SEISMIC IMAGING AND VELOCITY MODEL BUILDING

IN THE THRACE REGION,

NORTHWESTERN TURKEY: A CASE STUDY

A Thesis Presented to

the Faculty of the Department of Earth and Atmospheric Sciences

University of Houston

In Partial Fulfillment

of the Requirements for the Degree

Master of Science

By

Gokhan Alkir

May 2016

SEISMIC IMAGING AND VELOCITY MODEL BUILDING

IN THE THRACE REGION, NORTHWESTERN TURKEY:

A CASE STUDY

_____

Gokhan Alkir

APPROVED:

_____

Dr. Hua-wei Zhou, Chairman

_____

Dr. Shuhab Khan, Member

_____

Dr. Edip Baysal, Member

_____

Dr. Dan E. Wells

Dean, College of Natural Sciences and Mathematics

Acknowledgements

I am very grateful to the people who believed in me and my academic education during my stay at the University of Houston.

I wish to express my sincere gratitude to my advisor Dr. Hua-wei Zhou and my committee member Dr. Shuhab Khan for their great support and belief in me as I finalized this research. Moreover, I am extremely grateful to my committee member, Dr. Edip Baysal, for his support and expertise. I would also like to thank Dr. Orhan Yilmaz, Irfan Tanritanir, and other employees at Paradigm for their enormous contribution to my project. I am very grateful to Turkish Petroleum (TP) for their financial support during my studies. I am very thankful to my wife for her endless support, patience, and faith in me while on this long scholastic journey. Lastly, I would like to send all my prayers and love to my father, who passed away one semester before my graduation.

SEISMIC IMAGING AND VELOCITY MODEL BUILDING

IN THE THRACE REGION,

NORTHWESTERN TURKEY: A CASE STUDY

An Abstract of a Thesis Presented to

the Faculty of the Department of Earth and Atmospheric Sciences

University of Houston

In Partial Fulfillment

of the Requirements for the Degree

Master of Science

By

Gokhan Alkir

May 2016

Abstract

The aim of this research is to apply several seismic processing and imaging techniques to a raw 3D-land dataset and examine the quality of the subsurface images.

This study uses a 3D-seismic dataset in the Thrace region of northwest Turkey that was acquired by Turkish Petroleum in 2006 covering an area of approximately 146 km². This region is primarily a gas-rich zone with drilling operations starting in the 1970s and demand continuing even now. The target zone in the region is Upper Oligocene Osmancik deltaic sandstone and minor shale. The region developed as a fore-arc basin during medial Eocene to Oligocene time. The thickness of the basin-fill deposits is estimated to be up to 9 km deep.

This work applied conventional seismic data processing and imaging techniques. Kirchhoff pre-stack time and depth migration are used. Tomography approach was used to refine the velocities to get the final interval velocity. Having the final interval velocity, reverse-time migration was used.

The tomographic velocity analysis was successful in yielding an accurate interval velocity. After application of all these imaging methods, I found that the RTM gave the best image of the subsurface. I was able to estimate the hydrocarbon reservoir at 1500 – 2200 m. The shot pattern used for this survey for station and shot distances along the receiver and shot lines may be too large for the purpose of imaging at this depth.

Table of Contents

List of Figures

List of Tables

Chapter 1: Introduction

1.1 Introduction

Seismic imaging is one of the key methods in exploration geophysics that investigates the subsurface geological structures and production zones. In reflection seismology, the data coming from the Earth's interior usually include several types of undesired events which cause many problems in the data. Seismic processing and several imaging techniques are major applications used to produce a clear outcome of acquired data.

The area where I applied imaging techniques is located in the northwestern part of Turkey, which is rich with the hydrocarbon reservoirs. The number of drilling fields at this location underscores the significance of exploration; there are more than twenty billion cubic meters of gas in proven reserves. I focused on the imaging part of this work. Having raw-data allowed me to apply all possible imaging techniques to see a better stack response. In the first part of my study, I analyzed the data with a conventional seismic-data processing method called fast-track-processing.

In the second part of my study, I employed the pre-stack time and pre-stack depth migration methods to have a final stack which includes the subsurface structures in their true positions. If the subsurface is complex, it is difficult to find the true velocities. However, reservoirs are located in these complex areas. For building a velocity model, pre-stack depth migration, and tomography methods are employed. The best way to achieve a useful image is to have a perfect velocity model. It has a major impact on the imaging because unreliable velocities generate noisier sections (Yilmaz, 2001). Geophysicists normally work with the data recorded in time, but imaging in depth

yields a clear picture given a good estimation of the interval velocity model. Migration needs the travel times between the source and receivers and these travel times belong to the velocity of the subsurface. In time migration, velocities can be effective root-mean-square (RMS) velocities, but depth migration needs an accurate interval velocity function. Velocity estimation is hard to determine for depth migration; however, several methods have been applied to determine interval velocities for depth migration.

I also applied tomography for interval-velocity model building. Several reflection tomography methods are based on the same principle and have similar challenges (Biondi, 2006). In the tomography part of my work, I tried to focus on a ray-based velocity model updates by using the residual move-outs obtained by the Kirchhoff depth migration. In every iteration, I designed parameters to correct velocity errors. These iterations are advantages of this method, as is the ability to recover resolution.

I finalized my work with the approach called reverse-time migration (Baysal et al., 1983; Whitmore, 1983). It is a sophisticated wave-field continuation method. The velocity model used in RTM is built by tomography. I have included this method as my last imaging technique to see the best outcome of my research and used it to develop a better velocity model to improve my results.

1.2 Geological Settings of the Survey Area

The Thrace region is located in the northwestern Turkey. My target survey area is called Alacaoglu, in the Kirklareli Province, Turkey.

The Thrace Basin plays an important role since it is the natural gas province of Turkey. Commercial gas productions started during the 1970s, and after this stage, the location became a major exploration zone for petroleum systems (Gurgey et al., 2005;

Hosgormez and Yalcin, 2005). Thrace Basin is an intermontane trough bounded to the north and west by granitic and metamorphic rocks of Strandja-Rhodope Massifs, and it is suspected that the North Anatolian Fault Zone has an effect on oil potential of the basin (Coskun, 2000). Also, the Thrace basin is proposed to be a fore-arc origin (Gorur et al., 1996).

The Thrace Basin consists of five different units: 1) Strandja-Rhodope Massive metamorphics, 2) Istanbul Paleozoic and Kocaeli Triassic sediments, 3) Upper Cretaceous island-arc volcanics, 4) Early Cretaceous-Paleocene aged Cetmi Ophiolitic Melange, and 5) Sakarya continental crust and overlying sediments found in the southern part of Thrace (Siyako, 2006).

Previous research definite clues about the deposition and erosion cycle of the Thrace basin consisting of siliclastic and volcanoclastic rocks with some carbonates. The thickness of the sediments can reach up to 9000 m and thins towards the margins of the basin (Siyako, 2006). The geology of the region was formed by an extension in the late middle Eocene to late Oligocene times (Turgut et al., 1991). Sedimentation began in the basin with a quick decrease over an older metamorphic and crystalline basement. The geological map of the Thrace Region is displayed in Figure 1.1.

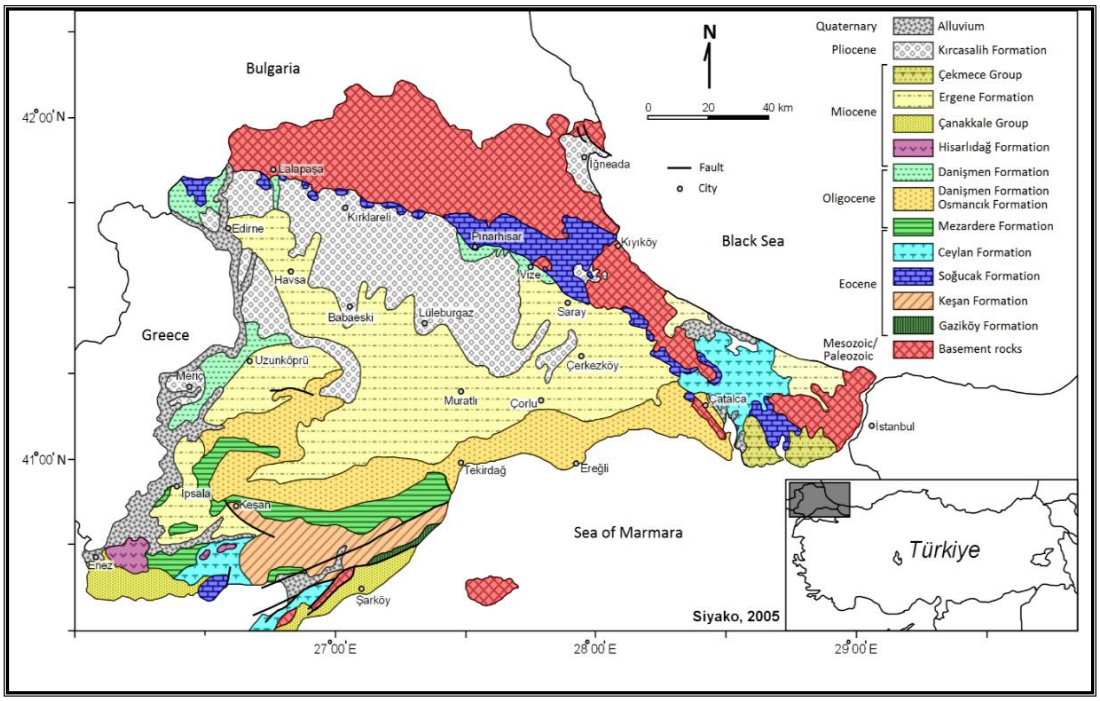

Figure 1.1: Geological map of the Thrace Region, in northwest Turkey (taken from Siyako, 2006).

1.3 Seismic Data

The raw 3D-seismic dataset and related files about acquisition used in this study were provided by the Turkish Petroleum Corporation. The 3D-data were acquired in 2006 by a swath shooting method. It consists of a total of 13 swaths where each swath consists of six receiver lines. The overlap between swaths were three receiver lines. The shot lines and receiver lines were perpendicular to each other. The seismic source used was buried dynamite. The whole survey covers approximately 146 km^2 (11.6 km X 12.6 km).

1.4 Methods and Applications

The seismic processing method is widely used in hydrocarbon exploration and is used to extend known production fields to increase the oil-production rates. The modern

seismic imaging techniques allow detailed subsurface images for structural and stratigraphic interpretation of geologically complex areas. Specially acquiring 3D-seismic data and creating three-dimensional images of the subsurface in depth (pre-stack depth migration methods) allows us to obtain interval velocities of the subsurface cube as well as the detailed image of the reflectors.

In my research, I was careful to obtain the best information from this 3D-land dataset. I used "conventional-processing workflows", such as common-depth-point (CDP) stacking and post-stack time migration, as well as up-to-date processing and imaging methods widely used in the industry. These workflows also allowed the construction of interval velocity cube for the area as opposed to the normal move-out (NMO) and RMS velocity information produced by the CDP stacking and time migration. My applications are divided into three stages.

1) In the first stage, a "conventional seismic processing" which may be considered as "fast-track processing" was applied. This stage includes the application of the field acquisition parameters by building databases for the information as well as creating an appropriate binning grid (CDP grid) for the processing of this dataset. I applied amplitude corrections such as spherical divergence and lateral balancing to the data, proper signal analysis and signal shaping operator, and necessary signal/noise improvement applications. After making these corrections, the data were binned to CDP for NMO, mute, and stacking. Following the CDP stack, the data were time migrated. The velocity field was refined to RMS velocities, which yielded the time-migrated cube of the seismic data. At this stage, I applied a post-stack time migration (exploding-reflector concept) to yield the results.

2) In the second stage, a detailed velocity (interval) model was created by employing ray-tracing methods for pre-stack depth migration and tomography iterations. The initial interval-velocity model for this stage was created from an RMS-velocity cube by a "constraint Dix" method.
3) In the third stage, from the final interval velocity model, I created images using different pre-stack depth-imaging methods such as ray-tracing and wave-equations (Kirchhoff migration and RTM). RTM is the most up-to-date pre-stack depth-imaging algorithm. It employs a two-way wave equation and is capable of imaging complex geological structures better than other methods.

Although the data is not shot as a wide azimuth, as most of the surveys are shot today, it is still expected and succeeded to give good imaging results for structural and stratigraphic interpretation.

1.5 Software Packages

All of my research studies were completed by using Paradigm's Echos, GeoDepth, and Tomography packages which include seismic data processing, migration algorithms, and seismic velocity implementations and refinements.

Chapter 2: Conventional Seismic Processing (Fast-Track Processing)

2.1 Introduction

In seismic exploration, reflection-seismic data, which are acquired in the field that contain reflections of the sound waves, are generated by a seismic source. Seismic processing is a technique that is applied to the recorded seismic traces in the field, so that one can have the ability to investigate the interpretation of the geological structures. Seismic reflection surveys are the most accepted method that the industry utilize. In this method, seismic records only contain the reflections, in fact only the primary reflections. In many cases the assumption of layered media is valid. The main goal of seismic data processing is to improve the signal-to-noise ratio and enhance the desired seismic signal.

In my research, seismic processing, and imaging tools were used to reach my objective. A seismic workflow should be designed to implement all of the seismic processing steps. Before starting any method, the seismic data needs to be carefully conditioned and created. The first step is to import the data from the SEG-Y disc files to the software package.

This chapter will briefly explain all the seismic-processing steps that are applied to the seismic data, and then it will provide the outcomes.

2.2 Acquisition Parameters

The acquisition parameters that were used in the survey are displayed in Table 2.1.

Table 2.1: The acquisition parameters used in the survey

Spread Geometry and Receiver		Source Parameters	
Spread	*6 Line*	**Source**	*Dynamite*
Channels	*768 (128 per line)*	**Depth**	*15 m.*
Group Interval	*50 m.*	**Shot Interval**	*50 m.*
Bin Size	*25 x 25*	**Charge**	*2 Kg.*
Total CDP Fold	*30*	**Shot per Salvo**	*18*
Receiver Line Interval	*300 m.*	**Source Line Interval**	*400 m.*
Receiver Line Direction	*W - E*	**Source Line Direction**	*S - N*
Near Offset	*35 m.*	**Recording**	
Far Offset	*3385 m.*	**Instrument**	*Sercel - SN388*
Geophone Type	*SM4 – U, 10 Hz*	**Tape Media and Format**	*3490 Cartridge, IBM Interchange*
Geophone/Station	*24*	**Record Length**	*5 s.*
Receiver Array	*1 * 24 inline*	**Sample Rate**	*2 ms.*
Array Length	*50 m.*	**High-Cut Filter**	*200 Hz*
Inline Geophone Space	*2.08 m.*	**Pre-amp. Gain**	*0 dB*

2.3 Processing Flow

Each seismic project requires a convenient seismic processing workflow. Before designing a flow, several tests should be undertaken to determine the parameters to get the best result. The main objective of seismic-data processing depends on the raw data quality acquired in the field, and interpretation of the data depends on the quality of this information. The general tasks in processing are the data conditioning, parameter analysis, data enhancement, migration/depth conversion, modeling and interpretation, and exploration decision making (Zhou, 2014). In this study, in my first part, which is conventional seismic data processing, I have designed a workflow which meets this criterion. The quality of the seismic data and the structural format of the surrounding location are key elements to implement seismic processing workflow. To enhance the signal, parameters have to be identified. The quality of a process depends, not only on the correct choices of the parameters, but also the efficiency of the preceding processing steps (Yilmaz, 2001). The processing workflow that is applied to this study is seen in Figure 2.1

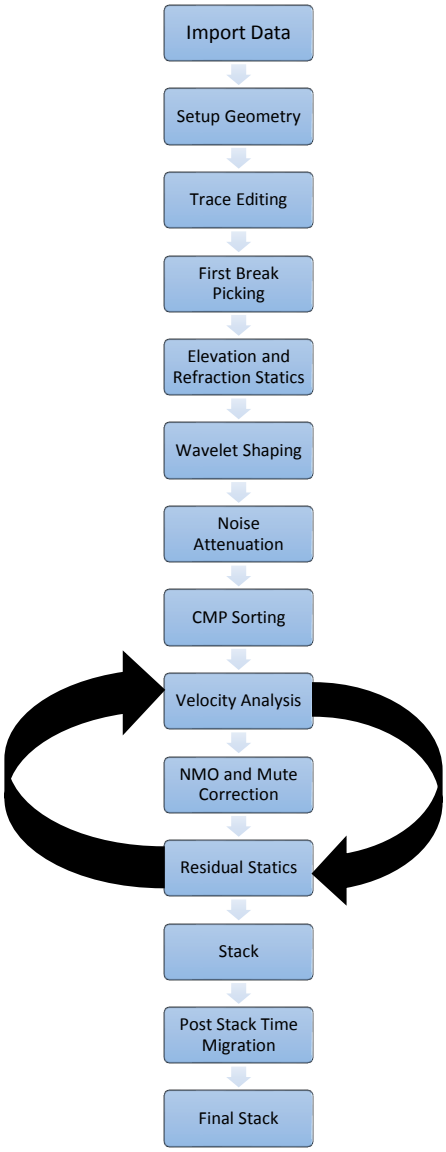

Figure 2.1: Conventional seismic processing workflow.

2.3.1 Geometry Set-up

The raw 3D-seismic data were acquired by the swath-shooting method, and it was supplied in SEG-Y files for each swath. First, it is imported into Echos software. The acquisition information was also supplied as Shell processing support (SPS) files for each swath. Shots and receiver locations are arranged to set up the correct geometry since geometry information is unquestionably crucial for the sake of any seismic

project. Combining the data with the acquisition information is the first important step for any data processing. The seismic data is read, and the information is stored contained in SPS files. These files are first transferred into the database, and consequently into the trace headers. Careful inspection of the data is essential since any incorrect information will severely affect the outcome (Yilmaz, 2001).

In Echos, the geometry check is done by the spreadsheet method and before the start of processing the data needs to be double-checked for any missing information. The 3D-layout of the shots and receivers is seen in Figure 2.2. In this study, the data is three dimensional. While filling the spreadsheet cells in the program, shot numbers, receiver numbers, and the relation files should match. Even though the processor confirms that the geometry setup is correct, the program also double-checks before starting the processing step. For the CDP stacking, the fold map covering the survey area is also created after assigning the geometry specification (Figure 2.3).

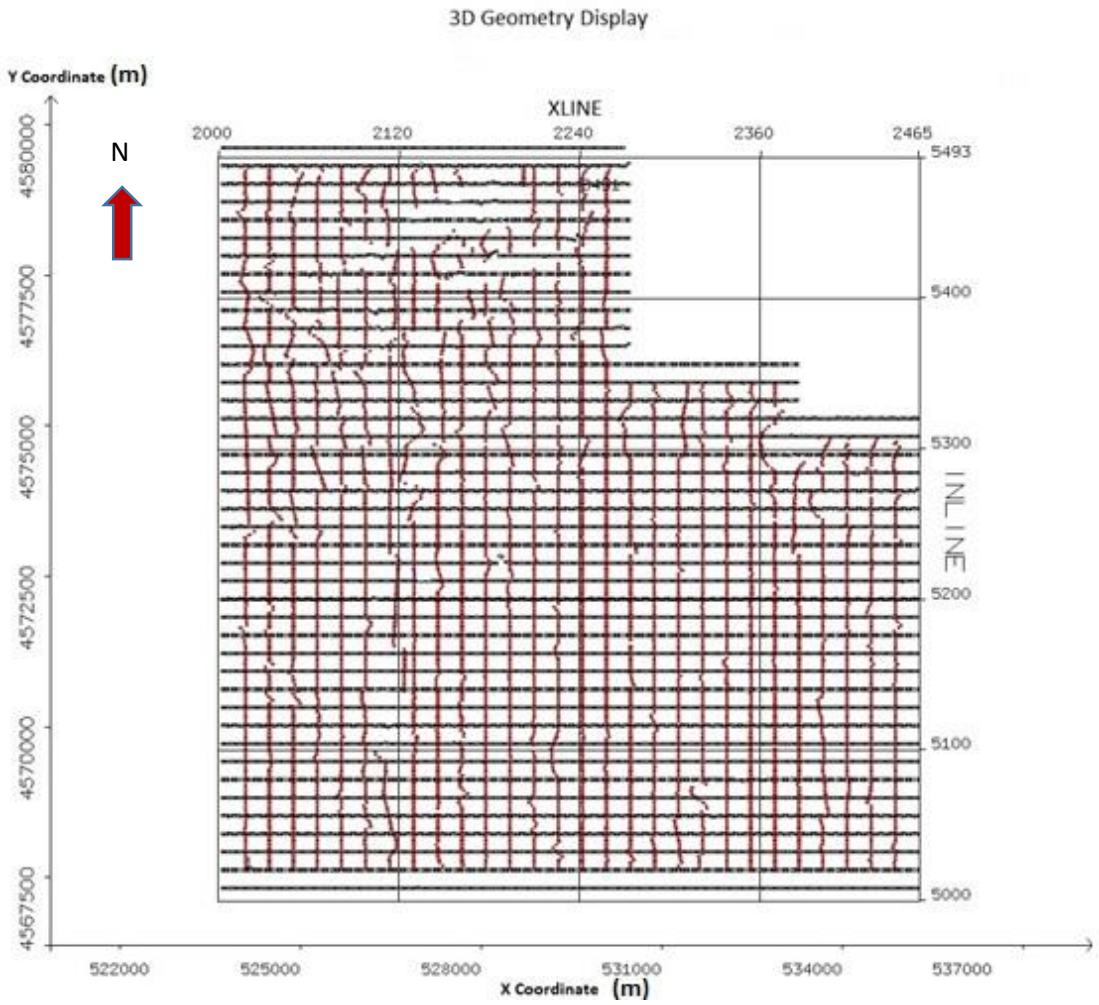

Figure 2.2: 3D geometry display of shots and receivers. Shots are shown in red and deployed as north-south direction. Receivers are shown in black and deployed in an east-west direction.

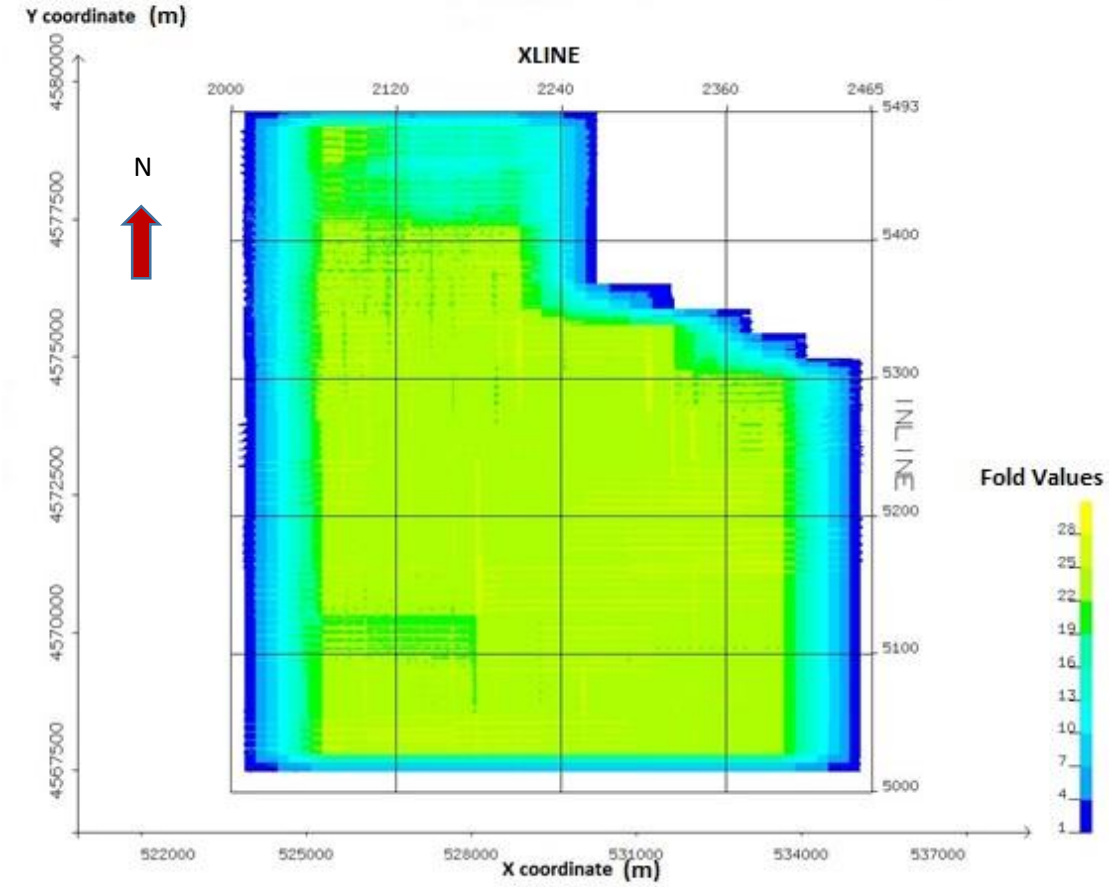

Figure 2.3: A map of the area covered for CDP stacking and resulting fold map of the data.

2.3.2 Trace Editing

The next step is the editing of bad shots and bad traces after the geometry with raw shots are finished (Figure 2.4). In this part, every single shot record is checked one by one to eliminate polarity reversals, bad traces, noise spikes, and mono-frequency signals. This is an essential step to pay attention to because if any undesired signal is processed, it may result in a poor condition in the upcoming processing stages. In my data, almost in every shot record, the main issues were the spiky noises, power line noise at 50 Hz because of the active railway in the survey area, and the organized noise,

i.e. ground roll. To remove unwanted noises, certain processing modules were applied to the data and yielded an enhanced signal.

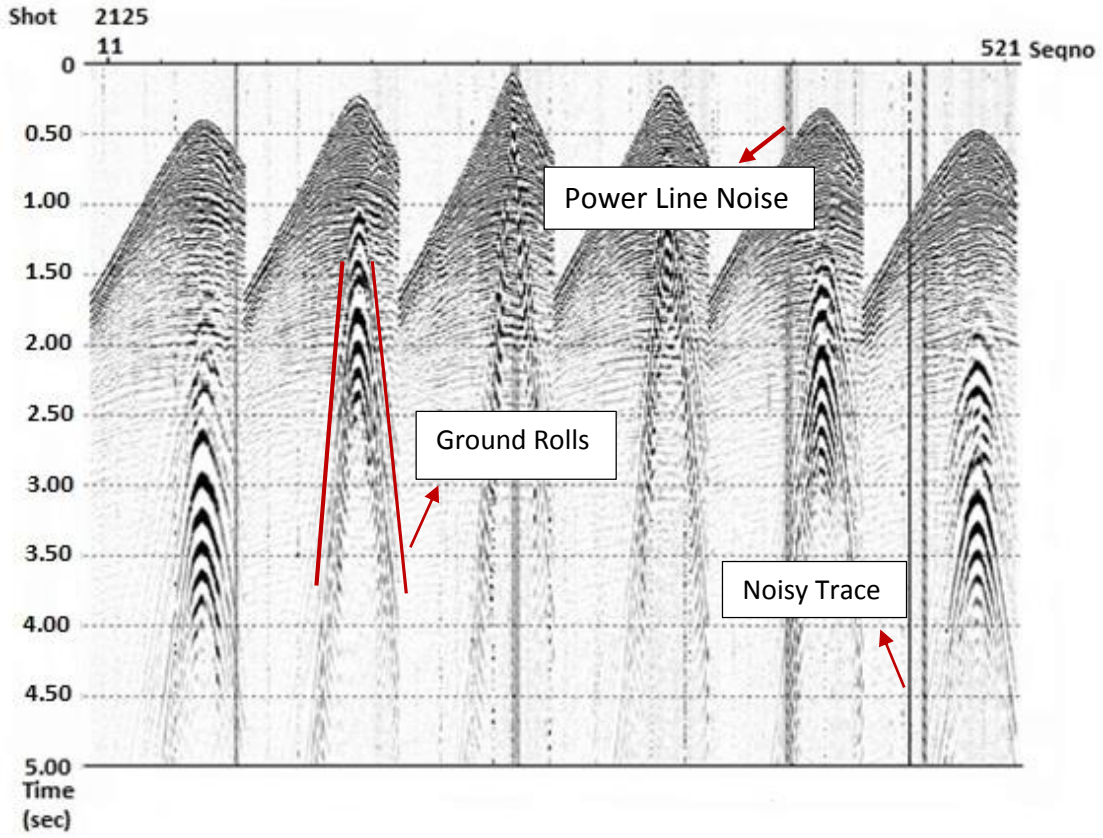

Figure 2.4: Raw-shot gathers from shot number 2125. The raw-data consists of all energy coming from the subsurface including noisy traces, ground rolls, and power line noise.

2.3.3 Spherical Divergence and Gain

To scale the amplitudes, spherical divergence, and exponential gain corrections were applied to accommodate for energy loses due to spherical spreading and transmission losses. During a seismic data record, coherent noise may have a stronger response than geological structures. Thus, before applying deconvolution of a time

variant the signal-to-noise ratio should be enhanced. Gain should not damage the signal. The proper gain depends on the velocity of the layer and the travel time;

$$\text{Spherical Divergence Correction: } (V * T_0^{Vpower}) * (T_x^{Tpower}) \quad (2.1)$$

Where,

Vpower is the power value of the average velocity at time T,

Tpower is the power value of time T.

Many gain corrections used in the industry are based on different scenarios. Automatic gain control (AGC) is one of the best methods used in seismic processing. Geometric spreading correction and trace balancing are also valued. In this study, the 1/T function is applied for spherical divergence followed by an exponential gain of 3 dB/s was used for amplitude recovery. Following the gain corrections as a function of time a lateral balancing of the trace amplitudes in a surface consistent manner was done. A scaler per shot and a scaler per recording station was calculated by Gauss-Seitel method and the resulting scalers were applied to the data. This lateral balancing step was also repeated after signal analysis and resolution enhancements and used in pre-stack 'true amplitude' migrations.

2.3.4 Deconvolution

Deconvolution is a major step in seismic-data processing which attempts to attenuate noise. Deconvolution is mainly applied before stacking. It improves the temporal resolution of the seismic-data by compressing the basic seismic wavelet. Deconvolution is the inverse process of convolution (Kearey et al., 2002).

$$s_k = r_k * w_k \quad (2.2)$$

Deconvolution operator is an inverse filter (i_k), which when convolved with the seismic wave (w_k), yields a spike function (d_k)

$$d_k = i_k * w_k \tag{2.3}$$

Then, logically convolution of the same operator (i_k) with the seismic trace, yields the reflectivity function.

$$r_k = i_k * s_k \tag{2.4}$$

In the real data, to achieve a seismic impedance from the seismic record through deconvolution is not possible. The input waveform and the Earth's impulse response are not known. Consequently, the inverse filter (deconvolution) is specified using statistical methods and deterministic methods (Yilmaz, 2001).

In my study, after several tests run on deconvolution, I have employed the spiking deconvolution method. Gain and deconvolution are applied on the raw-data as seen in Figure 2.5. My parameters were as follows;

- Design Window: 250 – 3284 ms for near offset, and
  2048 – 4646 ms for far offset
- Operator Length: 61
- Percentage of White Noise: 0.1

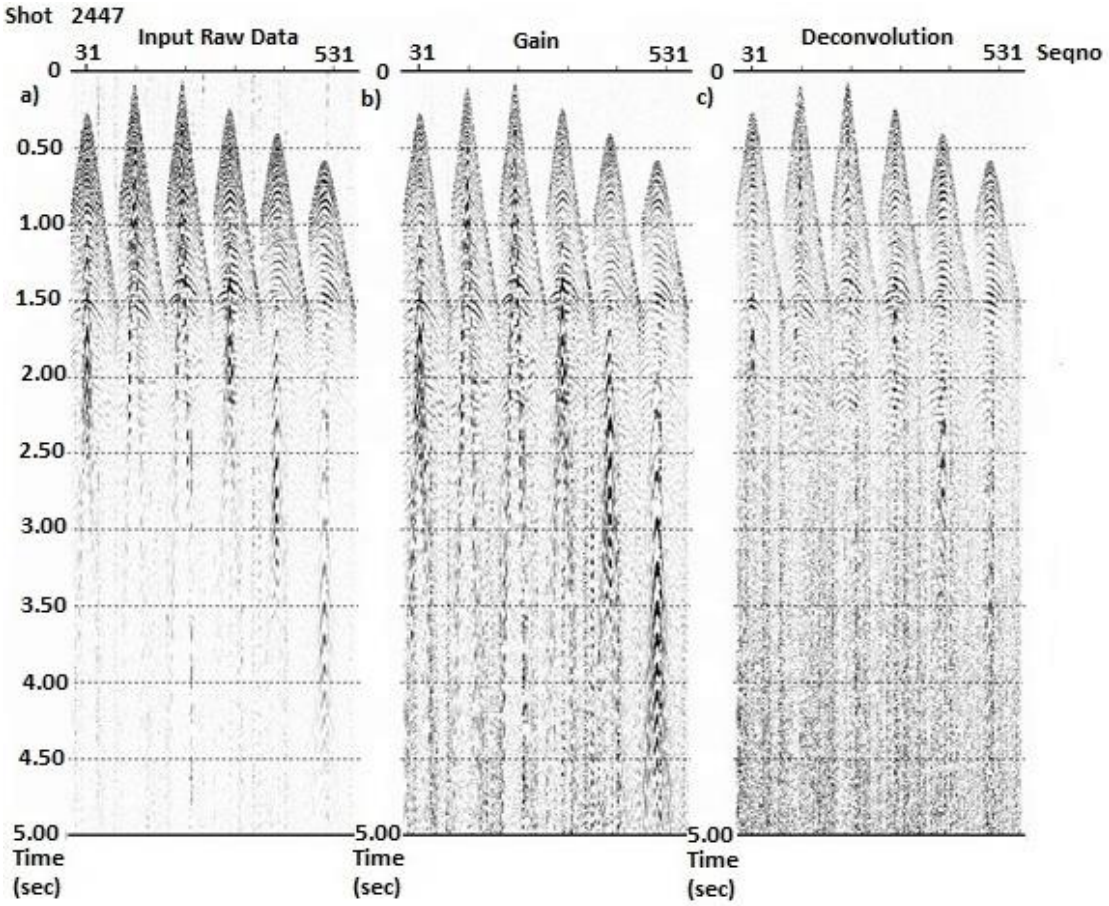

Figure 2.5: Gain and deconvolution are applied to the raw-data, the shot number is 2447. a) Raw shot gathers, b) after gain applied, c) after deconvolution. After these operations the signal quality is increased.

2.3.5 Noise Suppression

Seismic data contains both signal and noise and for an improved imaging, noise attenuation techniques are important. In general, the noise can be divided into two categories, coherent noise, and random noise. Coherent noise can be defined as a similar constant pattern along the shots, and random noise can be defined as outer factors like wind motion and cable vibrations. For noise suppression, I included 1 Hz as low frequency, and 15 Hz as the high frequency for band-limited noise. Scalar number for noise band was 0.25, and smoothing operator length was 60 ms.

2.3.6 Filtering

Filtering is an essential tool applied in all seismic signal processing projects. Major applications of filtering include removing unwanted frequencies, featuring some critical frequency values, identifying harmonic signals in the data, bypassing the aliasing effect, down-sampling, and revising the phase and amplitude uniqueness. Several types of filtering operation are widely used in the industry, and most common ones are low-cut filters, high-cut filters, and bandpass filters. Bandpass filtering is a key option since it overcomes the low-frequency ground rolls in the data.

In this study, some filtering tests were run to understand the optimum frequency values for the desired signals. I have implemented bandpass filtering tests to overcome the noise effects. To use a bandpass filtering, four frequency values have to be selected to apply to seismic data. A bandpass filter passes the frequencies within a certain range and rejects the frequencies outside. I selected my frequency bandwidth parameters depending on test results. I chose 5 – 15 – 80 - 120 Hz as my bandpass filtering parameters. The output of the noise suppression and filtering is displayed in Figure 2.6.

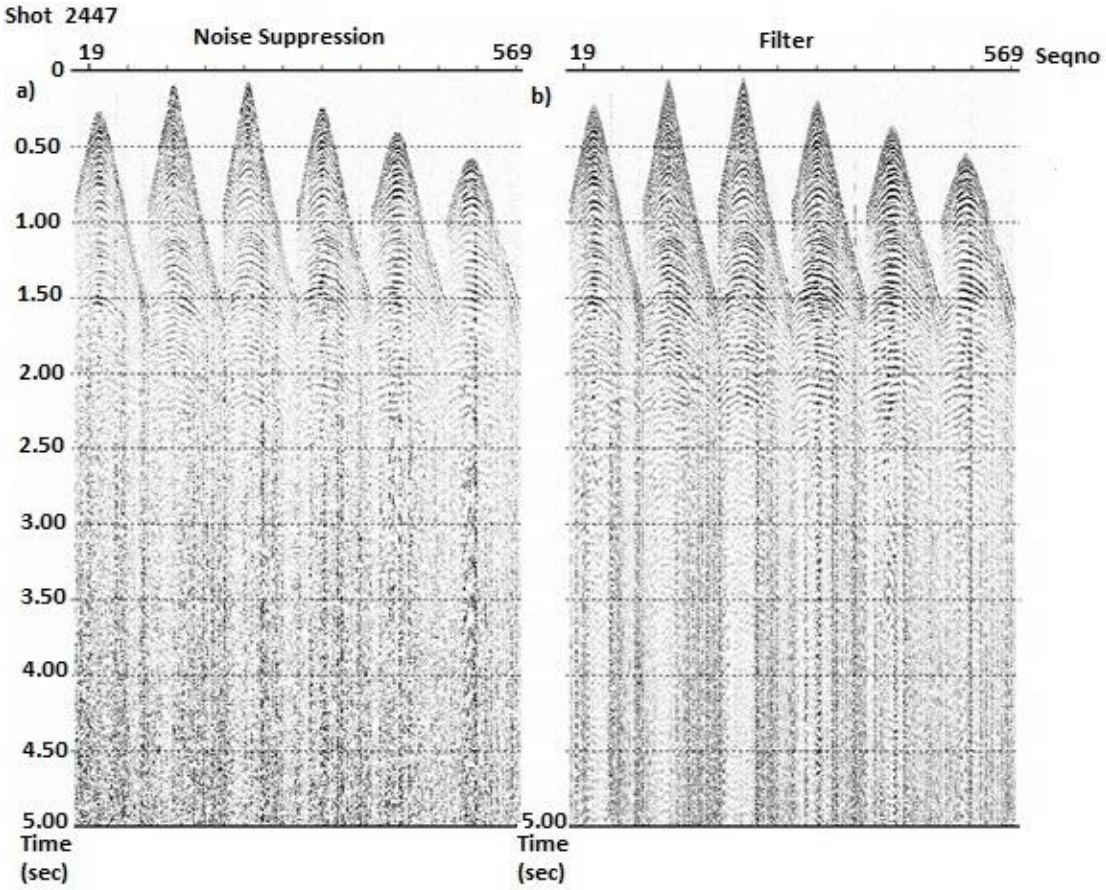

Figure 2.6: Noise suppression and bandpass filtering methods are applied to the raw-data, the shot number is 2447. a) The noisy traces and ground rolls are attenuated after noise suppression, b) the undesired frequency values are attenuated by applying the filter.

2.3.7 Amplitude Balancing

The main objective of amplitude balancing algorithm is to minimize counterfeit variations in the trace amplitudes (Lovelady et al., 1984). One of the main problems that affects the amplitude values is the coupling issue due to the poor contact between the source and receivers. It is possible to remove these undesired anomalies by applying an amplitude balancing operation.

In Paradigm's Echos software, there are these modules called Balan, Balsol, and Balapp which operate to perform surface-consistent amplitude balancing on pre-stack

seismic data. In essence, Balan is built to analyze a gate in the data from each input trace and to measure an amplitude corresponding to each trace. Balsol reads the output file of Balan and scales down the trace amplitude information to surface consistency by using the Gauss-Seitel method and finds scalers for each shot and receiver stations. The solutions are done in two passes, where the information from bad traces are determined and ignored from the consideration in the second pass. The database attributes are written for the calculated scalers. These are retrieved by the Balapp module and applied to the data. Scale factors are classified and applied to the seismic data.

A shot-related effect affects all traces within a shot-gather in the same way, independent of their receiver positions. A receiver-related effect affects all traces within a receiver-gather in the same way, independent of their shot positions. Equation is created for the surface-consistent model (Yilmaz, 1987):

$$x_{ij}(t) = s_j(t) \text{ X } h_{\frac{i-j}{2}}(t) \text{ X } e_{\frac{i+j}{2}}(t) \text{ X } q_i(t) + n(t) \qquad (2.5)$$

where, $x_{ij}(t)$ is the waveform of the trace with source location j and receiver location i, $s_j(t)$ is the waveform component associated with the source location j, $q_i(t)$ is the waveform component associated with receiver location i, $h_{\frac{i-j}{2}}(t)$ is the component associated with the offset dependence of the waveform $\frac{i-j}{2}$, $e_{\frac{i+j}{2}}(t)$ is the Earth's impulse response at the source to receiver midpoint location, and n(t) is the component that cannot be associated with the shot, receiver, offset or CMP.

2.3.8 First Break Picking

First breaks are the onsets of the signals and need to be picked as precisely as

possible because they are important for the geometry. Practically, these arrivals are affiliated with the energy of refracted waves at the bottom of the weathering layer, or with the direct waves traveling from the source up to the receiver (Figure 2.7).

First break quality is related to the near surface structure, source type, and signal-to-noise ratio conditions (Sabbione and Velis, 2010). It can be difficult to pick the first breaks if the structure is complex. Hence, in this research, the picking was handled in common shot gathers by applying an automatic picking algorithm based on neural network methods followed by manual editing to achieve the best results. Then a static correction set for shots and receivers was calculated with refraction algorithm (Figure 2.8). As discussed later the first break picking is essential for statics correction.

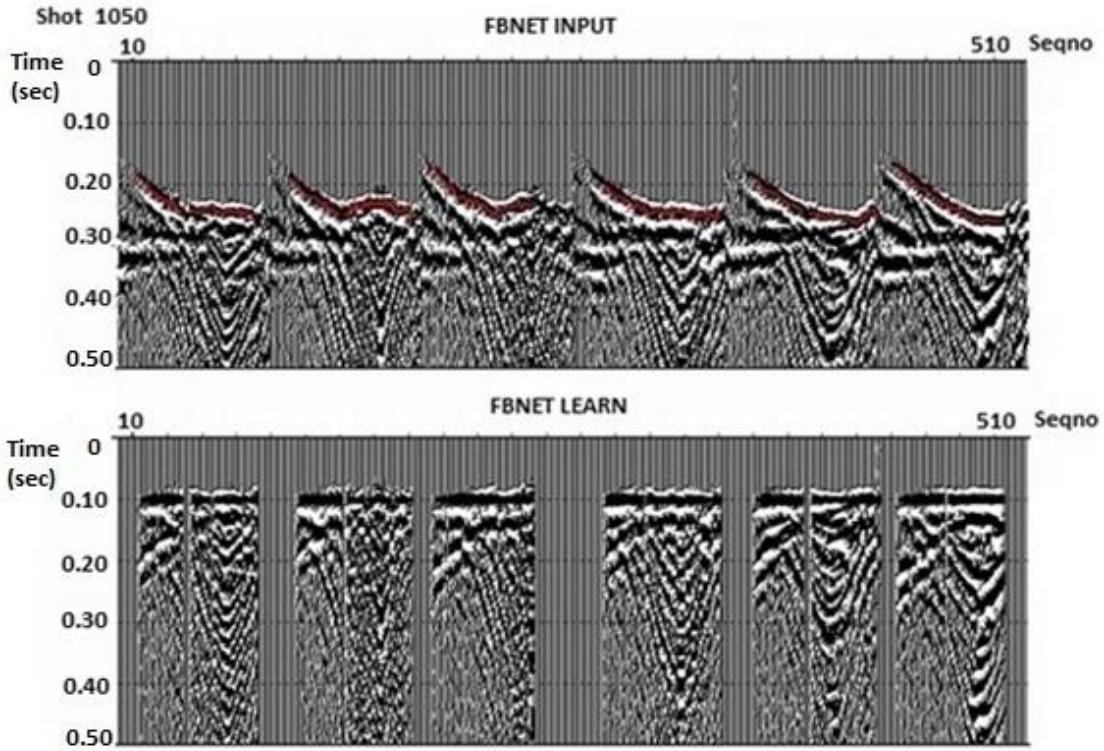

Figure 2.7: First break picking approach based on the automatic picking algorithm based on neural network method followed by manual editing for shot no: 1050. Upper figure is the input for first breaks, and the below figure represents the learning of the first breaks after automatic and manual picking.

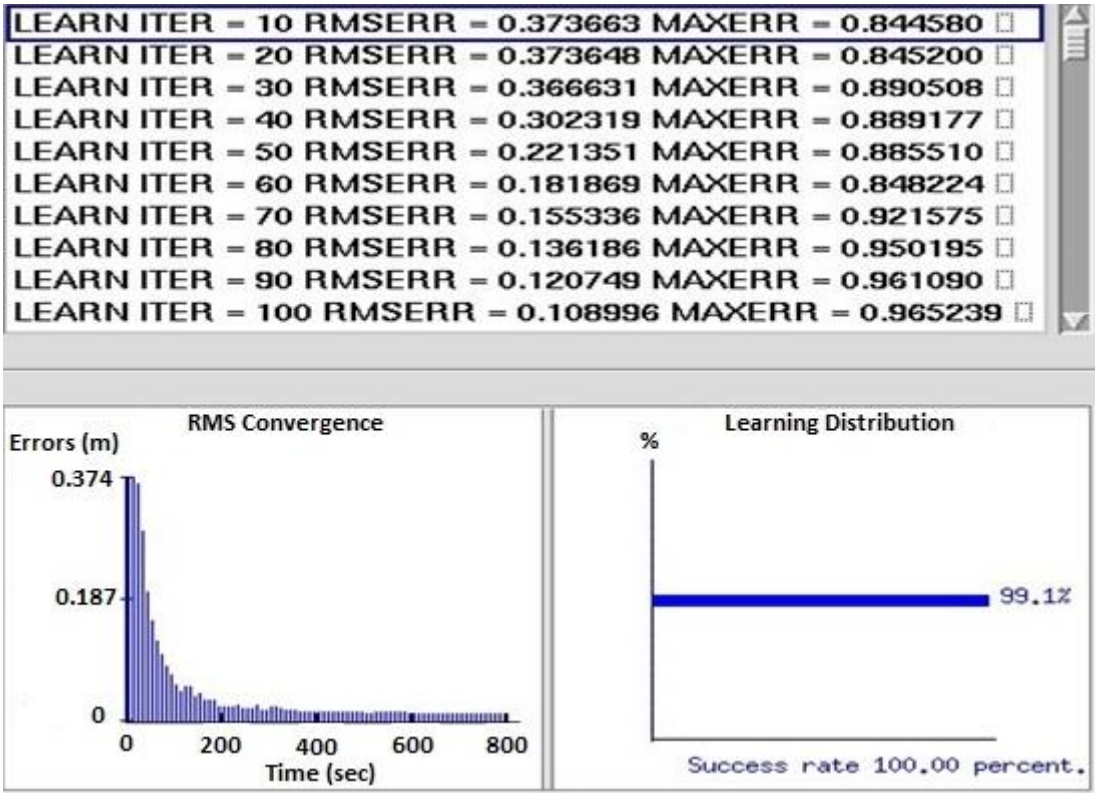

Figure 2.8: Iterations of RMS velocities and errors for learning confidence of the first break picking quality. The errors in RMS are decreased with the iterations of the learning process and resulted in a high success rate.

2.3.9 Refraction Statics

The estimation of the velocity and the thickness of the weathering layer is done depending on the first arrivals. Automatic residual statics methods perform best if refraction statics correction has been applied first since correlation across a common-midpoint gather depends on the quality of the stacked trace (Lawton, 1989). Refraction statics are applied to seismic data to compensate for the effect of near-surface low-velocity layers and differences in the elevation of shots and geophones (Yilmaz, 2001). Time shifts were applied to the seismic reflection traces to correct the time delays which are known as static time shifts.

Refracted arrival times are used to derive static corrections for the seismic-reflection data. Refraction static correction can be considered as a three stage process; decomposition of refraction travel times into surface consistent delay times, construction of a refractor elevation model, and computation of the static correction (Daly and Diggins, 1988).

To calculate the refraction statics, the following equation for delay time was used;

$$\text{Delay Time} = \frac{Z_1 \cos i_c}{V_1} \tag{2.6}$$

Where, Z_1 is the vertical depth to the refractor, i_c is the critical angle, and V_1 is the weathering velocity.

We require two corrections. For the first one, we need the weathering and sub-weathering velocities in addition to the delay times. For the second one, we need the information on the weathering velocity to establish the refractor elevation and information about the sub-weathering velocity to make the static correction. The weathering velocity is usually assumed, but the sub-weathering velocity can be assessed from the raw-shot records.

Refraction statics are remarkably effective for the estimation of long-wavelength statics. Wavelength of statics is related with the range of lateral change in the weathering layer. A brute stack with the refraction statics is seen in Figure 2.9.

The parameters used for refraction statics are;

- Replacement Velocity: 2150 m/s
- Datum Elevation: 100 m.

- Weathering Velocity: 1000 m/s

2.3.10 Elevation (Field) Statics

Elevation statics involve computation and removal of the effect of different source and receiver elevations. Usually, a flat datum which is below the lowest source-receiver pair is used to bring the source and receivers elevation. A replacement velocity is needed, and this can be obtained either from the general knowledge of the area or estimation of the up-hole times or direct arrivals. The elevation correction t_D is made with using the equation:

$$t_D = [(E_S - Z_S - E_D) + (E_R - Z_R - E_D)]/V_r \quad (2.7)$$

Where, E_S is the ground elevation at the shot location, Z_S is the depth of shot, E_D is the datum elevation, E_R is the ground elevation at the receiver location, Z_R is the depth of receiver, and V_r is the replacement velocity.

The surface elevations in the survey area differ in the range of 35 m and 116 m; therefore, a reference datum elevation of 100 m is chosen for processing. Field static corrections are calculated and applied to bring the sources and receivers to the reference datum. A brute stack of the data with field statics is shown in Figure 2.10, and a close-up section is displayed in Figure 2.11.

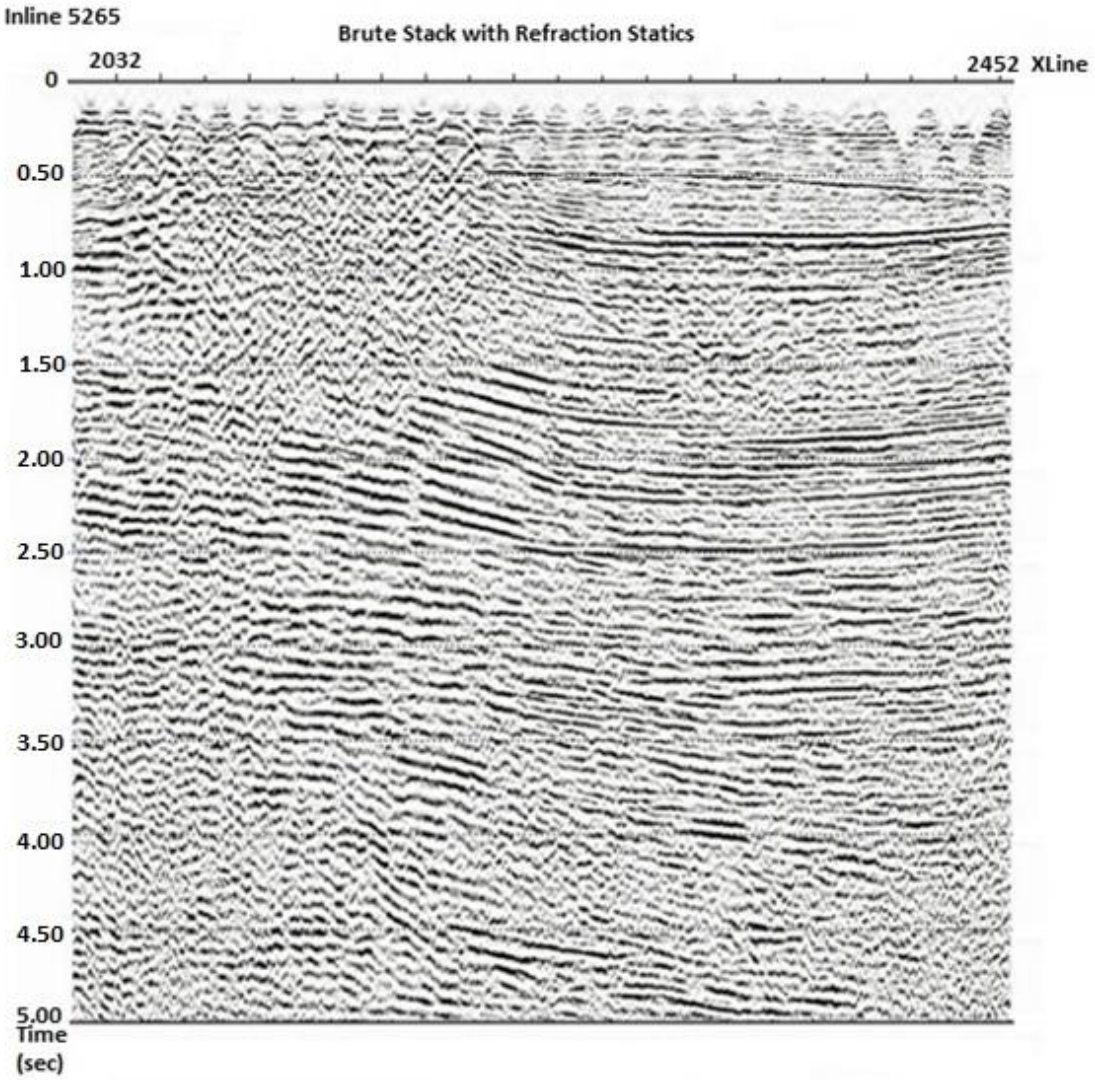

Figure 2.9: Brute stack view of the data with refraction statics for inline number 5265.

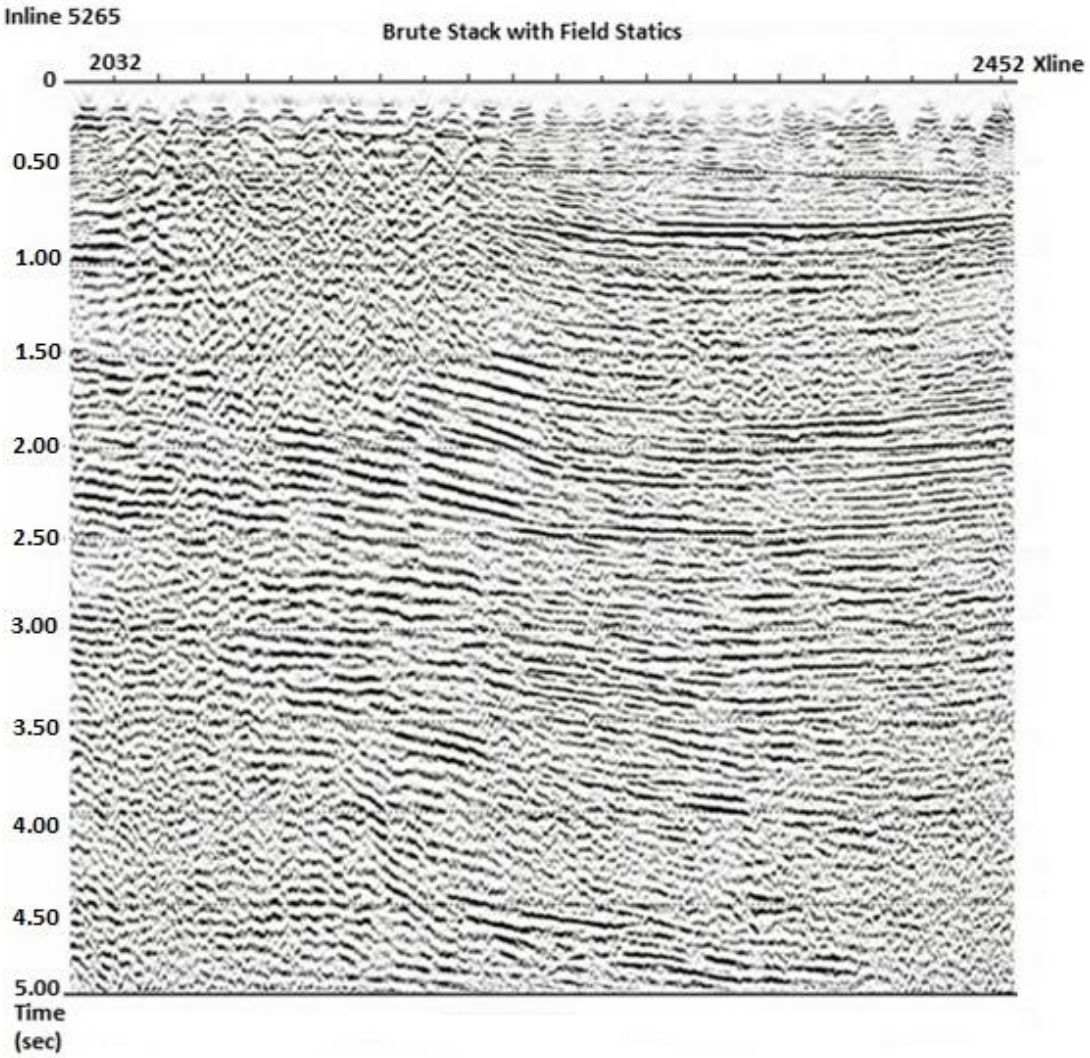

Figure 2.10: Brute stack view of the data with field statics for inline number 5265.

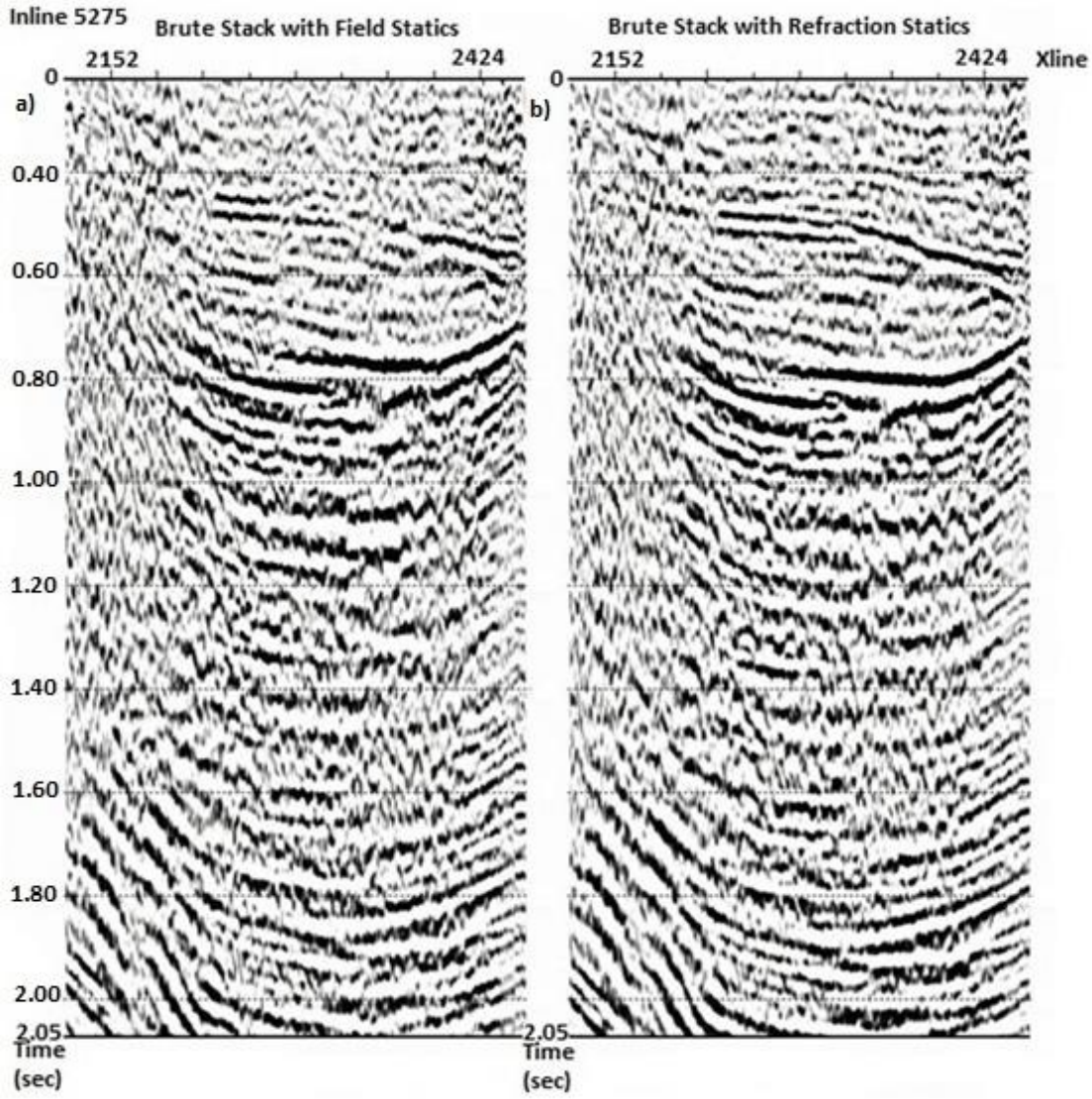

Figure 2.11: Zoomed view of the brute stacks of the data. a) Brute stack with the field statics, b) brute stack with the refraction statics.

2.3.11 Wavelet Shaping

The main goal of wavelet shaping is to secure the Earth's reflectivity by eliminating the effects of source and receivers. Its most common purpose refers to the estimation of the basic wavelet embedded in the seismogram. Wavelet shaping designs a shaping filter to convert the estimated wavelet to the desired form, usually a broadband zero-phase wavelet, and applying the shaping filter to the seismogram

(Yilmaz, 2001). In all wavelets with the same amplitude spectrum, the zero-phase wavelet has the largest resolution, hence the most desirable wavelet.

In this study, a surface-consistent wavelet shaping is applied, where a source wavelet and receiver wavelet is extracted from the data, and a single filter for individual shots and individual receiver stations are applied. So, it yields to a desired zero-phase Butterworth type wavelet. The analysis window (300 - 3000 ms) was used for extraction of one wavelet per shot gather. The following equation is used for Butterworth wavelet;

$$A(f)^2 = \frac{(\frac{f}{f_a})^{2N}}{(1+(\frac{f}{f_a})^{2N})(1+(\frac{f}{f_b})^{2M}} \quad (2.8)$$

Where, f_a is the low cut-off frequency (FL), f_b is the high cut-off frequency (FH). N is the slope on the low-cut side, and M is the slope of the high-cut side.

In this study, a zero-phase desired Butterworth wavelet is chosen with the parameters, in the frequency range of 10 Hz. to 60 Hz. where the slope on the low-frequency side are 18 dB/octave, and on the high-frequency side 36 dB/octave.

2.3.12 Amplitude Quality Control (Ampqc)

Amplitude quality control is done to eliminate the noisy traces in seismic records and improve the desired signal. This step needs to be applied to remove the bad effects of spikes or direct currents. Usually, this process contains two steps; firstly the average amplitude values within a specified time gates are calculated by using the equation and then displayed. Afterward, a mathematical scaling factor should be implemented to edit the noisy traces. In this case, the scaled amplitude values are

disregarded from the seismic record which may show unexpected changes in the later stages.

$$A_{ave} = \sqrt{\frac{\sum_{i=1}^{N} |a_i|}{n}} \tag{2.9}$$

Where, A_{ave} is the average amplitude, and N is the number of non-zero samples. The noisy trace removal from the raw data is shown in Figure 2.12.

2.3.13 Common Mid-Point (CMP) Sorting

In seismic surveys, the shots are recorded sequentially, and it is determined that the records which are coming from the sensors are for a single shot analysis. Shot positions, receiver positions, and the reflection positions are the most important measures in the survey. The real positions of the sublayers are unknown before starting the processing. Organizing the data in common mid-points is an outcome of the field logistics. The mid-point is defined as the mid-point between source and receivers. Once we gather all these information from the shot-receiver pairs, it shows the subsurface model. The signal-to-noise ratio has to increase after applying these steps.

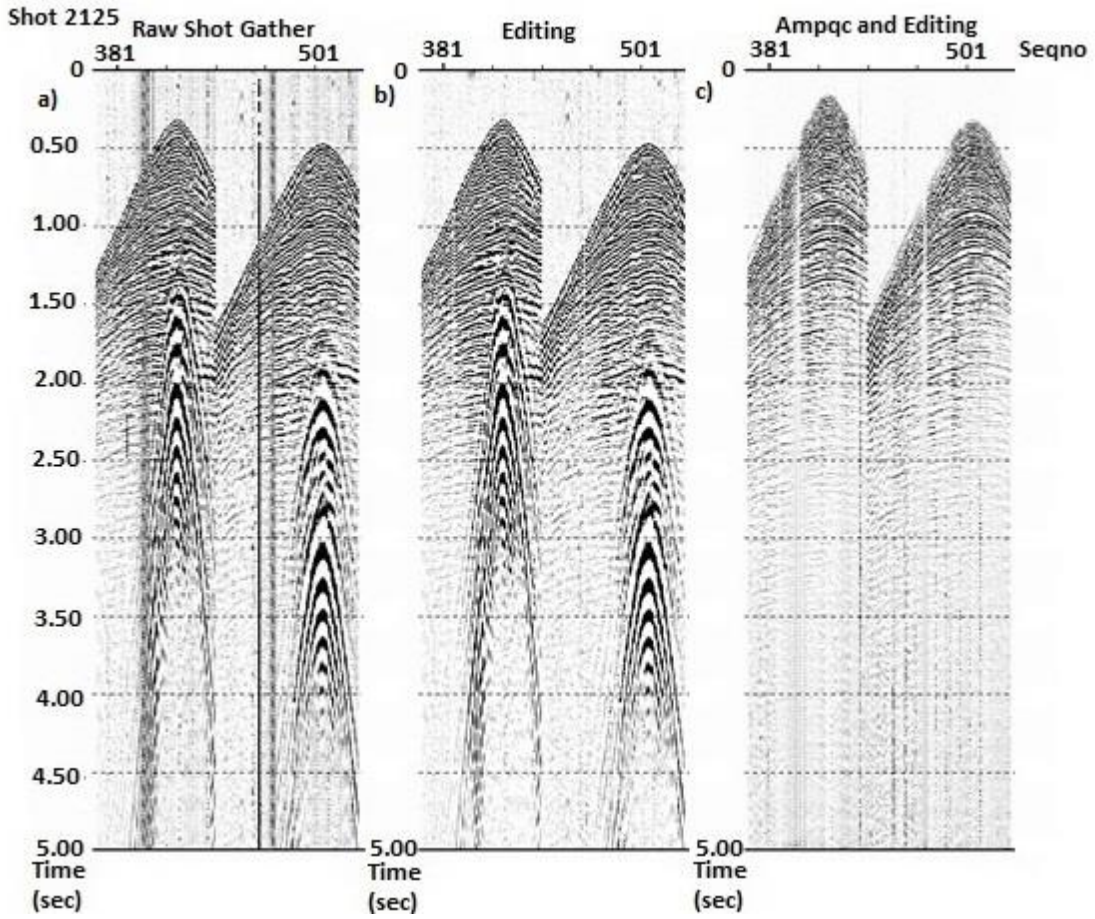

Figure 2.12: a) Raw-shot gathers for shot number 2125, b) after editing of undesired noisy trace removal which causes poor data quality, c) after editing and Ampqc.

2.3.14 Velocity Analysis

To achieve the final image of the subsurface, seismic velocities are crucial for data processing and should be picked carefully. Velocity analysis is done to correct the effects of normal move-out on reflection times. In my study, the velocities are picked with the 'Interactive Veldef' module in Echos. The data has been ordered in common-depth-points and offset. To pick appropriately, the 3D-data input has been sorted in group range as follows:

- First Inline: 5050

- Last Inline 5450
- Inline Increment: 100
- First Crossline: 2050
- Last Crossline: 2400
- Crossline Increment: 100

The number of the gathers in each group is also an important parameter in this module, since it gives us a decision about surrounding layers. If the number of gathers is too small, then the gathering display shows only a portion of the area. In this case, I have chosen this number as 41 to give me a clear section of the general gathers. I used both the semblance velocity spectrum and the constant velocity stack.

The stacking velocity can be described as RMS velocity, and it attains the maximum amplitude of the events in the stacked section. For the first part of my study, I have used semblance velocity analysis as shown in Figure 2.13. The semblance is the measure of a coherency in the seismic data, and in a mathematical expression, it can be calculated as in equation (2.10). The semblance panel reflects the optimum stack response in the sense of contour plot. For the accuracy of the velocities, the coherency of the ratio needs to be picked at its highest.

$$\text{Semblance} = \frac{1}{M}\frac{\Sigma_t s_t^2}{\Sigma_t \Sigma_{i=1}^{M} f_i^2} \tag{2.10}$$

Where, M is the number of traces in a CMP gather, f_i is the amplitude on the i^{th} trace at two-way-time, and s_t is the stacked amplitude.

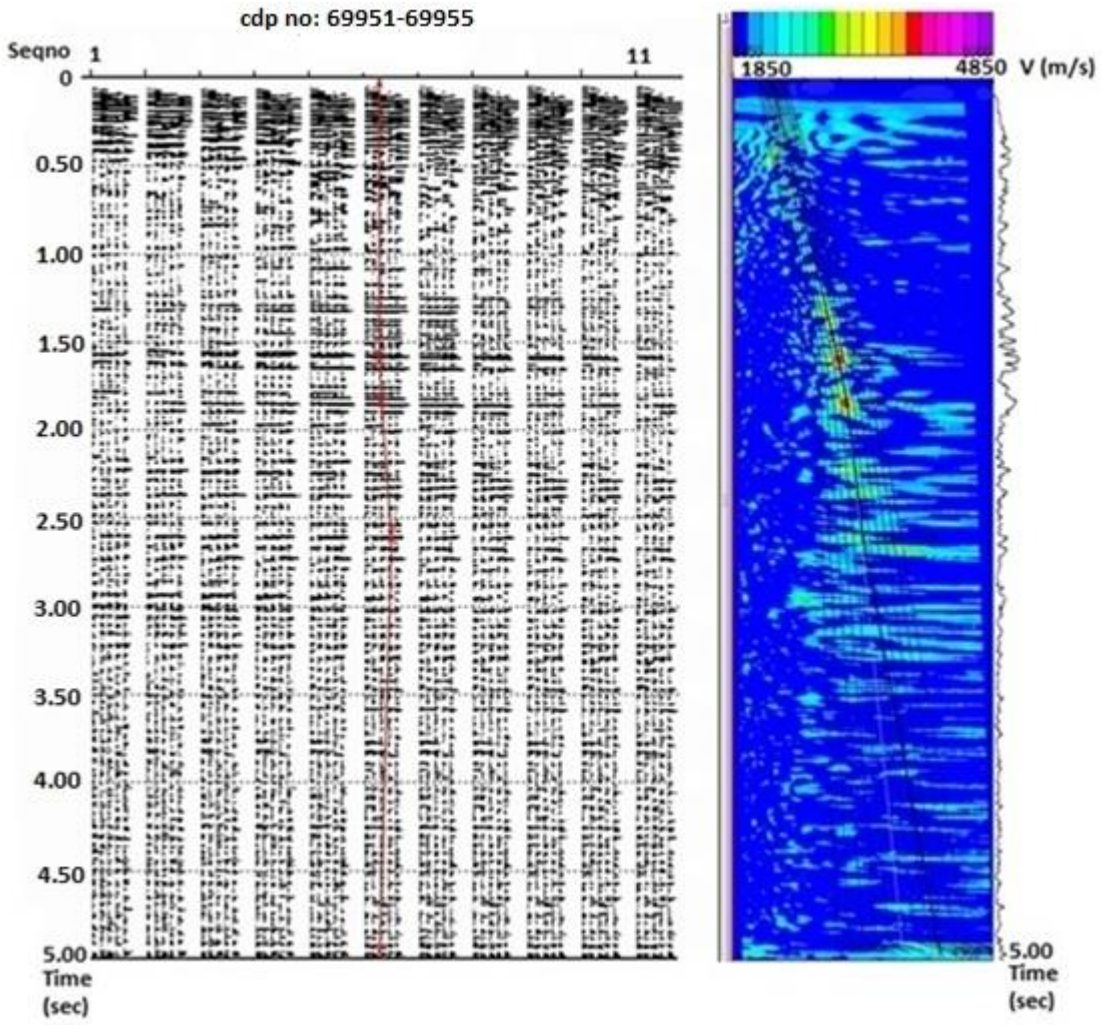

Figure 2.13: Semblance velocity analysis on the common-depth-point (CDP) gathers. Right panel represents the constant velocity stack with picked time-velocity pairs from amplitude spectrum. Left panel represents the different velocities on stacked amplitude spectrum. The colored panel on right displays semblance of the stacked seismic traces as a function of stacking velocity in horizontal direction and two-way-traveltime in vertical direction.

2.3.15 Normal Move-out (NMO) Correction

The normal move-out time is the time difference between the two-way time at a given offset and two-way zero-offset time. In a basic definition, it is a seismic processing step which flattens the events in the common-midpoint gathers before

stacking. The main target of NMO is to remove the hyperbolic curvature in the reflection events. In other words, it is applied to remove the effect of the offset. If this step is successful, then for all the offsets, all the reflection points should come at the same time (Liner, 1999). Depending on a flat reflector, normal move-out is applied with the following equation;

$$t_x^2 = t_0^2 + \frac{x^2}{V_{st}^2} \tag{2.11}$$

Where, t_x is the actual reflection time of the seismic event, t_0 is the zero offset reflection time of the seismic event, x is the offset distance between source and receiver, V_{st} is the NMO or stacking velocity for the reflection event.

In larger offsets and shallower times, the frequency distortion increases (Yilmaz, 2001). Before getting into stacking operation, this undesired effects should be removed by applying a mute function. In the NMO module of Echos, there is the option of implementing a stretch mute. Therefore, a stretch mute of 45% was applied.

In the static corrections when a new velocity is picked, a new NMO correction is produced every time. How many times these iterations should be employed depends on the quality of the data. Two iterative corrections are run to achieve an acceptable result.

2.3.16 Residual Statics

The next step in the static correction is the residual statics. This is done because the reflection times are affected by the inconsistency of the near surface. Residual statics are useful for estimation of short wavelength statics. In general, refraction statics corrections remove a significant part of these distortions, but in the case of rapid

changes in elevation, the base of weathering, and the weathering velocity, that step alone is not sufficient to handle the problem. It always contains the errors or residuals, which have the effect of blurring the coherency of the reflectors on the CMP stacks (Yilmaz, 1987). A widely used method for residual statics is the surface consistent method. As an explanation, it presumes that static shifts are time delays that depend on the source and receiver locations in the survey. In addition to this, if the ray-paths are vertical in the near surface, the assumption is accurate. Using the surface consistent method is effective and reliable because weathering layer usually has a low velocity and refraction towards the normal at its base tends to make ray-paths vertical. The total residual time shift (t_{ijk}) can be calculated by using the equation:

$$t_{ijk} = r_i + s_j + G_k + M_k x_{ij}^2 \tag{2.12}$$

Where, r_i is the residual static time shift associated with the i^{th} receiver, s_j is the residual- static time shift associated with the j^{th} source, G_k is the difference in two-way traveltime at a reference CMP and the traveltime at the k^{th} CMP, and $M_k x_{ij}^2$ is the residual move-out that accounts for the imperfect NMO correction.

To calculate the residual statics corrections, the algorithm works in three stages:

1) Picking the time shifts, by cross-correlating each NMO corrected input trace with a 'pilot' trace belonging to that CDP location.
2) Decomposition of time shifts into receiver, source, structural, and residual terms,
3) Application of derived source and receiver terms to travel times on pre-NMO corrected CMP gathers.

In my study, I have applied an algorithm that allowed the pilot trace to be accepted from outside rather than being calculated internally. To clarify this method, a stack data is created and used as pilot, where post-stack data enhancement methods create a better signal-to-noise ratio for the pilot traces. A specific horizon is picked which is the base for the cross-correlations with the pilot.

In many land data examples, especially in areas with low signal-to-noise ratio, it is helpful to repeat the velocity analysis and to build the pilot traces, solve the residual statics and apply to the data to be stacked. Repeating these steps several times, yield a finer residual statics, and produces a finer velocity model for stacking the data. The resulting stacks of each iteration are carefully examined to observe improvements. The second iteration or sometimes the third iteration yields an improved velocity model and stack results. In this dataset, two iterations were found sufficient.

A true picture of the subsurface should be achieved from the data corrected for varying near-surface effects. After application of the residual statics, the arrangement of reflections can be clearly seen. The most important part is to catch the continuity of the reflectors in the stacked section. Accordingly, to improve the stacking quality, residual statics are enforced to the NMO corrected gathers.

2.3.17 Stacking

The stacking process is the sum of all NMO corrected gathers into one output trace. Each trace corresponds to a zero-offset trace, and the seismic trace should have been recorded by a receiver coincident with the source. It is fundamental to apply this step to enhance the signal-to-noise ratio and improve the seismic data quality.

Most of the time, after implementing the processing steps, I came up with a result called brute stack. It means a preliminary common midpoint stack, where final statics and velocity corrections have not yet been applied (Sheriff, 2005). After application of further methods, the final stack was done as seen in Figure 2.14.

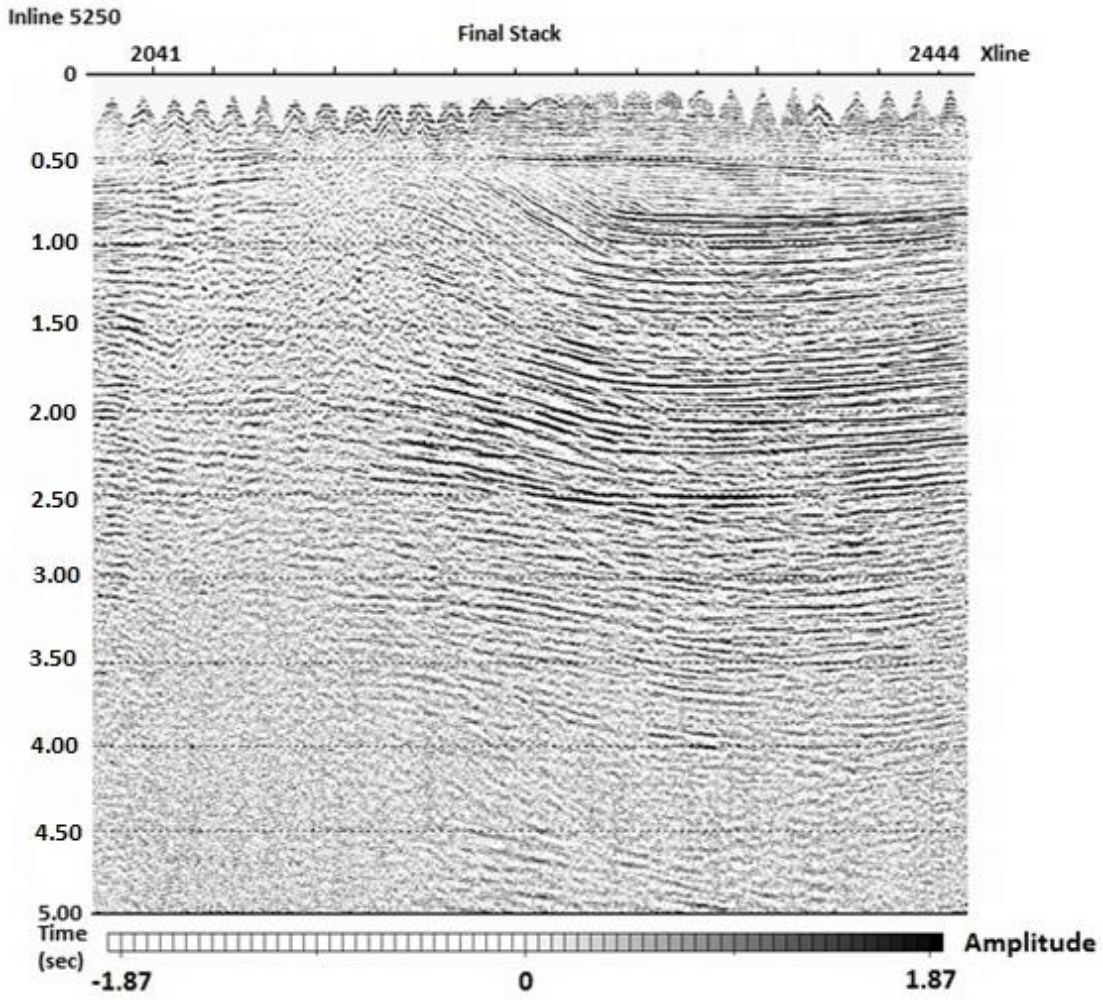

Figure 2.14: The final stack of the data after conventional processing techniques. In this image, inline number 5250 was used.

The image quality requires improvement to understand the subsurface and to enhance the data quality. So, a mute operation and AGC enhancement were

performed on the final stack. The final stack with mute is seen in Figure 2.15. The final stack by using mute and AGC is displayed in Figure 2.16.

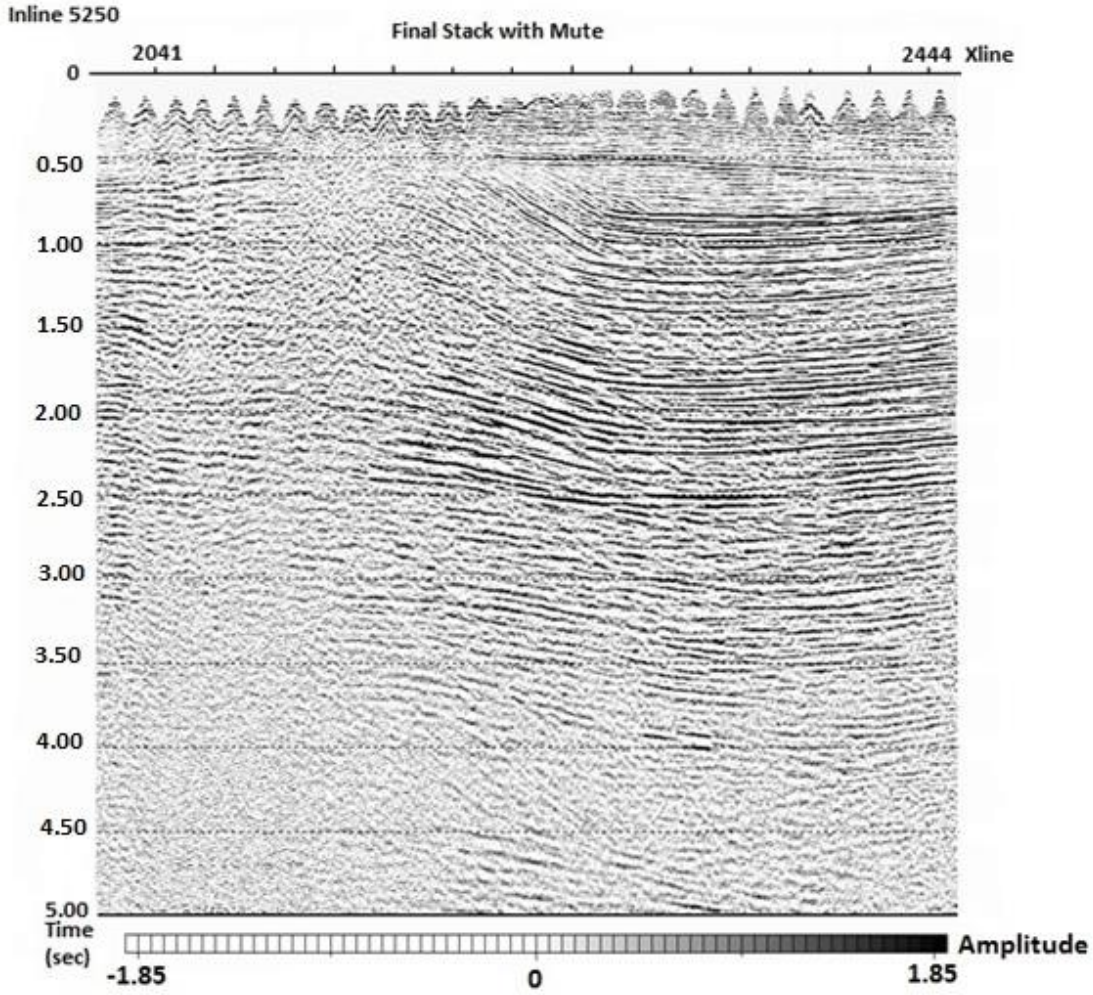

Figure 2.15: The final stack of the data with the mute operation. The inline number is 5250.

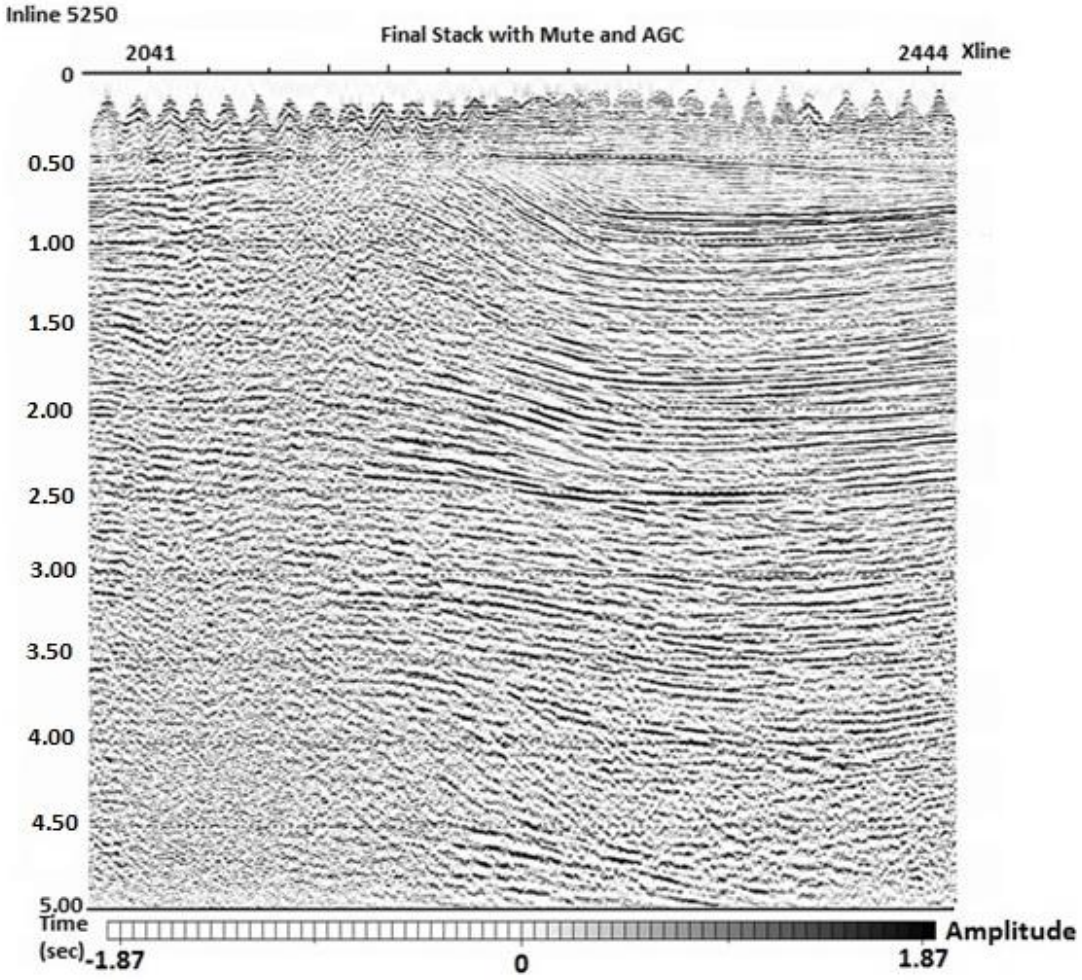

Figure 2.16: The final stack of the data with mute and AGC. The inline number is 5250.

2.4 Presentation of the Results of 3D Data

The interpretation and visualization of the 3D-data are done by using 3D-visualization tools. An example of such visualization of the stack volume is presented in the Figure 2.17.

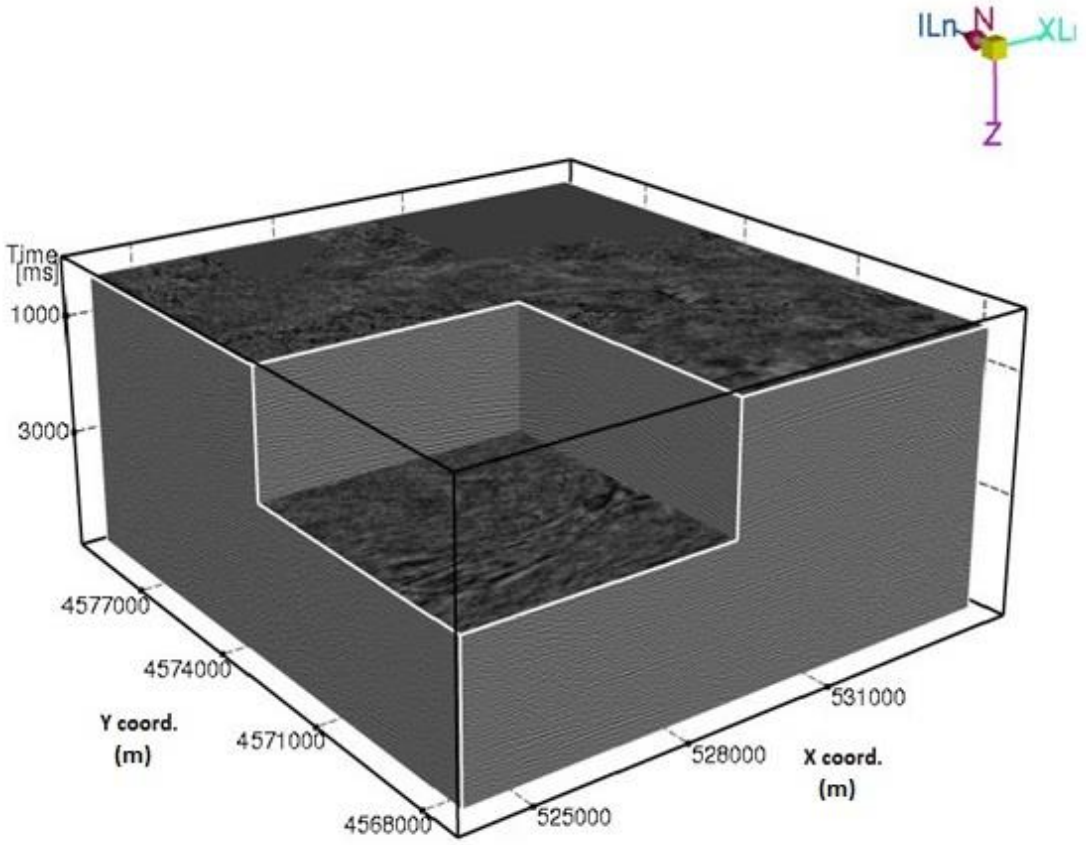

Figure 2.17: The 3D stack cube displayed in 3D visualization tools.

The pictures of 3D-data in visualization tools do not represent the detailed information. Therefore, throughout this report, I will use 2D-presentations with certain inlines and crosslines (xlines). I have chosen two inlines, 5204 and 5300 and three xlines, 2021, 2208, and 2240. Their locations are shown in Figure 2.18. I used the same inlines and xlines to present results of each imaging method.

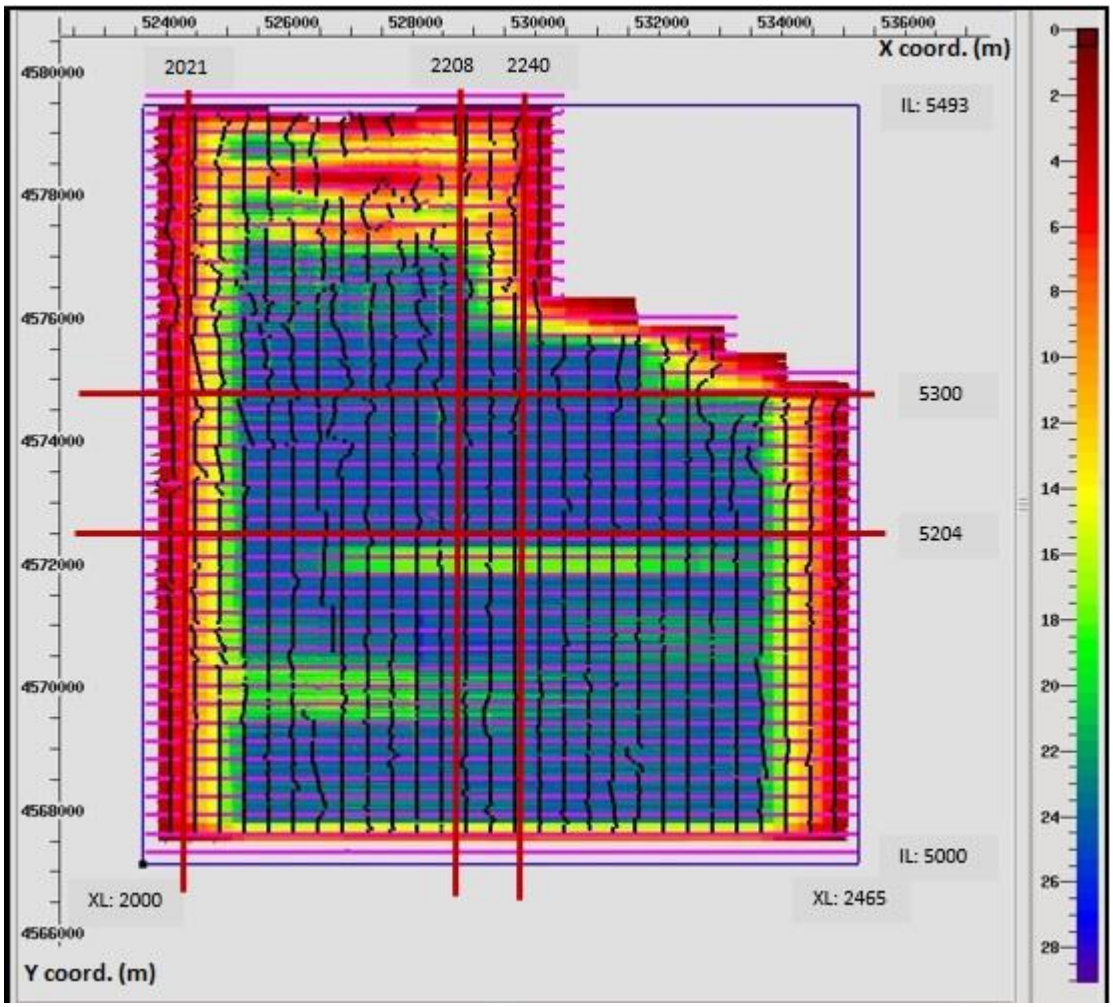

Figure 2.18: The fold map and geometry view of the 3D-data. The inline range is between 5000 to 5493, and the crossline range is between 2000 to 2465. Selected inlines and crosslines for presenting the results of each imaging methods are displayed in bold red lines. The displayed inlines are 5240 and 5300; the crosslines to be displayed are 2021, 2208, and 2240.

The final stack results for the selected inlines and xlines are presented in the following Figures 2.19 to 2.23.

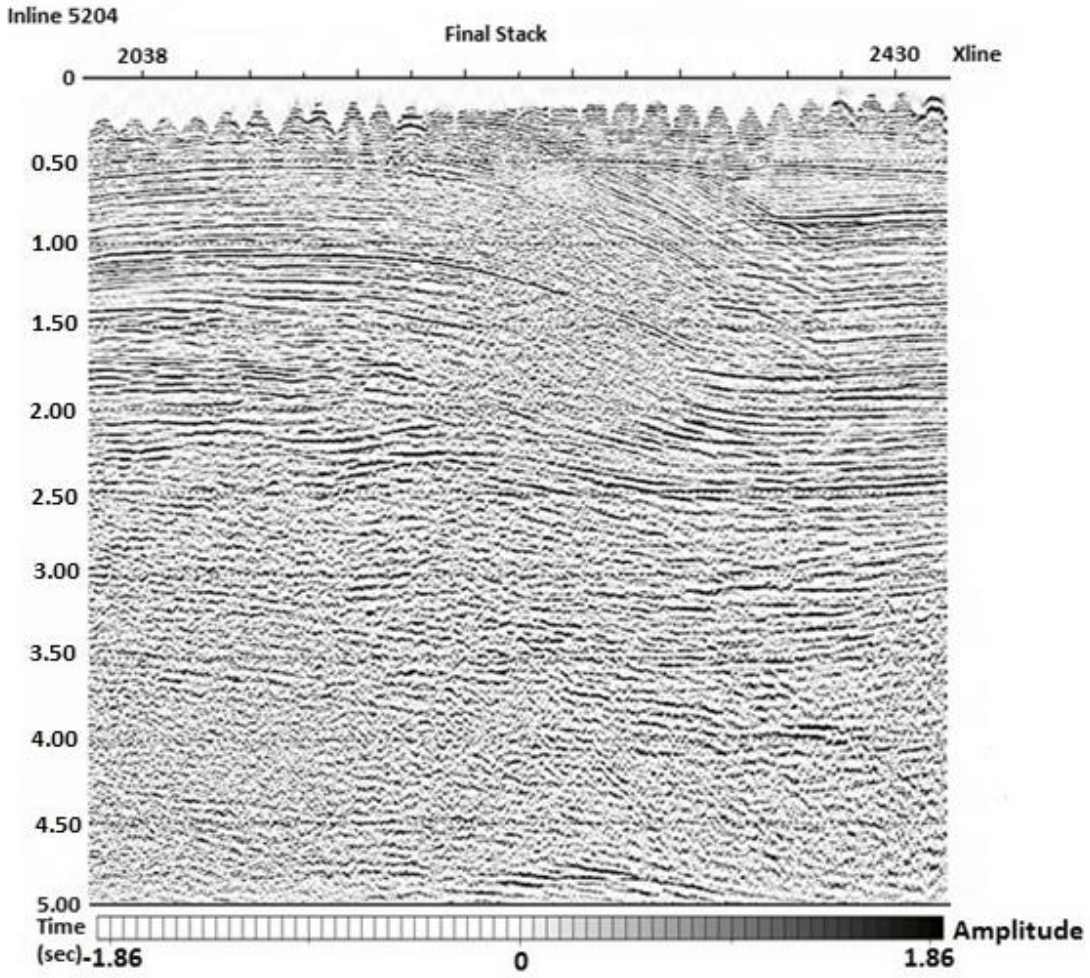

Figure 2.19: The final stack of the data, inline 5204.

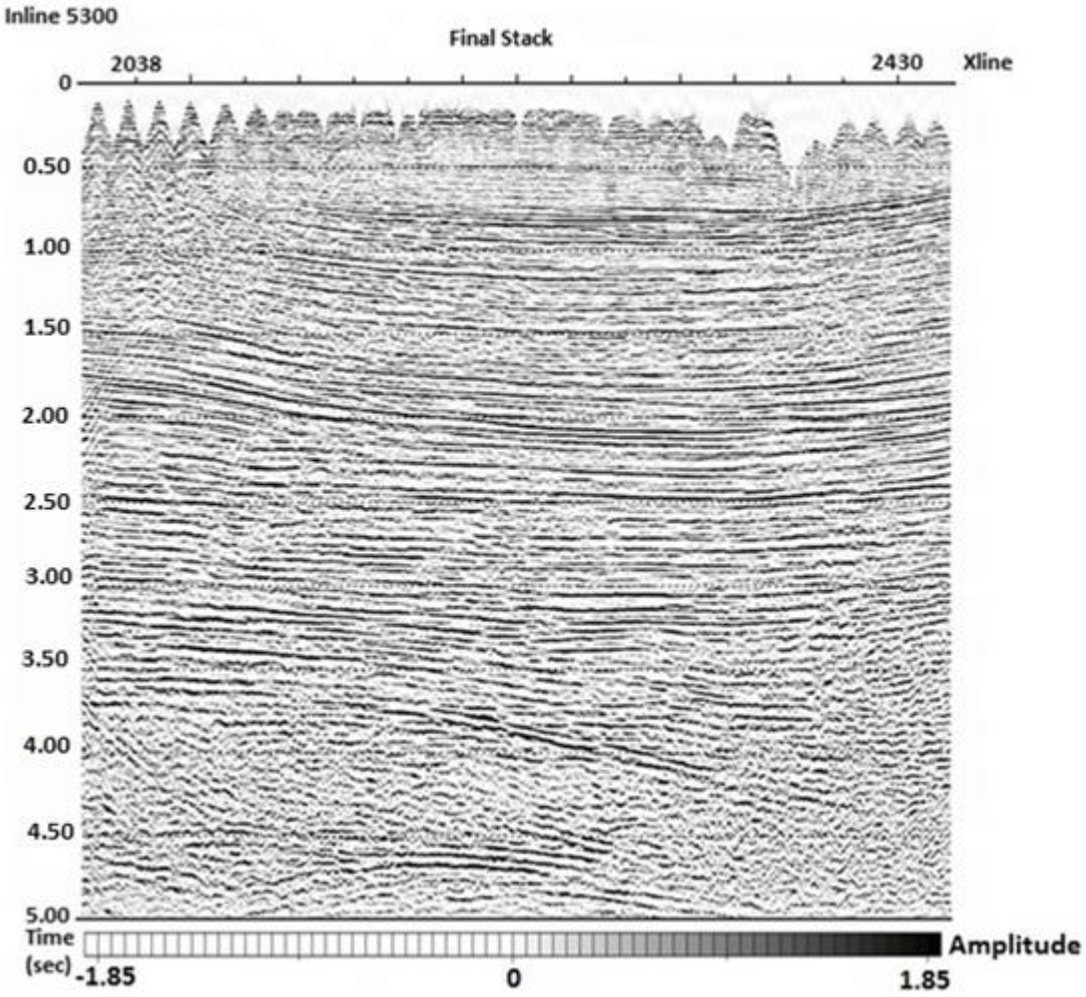

Figure 2.20: The final stack of the data, inline 5300.

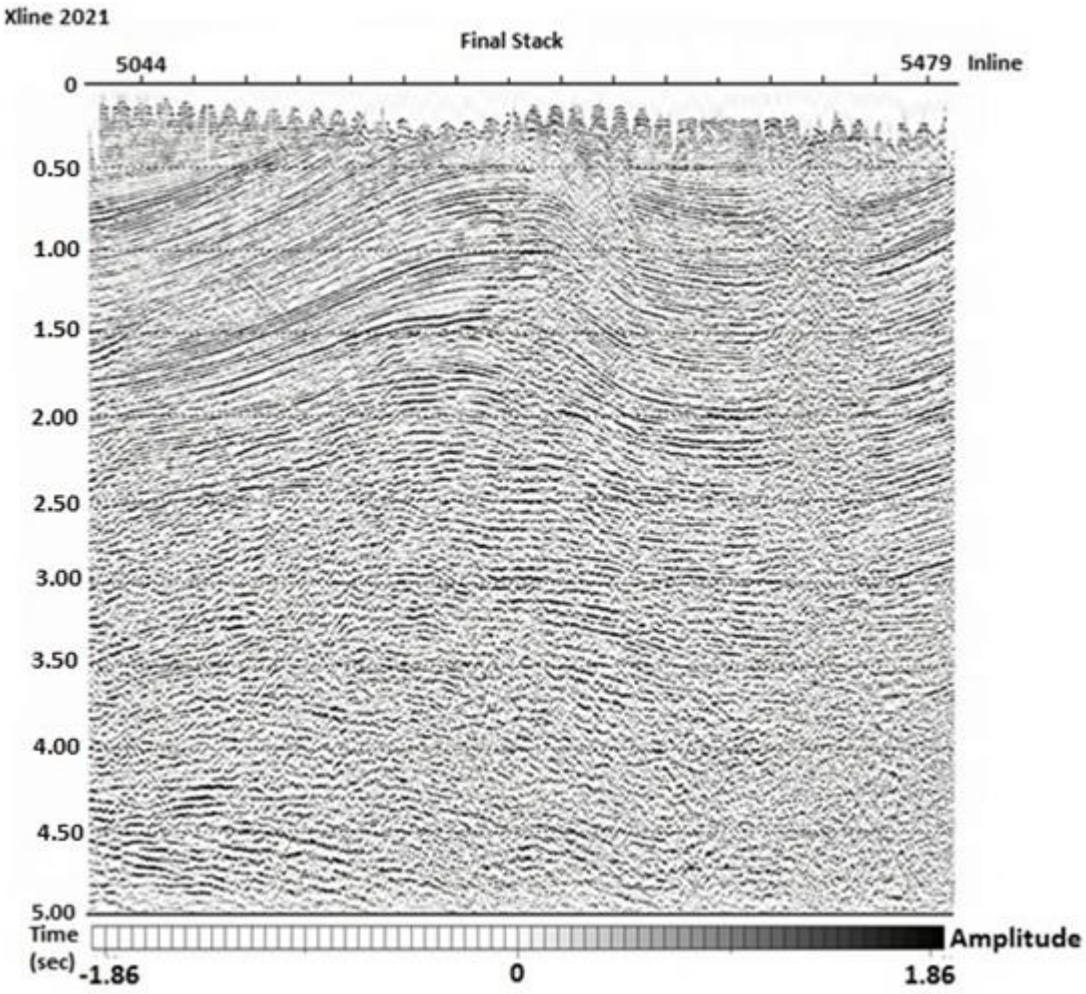

Figure 2.21: The final stack of the data xline 2021.

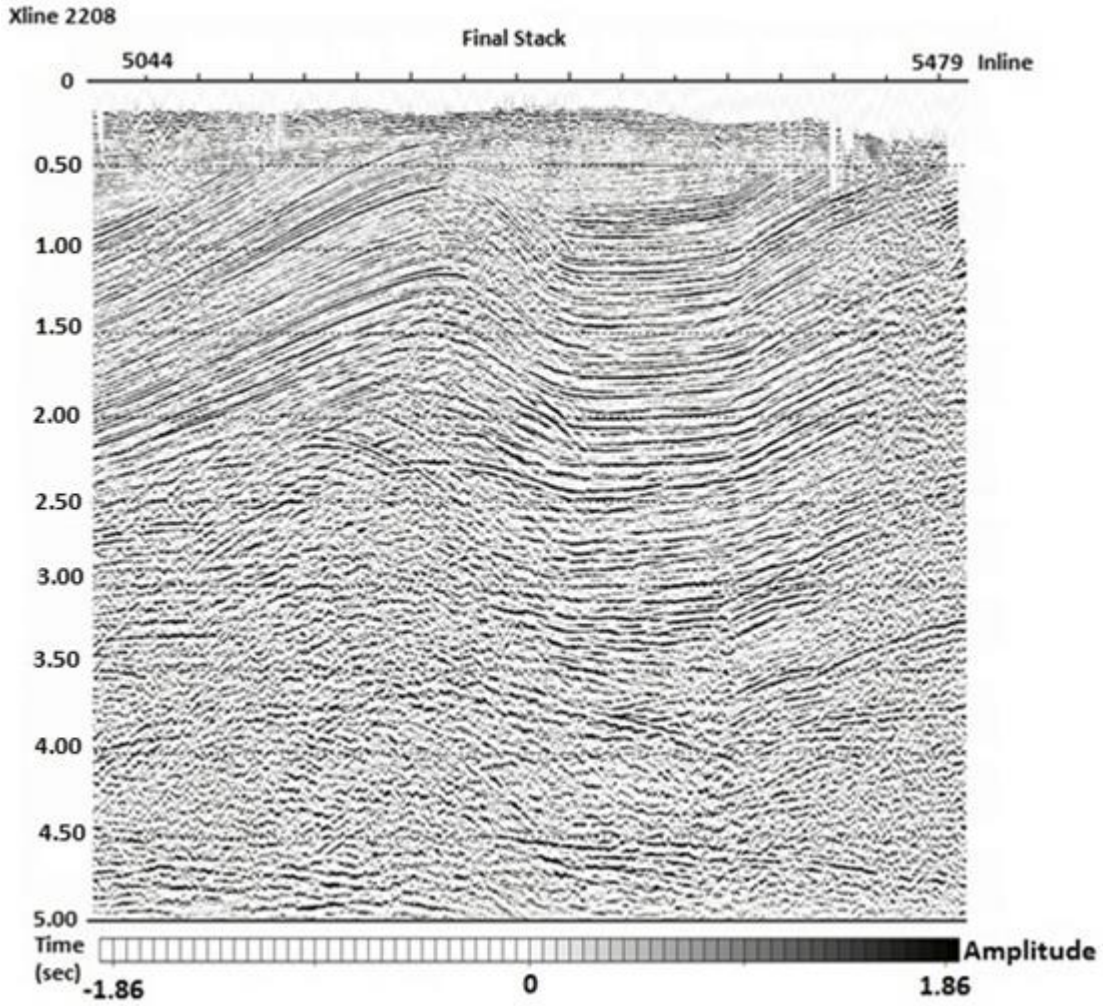

Figure 2.22: The final stack of the data, xline 2208.

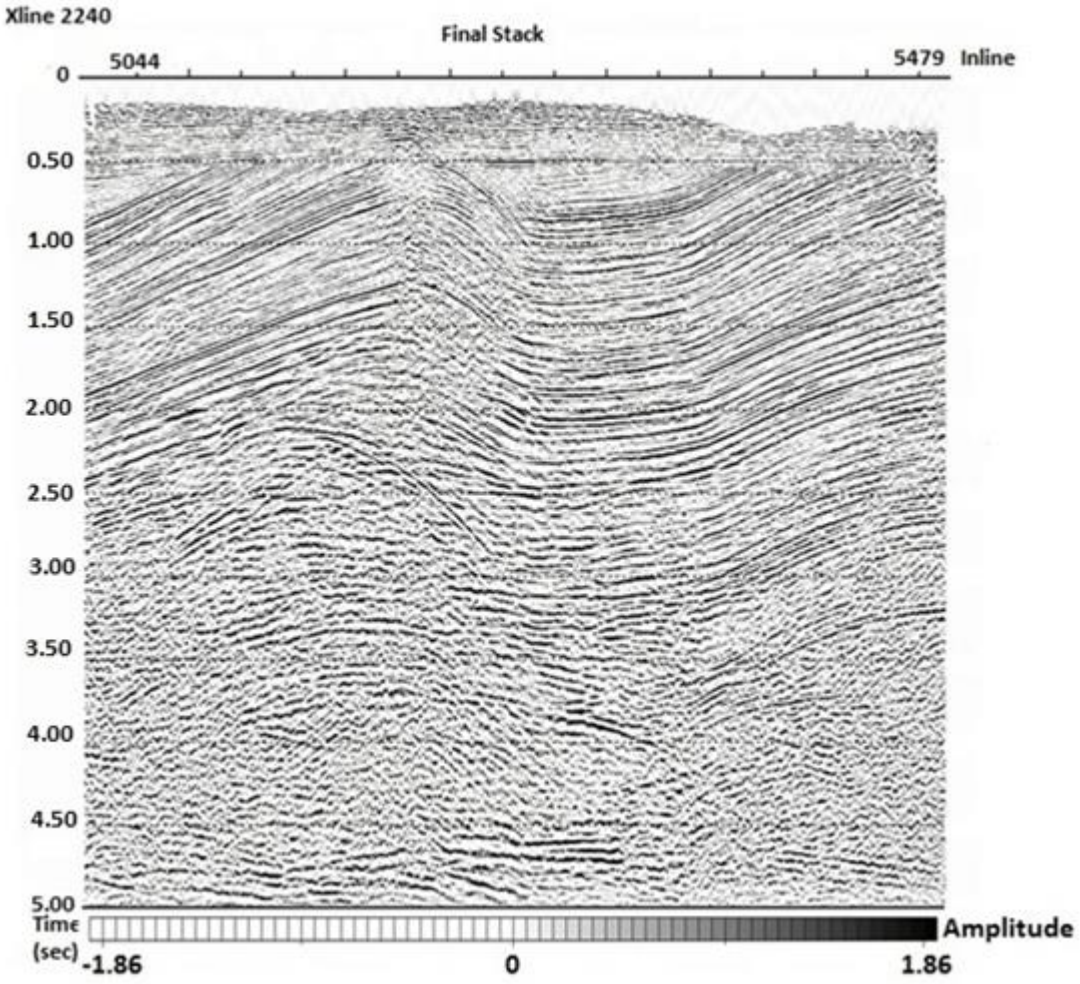

Figure 2.23: The final stack of the data, xline 2240.

Chapter 3: Post-Stack and Pre-Stack Time Migration

3.1 Introduction

The ultimate goal of recording seismic data is to restore an image of the geological features in the subsurface (Biondi, 2005). Seismic migration is a technique that is used in data processing which evacuates the distortions from reflections by changing events to their correct positions. Presently in the industry, migration is usually operated before stacking in order to give an idea about the amplitudes and structures. As a seismic imaging tool, migration is one of the earliest method and it has been used to display single-fold analog seismic records.

Migration is used in a wide variety of problems related to the imaging especially for complex structures. Associated with the subsurface problem needs, migration is used as time and depth migration, two or three dimensions, and before or after stacking operation. Migration algorithms are formed on the assumption of the wave equations (either integral or differential form of the wave equation). In order to identify the problem, the linearity of the model underlying the migration should be stated (Gray, 2001). Imaging the scatters individually makes the data easy to understand.

3.2 Kirchhoff Migration

Kirchhoff migration is described as a simple but a robust and versatile method. It is based on the integral of the wave equation. This method can be used either for pre-stack or post-stack migration. It uses the seismic record in the original space-time domain and fits both types of migrations. In my study, I have used Kirchhoff migration for both post-stack and pre-stack imaging.

Fundamentally, measurements are made only at the surface, hence integration must be narrowed to the surface of the Earth. This method is also known as diffraction summation method. There are two intuitive views of the process of this migration (Schneider, 1971). One is the gathering approach which loops over each image point in the solution model space and gathers the contributions of all the input traces that are within a migration aperture. The input zone for migration defined in the data space is seen in Figure 3.1. The output consists of stacking all input traces along the two-way travel-time curve. If the velocity is constant, the travel-time curve will be a hyperbola over the image points. In the complex velocity areas, the curve will be calculated by ray tracing.

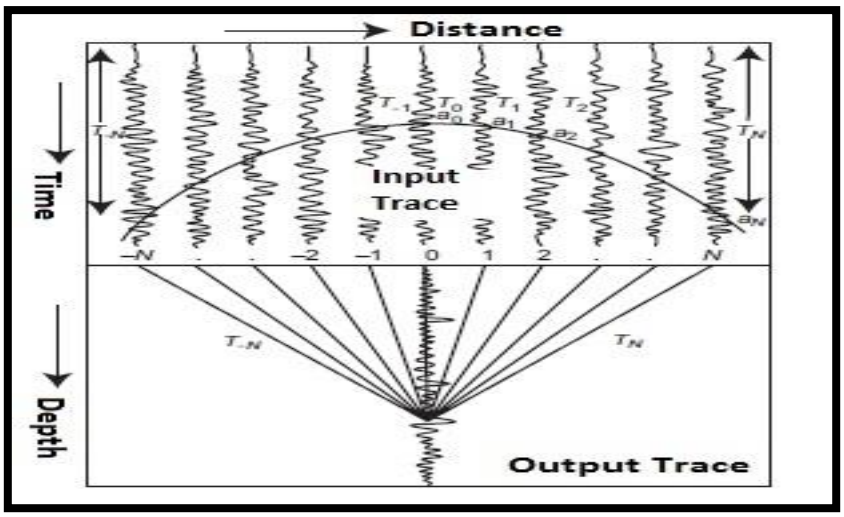

Figure 3.1: The gathering approach (after Schneider, 1971).

The other method is called the spraying approach, which loops over each input trace in data space and smears the data over all image traces within another migration aperture defined in solution model space (Zhou, 2014).

Kirchhoff migration is defined as a diffraction summation method, and it embodies three factors, which are: obliquity factor, spherical-spreading factor, and

wavelet-shaping factor (Yilmaz, 1987). The obliquity factor eliminates the backward going waves, and it is depicted as an angle dependence on the amplitudes. To implement the migration, the time derivative of the data is taken and all individual traces are multiplied by the obliquity factor, cos ø, and computed by the spherical spreading factor ($1/r^2$) which is defined as the amplitude decay of the wave front energy and summed along the diffraction curves. The wavelet shaping correction reconstructs amplitude and phase distortions that arise while the wave front is propagating.

3.2.1 Kirchhoff Post-Stack Time Migration

The main aim of post-stack migration is achieved by using the seismic data reflectivity series that are created in either (x, z) space or (x, y, z) space. Kirchhoff time migration collects the energy from the input traces within specified migration aperture (Bancroft, 1996). The arrival times for each input trace are calculated using the equation (3.1) which is identical to that used in a normal move-out (NMO) removal.

$$T^2 = T_0^2 + \frac{4x^2}{V^2} \tag{3.1}$$

Where, T_0 is the time of migrated sample, T is the time of an input trace, x is the distance from output to input, and V is the migration velocity. A 3D-volume of stack data, T is shaped like a hyperbola.

I have employed a 3D-Kirchhoff post-stack time migration to see the final migrated section. The post-stack Kirchhoff time migration was done for the inline range 5000 – 5493, and xline range 2000 – 2465. Migration half aperture was 6000 m.

The velocity used for post-stack time migration was RMS velocity, and I have created my velocity as volume instead of a vertical function. The result of post-stack

time migration can be seen in Figures 3.2 to 3.6. Comparing the result with the stack in an earlier chapter, the signal-to-noise ratio and the data is enhanced.

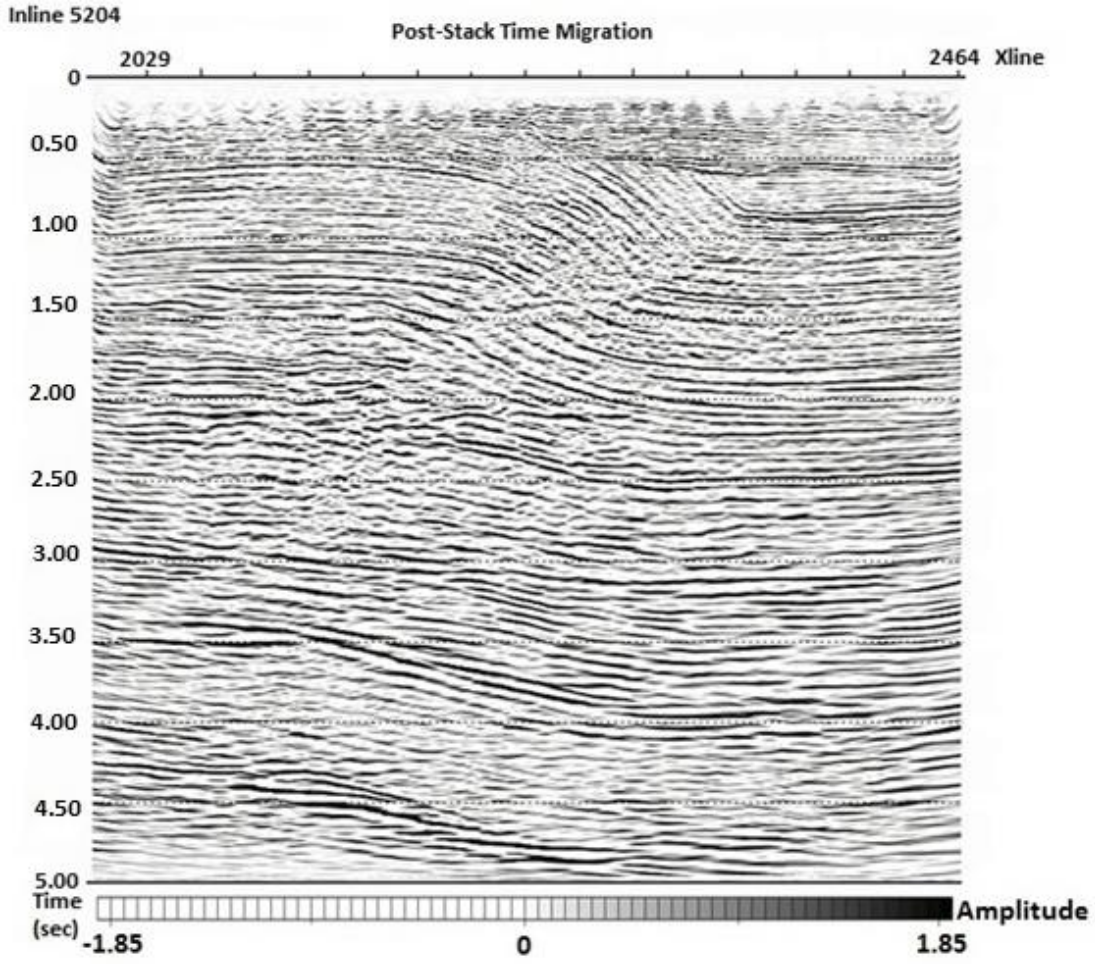

Figure 3.2: The Kirchhoff post-stack time migration result of inline 5204.

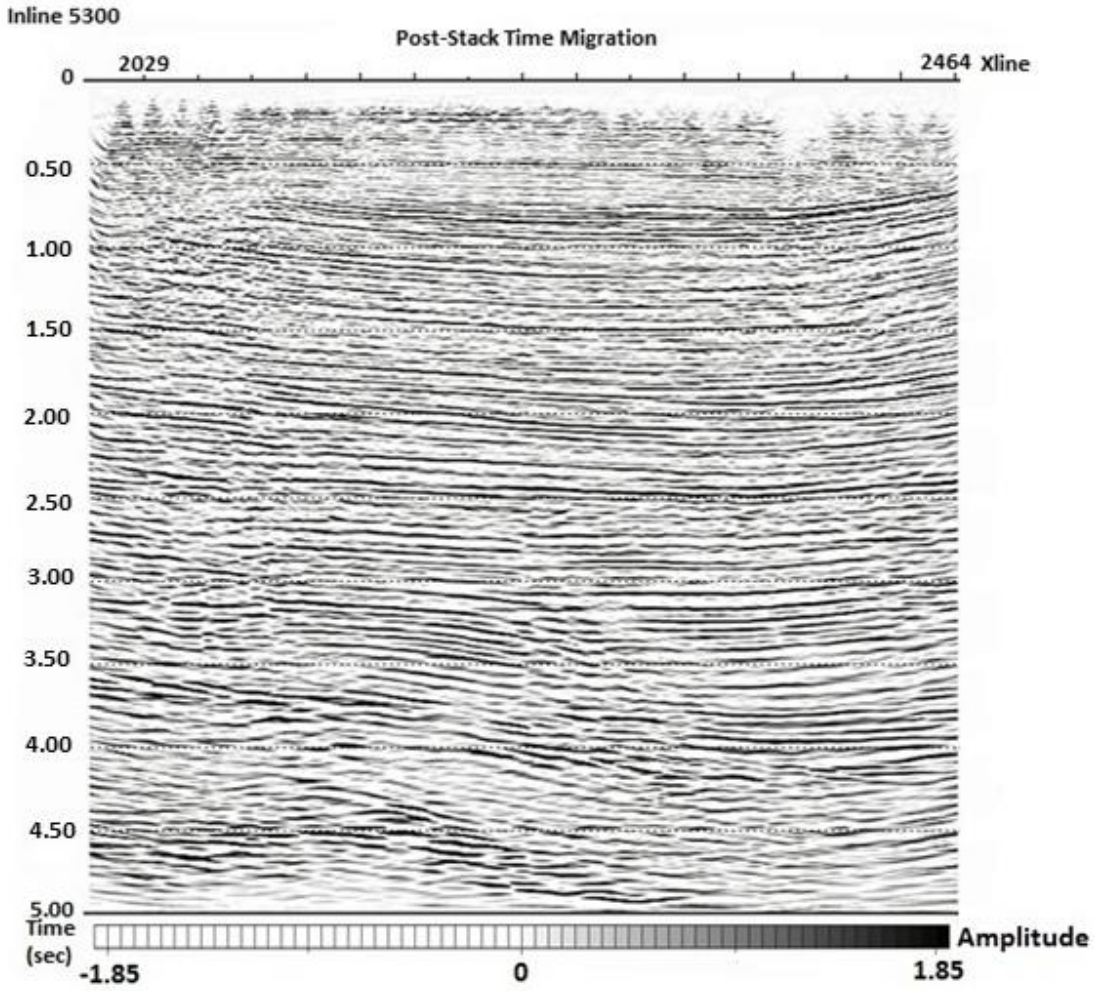

Figure 3.3: The Kirchhoff post-stack time migration result of inline 5300.

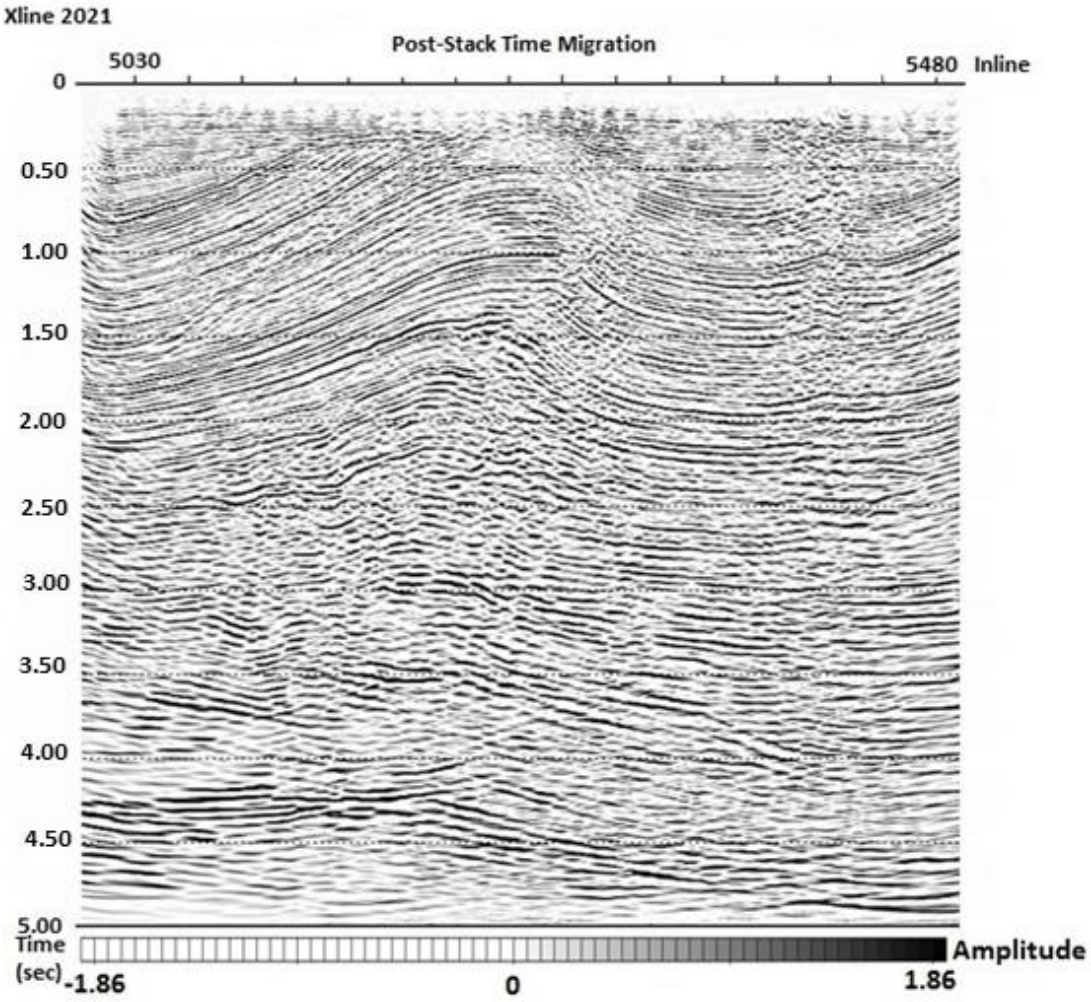

Figure 3.4: The Kirchhoff post-stack time migration result of xline 2021.

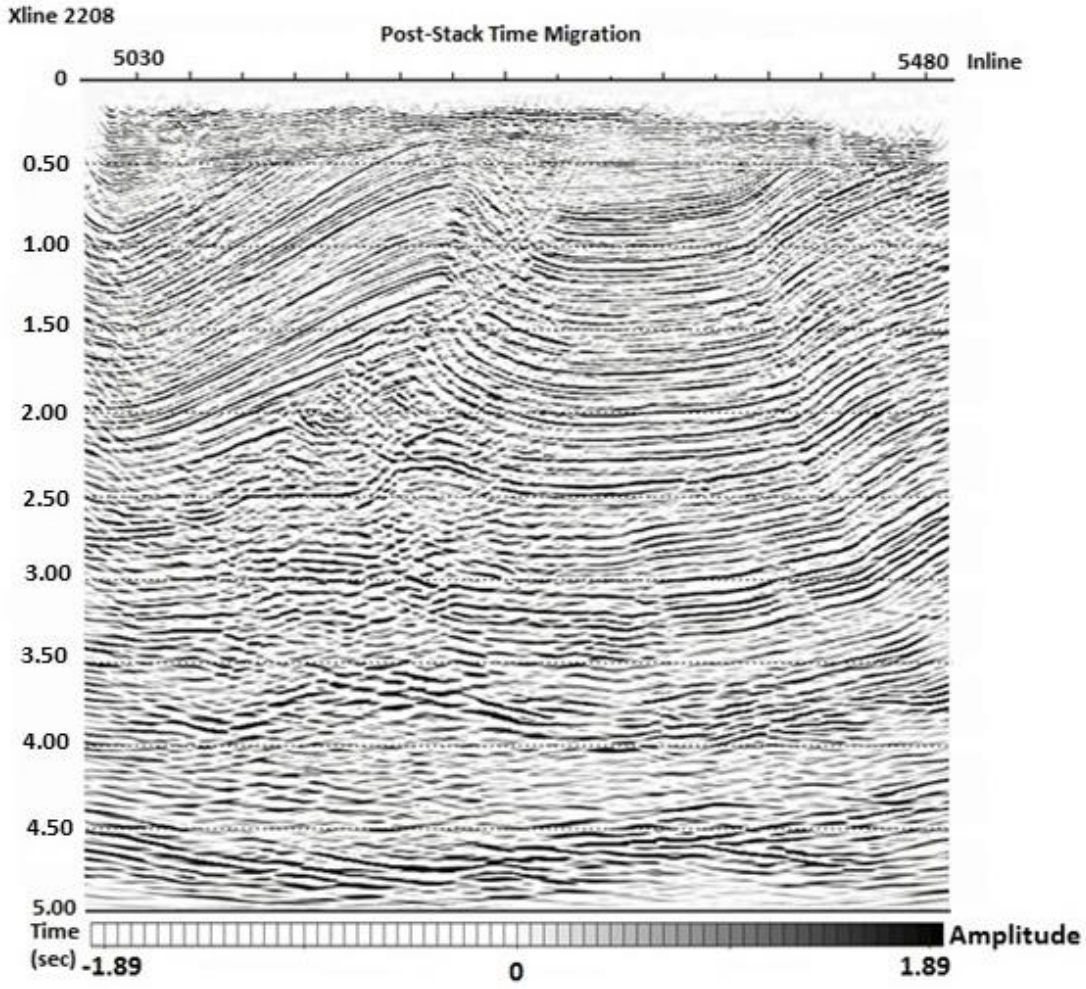

Figure 3.5: The Kirchhoff post-stack time migration result of xline 2208.

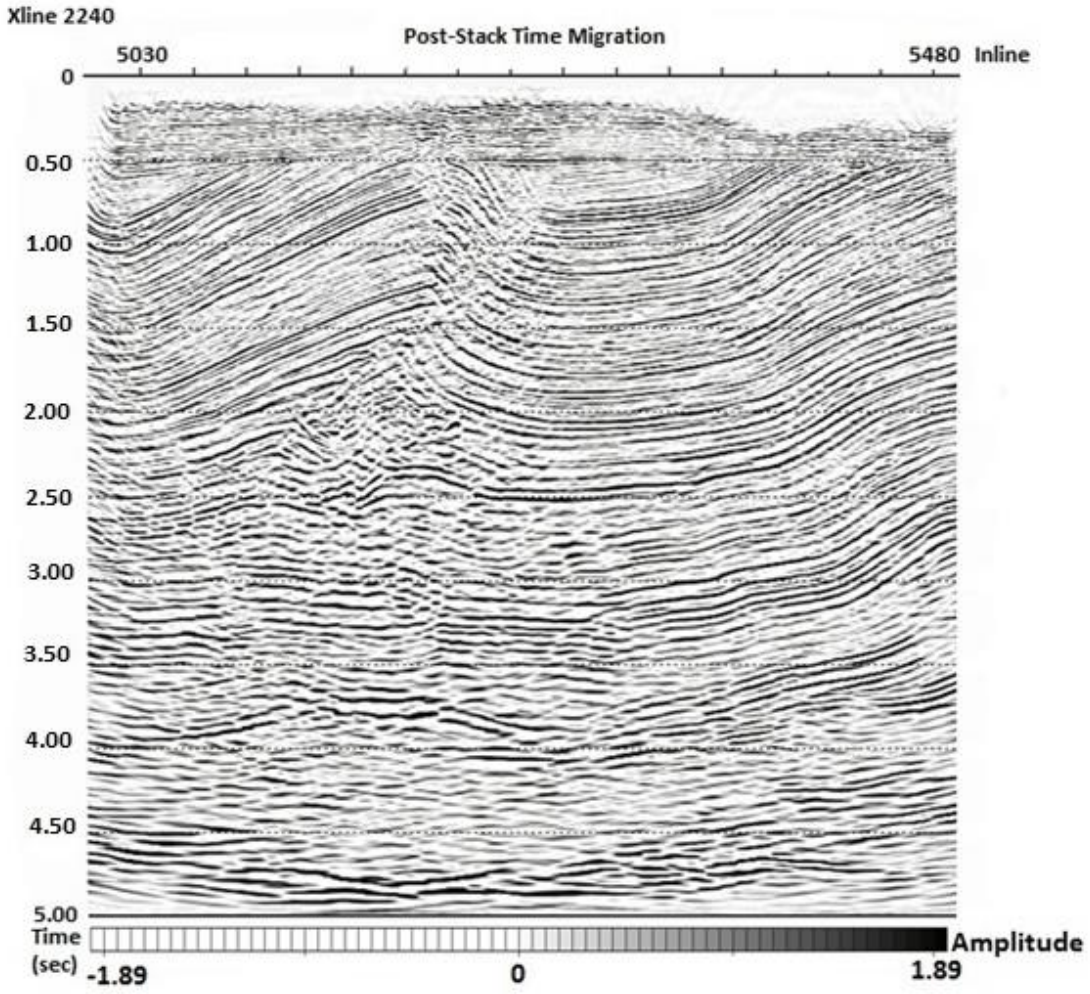

Figure 3.6: The Kirchhoff post-stack time migration result of xline 2240.

3.2.2 Kirchhoff Pre-Stack Time Migration

Kirchhoff pre-stack time migration is performed due to its efficiency and target-orientation for imaging. It can be employed for the lateral and depth velocity changes and it usually comes up with a reliable image by using a correct migration velocity model. In my study, the usual application of this method was demanding since the computation time and cost are challenging due to the large volume of a 3D-data input.

PSTM method is applied to CMP gathers before stacking with no NMO correction. The exploding reflector method is no longer accurate; therefore, a one-way travel-time approximation was used (Bancroft, 2002). 3D-Kirchhoff pre-stack time migration produced an image at the desired location in a 3D-space. Energy (from a trace to a shot and receiver) needs to be scattered to all locations of scatter-points conforming to the travel-time (Dai, 2004). Afterward, the energy is summed to a location by applying a weighting operation for ray-paths.

In my study, PSTM is applied to assess the functional changes and advancement that originated from different migration approaches. The pre-stack velocity analysis is undertaken by the tool named 'Velocity Navigator'. The function of this program is to present all information related to the velocity models (velocities along horizons, velocities like vertical function or velocity volumes). In consideration of velocity analysis after each migration application, the velocity has been reconstructed. In this step, a new residual move-out volume has been performed by using the pre-stack gathers. These volumes have been implemented by picking from semblance profile as shown in Figure 3.7. Picking the highest coherency in the semblance profile identifies the inlines and crosslines. For both inlines and crosslines a step-wise approach was done. The step value was 50.

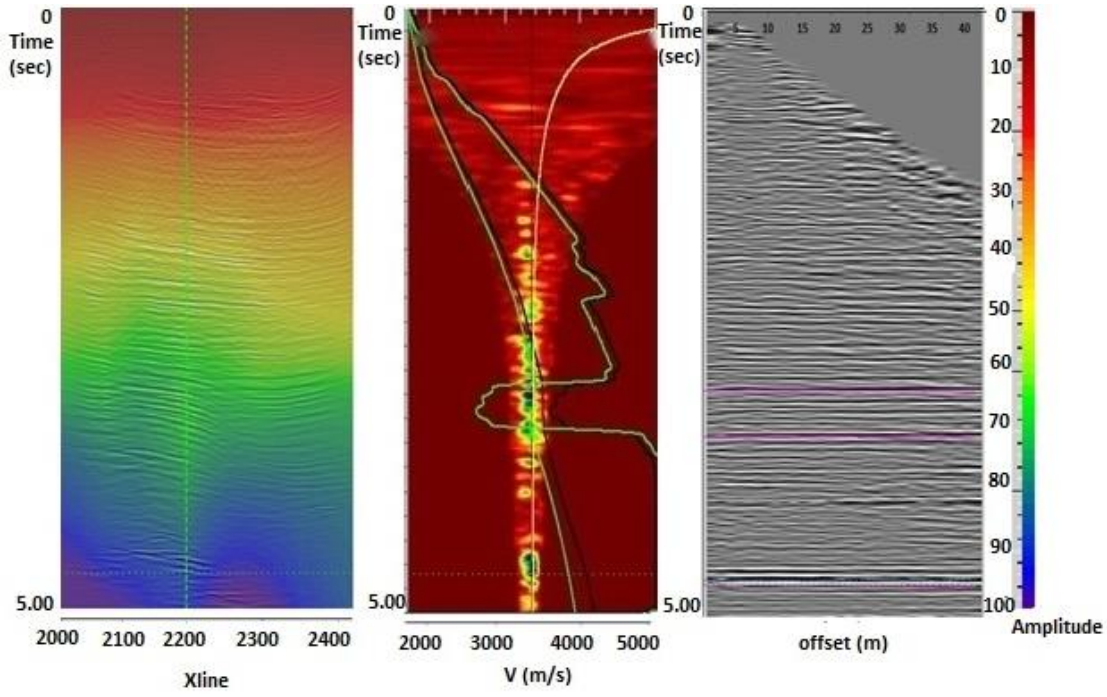

Figure 3.7: RMS velocity volume refinement. Left image is the migrated stack section with including the velocity variation for inline 5200. The middle image is the velocity error (residual move-out) picking semblance profile. The right image is the common-image-gather of xline 2220. Once the picking is accurate, gathers tend to be flat.

The residual picks are selected to create the residual move-out volume. The program calculates and displays the semblance plot of the time difference of the residual move-out calculated at a reference offset. The time residuals are evaluated from move-outs that remain on a reflection event of migrated gathers. Employing the velocity field correction with the measured data have flattened the move-out on the reflection event and formed a corrected time-migrated image.

The main goal of applying velocity model updating was to refine and establish the final model for RMS velocity which can be seen in Figure 3.8. Velocities are ranging from 1750 m/s to 4700 m/s. Later, RMS velocities are converted into interval velocity to

be used by depth migration. The final migrated stack of the section with the updated RMS velocity is seen in Figure 3.9 to 3.13.

In a way, time migration is equivalent to the depth migration if the medium is horizontally layered. If the lateral velocity variations are common in the structure, a depth migration needs to be performed. However, finding the best velocity for the depth migration is not easy. In this study, pre-stack time migration has been performed twice. In every resulting migration process, the velocity volume has been updated to obtain a result.

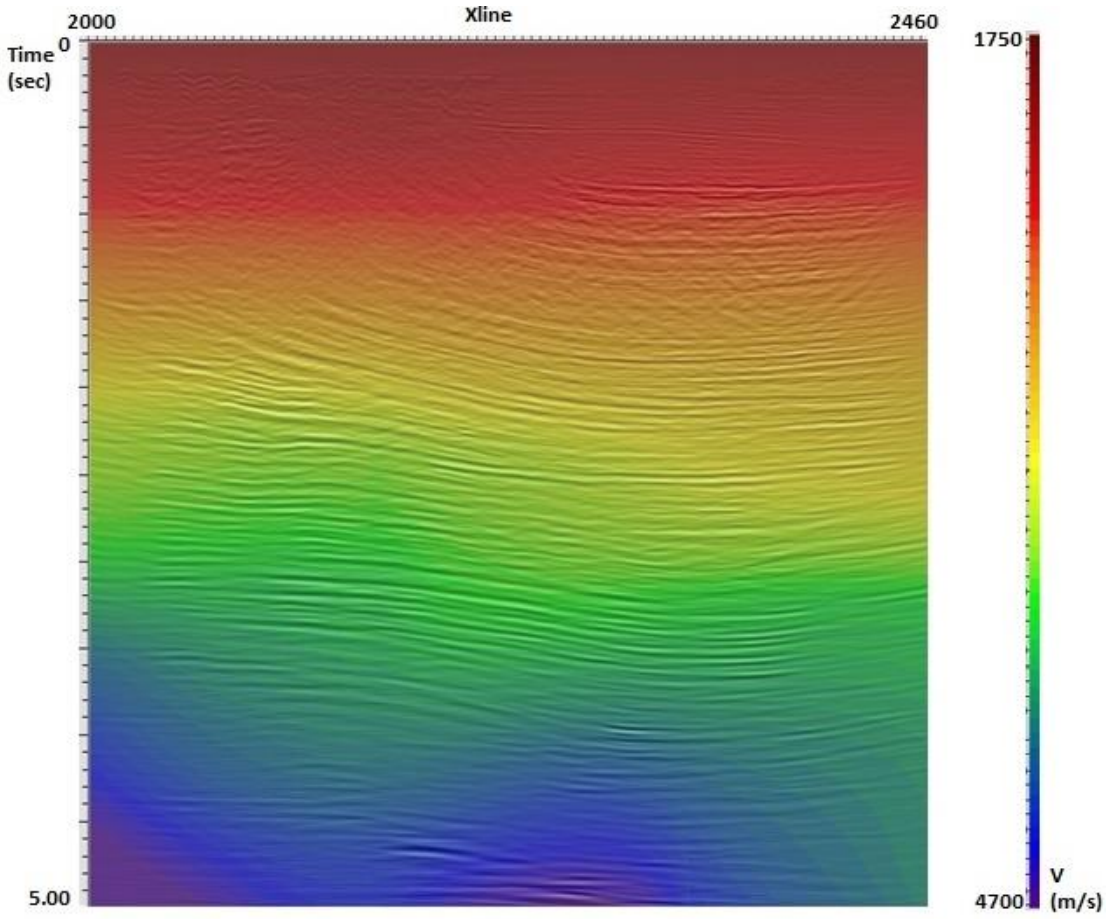

Figure 3.8: Pre-stack time final RMS velocity field. Velocities range from 1750 m/s to 4700 m/s. The inline number is 5250. The horizontal axis is the crossline values.

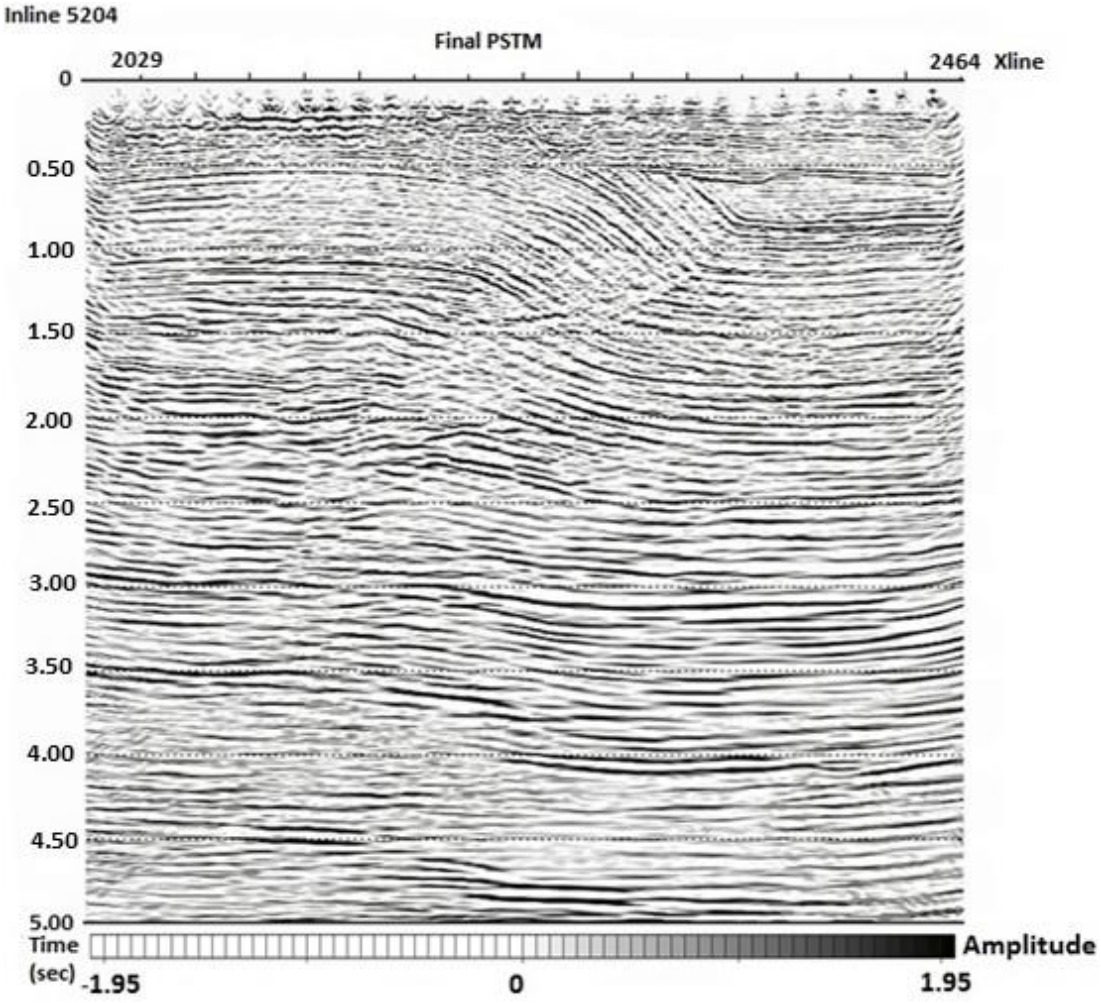

Figure 3.9: The final Kirchhoff pre-stack time migration result of inline 5204.

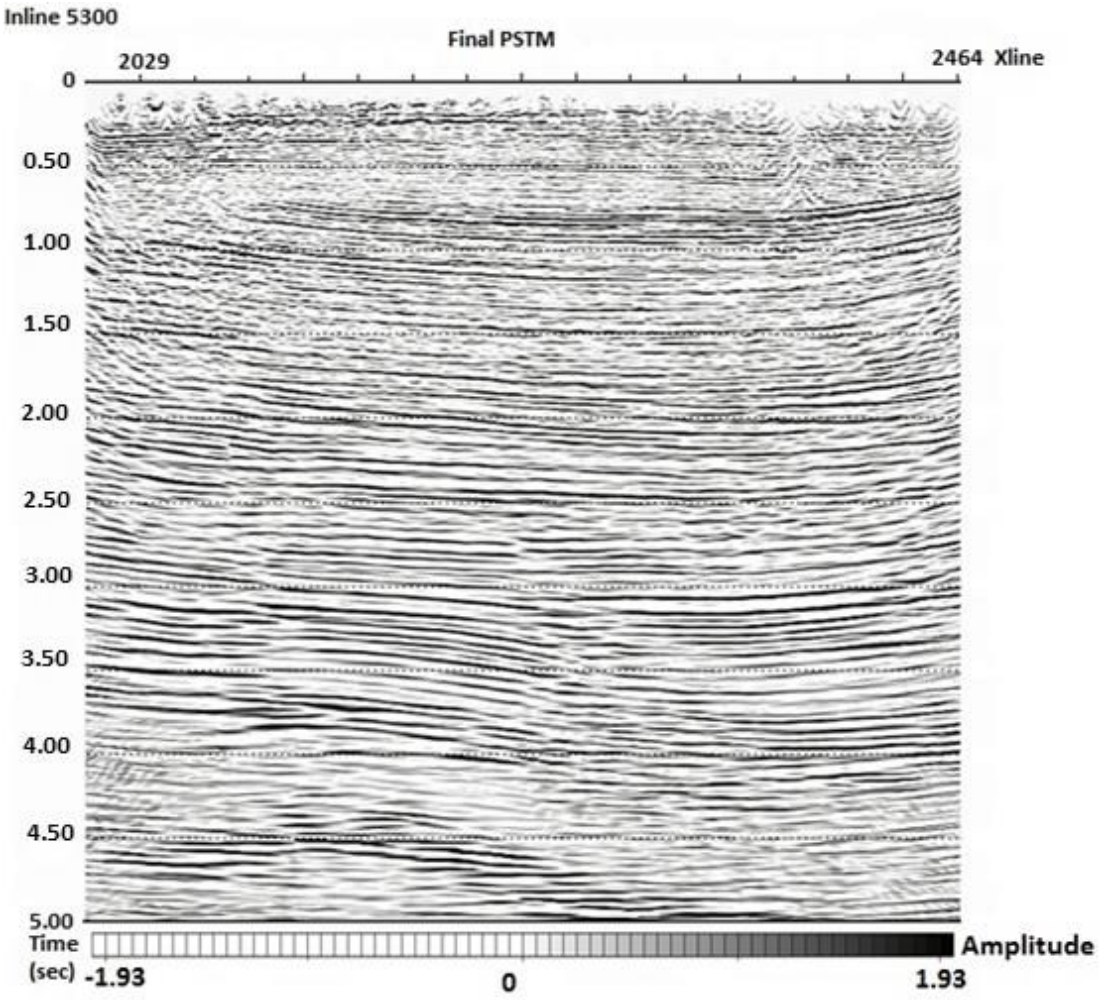

Figure 3.10: The final Kirchhoff pre-stack time migration result of inline 5300.

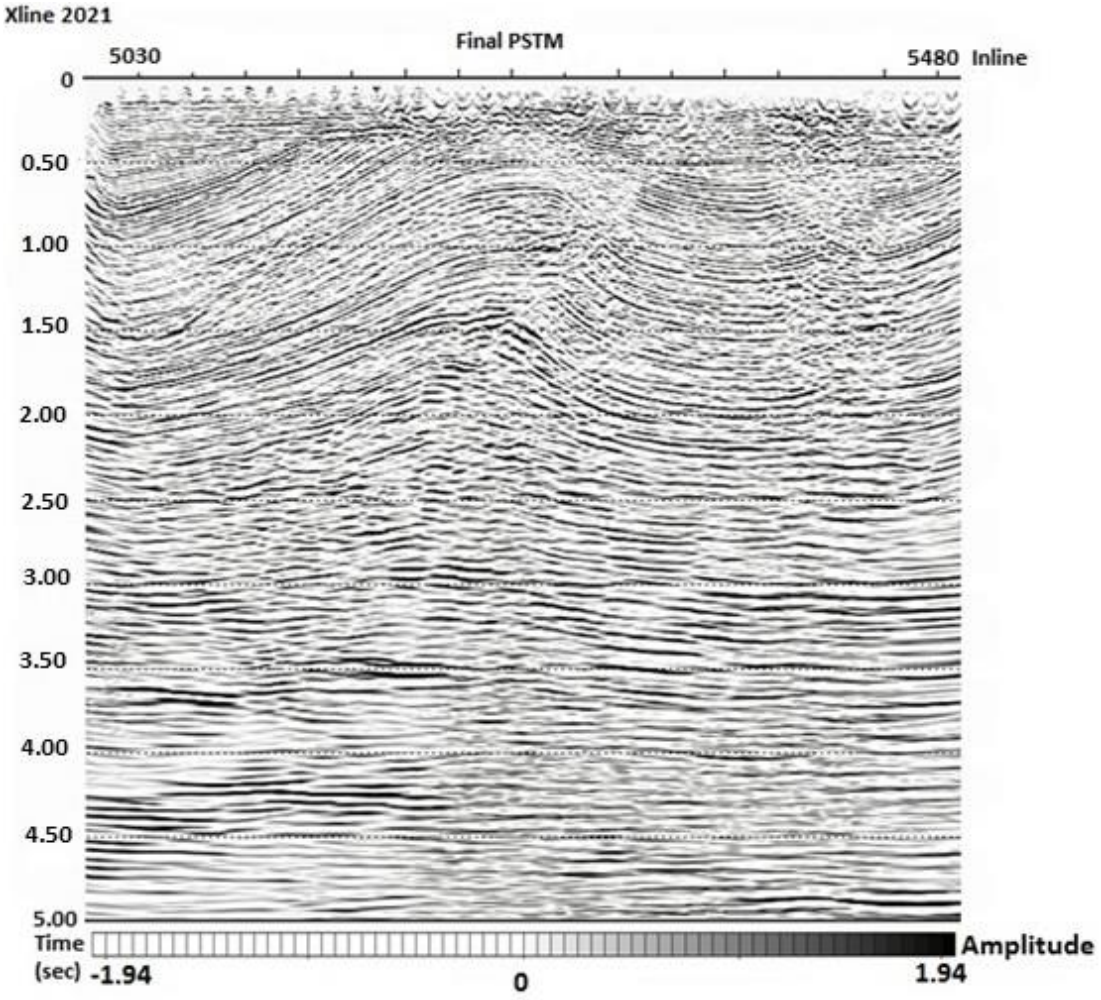

Figure 3.11: The final Kirchhoff pre-stack time migration result of xline 2021.

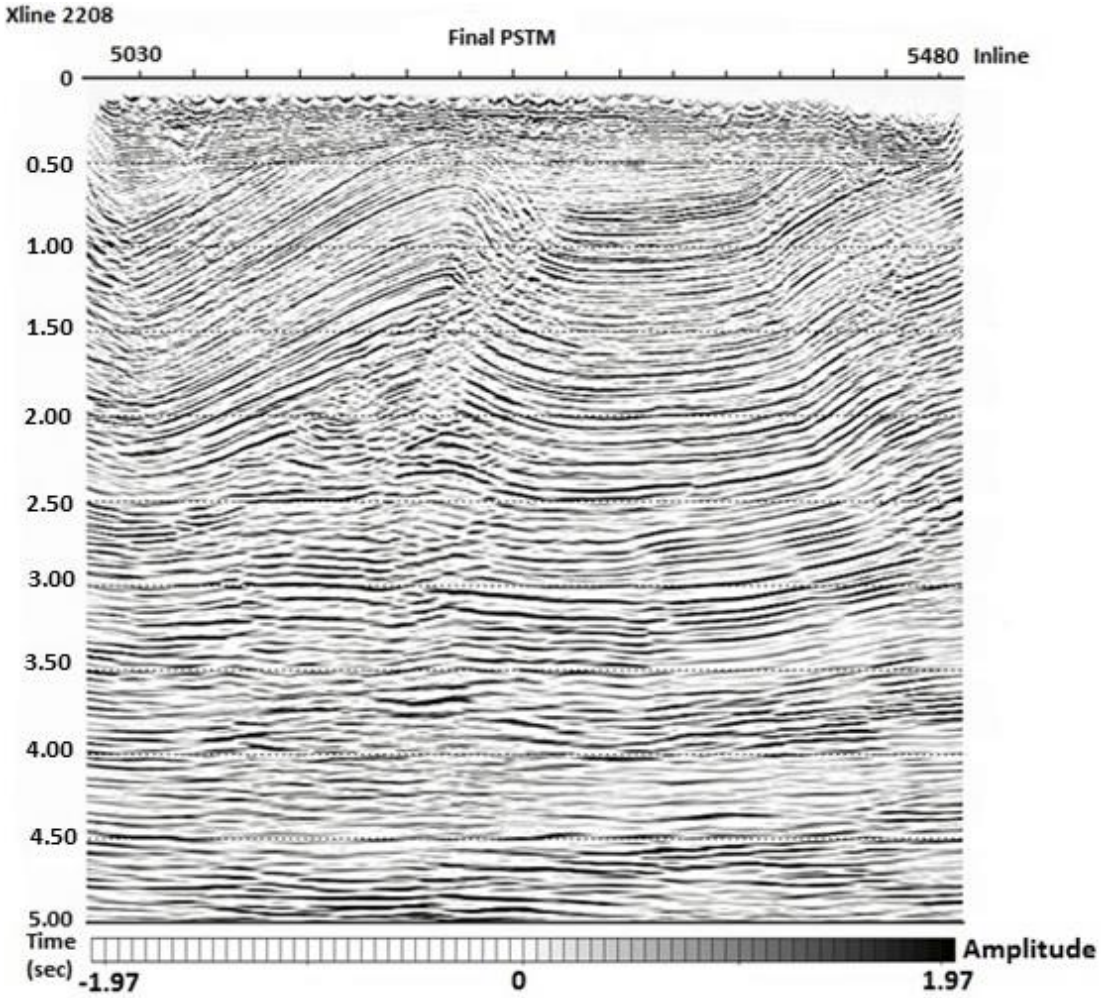

Figure 3.12: The final Kirchhoff pre-stack time migration result of xline 2208.

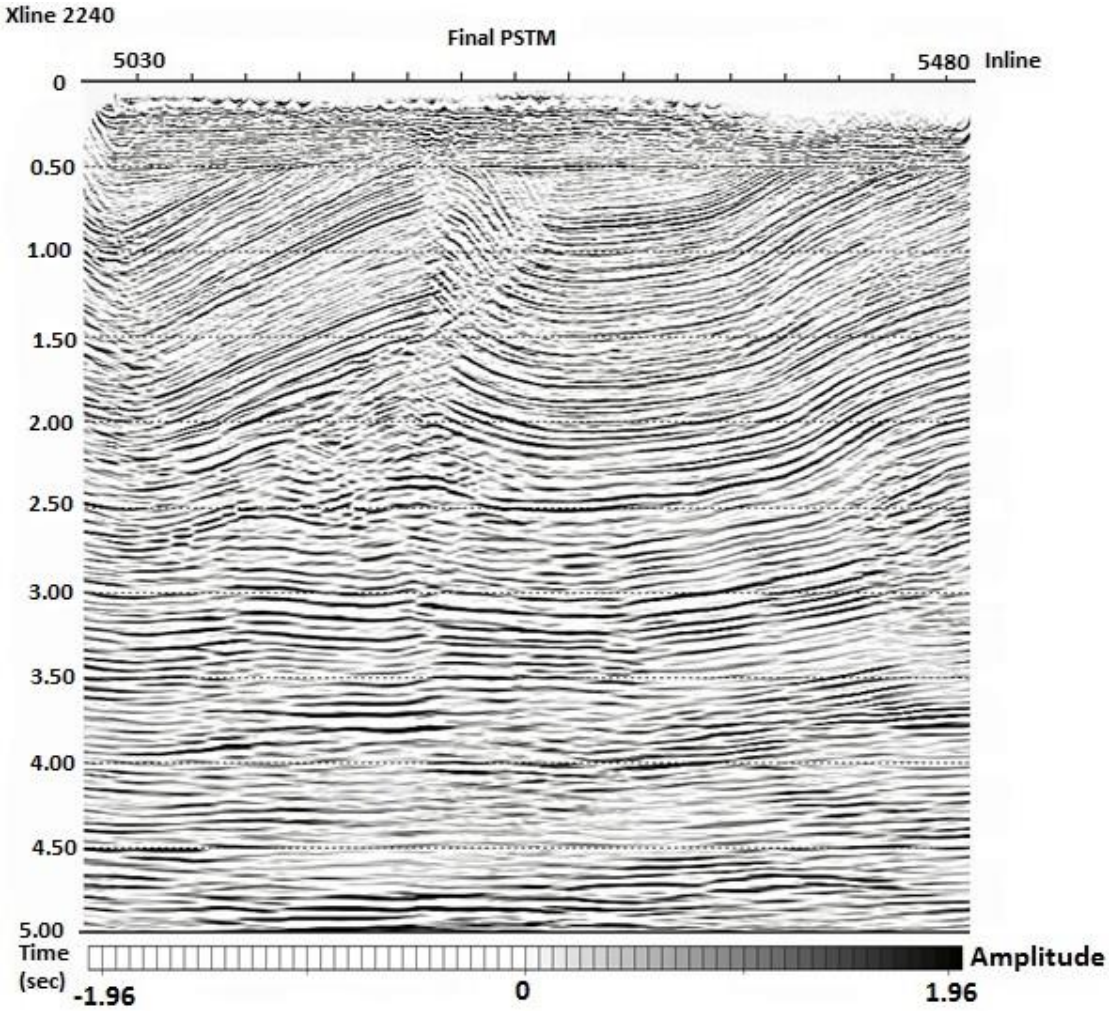

Figure 3.13: The final Kirchhoff pre-stack time migration result of xline 2240.

Chapter 4: Pre-Stack Depth Migration (PSDM)

4.1 Kirchhoff Pre-Stack Depth Migration

Time migrations are done using the effective velocity (RMS) models, and when the lateral velocity changes are taken into account, time migrations usually do not give a properly migrated section. To yield an accurate image of the subsurface, depth migration should be performed. Depth migrations require the interval velocity model of the subsurface. In my study, I have employed Kirchhoff pre-stack depth migration to receive a better and more detailed image of the subsurface. If the velocity model is defined perfectly, the distortions in the subsurface may be removed to achieve a good result.

Although the migration process requires the correct velocity model, the migration may be used as a tool to find the correct velocity models of the subsurface. The Kirchhoff depth migration, which uses ray-tracing through the given interval velocity model, will produce common-image-gathers (CIG) which can be examined later for their flatness of the events. The correct interval velocity model will produce CIGs at every surface location and at every depth. All events (reflections) need to be perfectly aligned (flat). Therefore, the "error" in alignments in CIGs (over or under-corrections) are measured. Updating the interval velocity model by minimizing the errors produces a correct interval velocity model and a correct image of the subsurface. This minimization process is called tomography. The workflow consists of iterations between the Kirchhoff depth migration and tomography is named the "Velocity Model Building".

The estimation of interval velocities is proposed by Dix (1955). The interval velocity that has been used in depth migration algorithm is produced by Paradigm's "Constrained Velocity Inversion" instead of applying the regular Dix equation (Koren and Ravve, 2005). The input was the RMS velocity volume used in the final pre-stack time migration, and the output was the conversion of this velocity volume, into the interval velocity volume.

The interval velocity cube that is produced by Constrained Velocity Inversion (CVI) is used for the first pass of the pre-stack depth migration. The resulting CIGs are used in tomography in order refine the interval velocity model.

4.2 Tomographic Velocity Update

To refine the velocity, tomography of depth migrated gathers is a method that is widely used. An incorrect velocity will result in a poor image. The degree of non-flatness of the common reflection point migrated gathers is a measurement of error in the model. The non-flatness of the migrated gathers are picked with a residual depth move-out at a specific reference offset. Generally speaking, tomography uses the measurement of non-flatness as an input and computes an alternative model with minimal errors. Tomography is a global solution for the velocity model. Tomography produces an error in time at one location and an error in velocity and depth at another location. In other words, the depth and velocity values in the velocity model will be updated, so that the zero-offset arrival times of the reflections in the data will remain unchanged.

In this study, 3D-grid tomography has been implemented. According to the workflow of this process, first of all, with the given parameters a matrix should be built.

Secondly, once the matrix is built, it is used to create an updated velocity volume for depth migration. For every iteration, an updated model is created and hence, travel-time calculations have to be performed each time.

During each iteration, the resolution is refined and newer updates are added and reviewed in sequence. When assessing each iteration a consistent improvement should be seen. The objective of a velocity update is to flatten the gathers, but this requires effort and more details are needed. In my tomography workflow, refining the final interval velocity model required two iterations. Hence, three pre-stack migrations and two tomography implementation were performed.

To implement the 3D-grid tomography, several pre-processing steps were done. The stack result of pre-stack depth migration, 'Auto Image Picking' tool was used. This is an automatic picking program for the interlayer horizons which implements the automatic picking of seeds and for the propagation of surfaces. From a 3D-migrated depth image, a distillation of main reflectors in the subsurface is performed. This method was useful since it saved time to employ the 3D-tomography workflow and accordingly it produced tomography-interlayer horizons as either grids or picks. A view of interlayer horizons as an output of the Auto Image Picking program is seen in Figure 4.1.

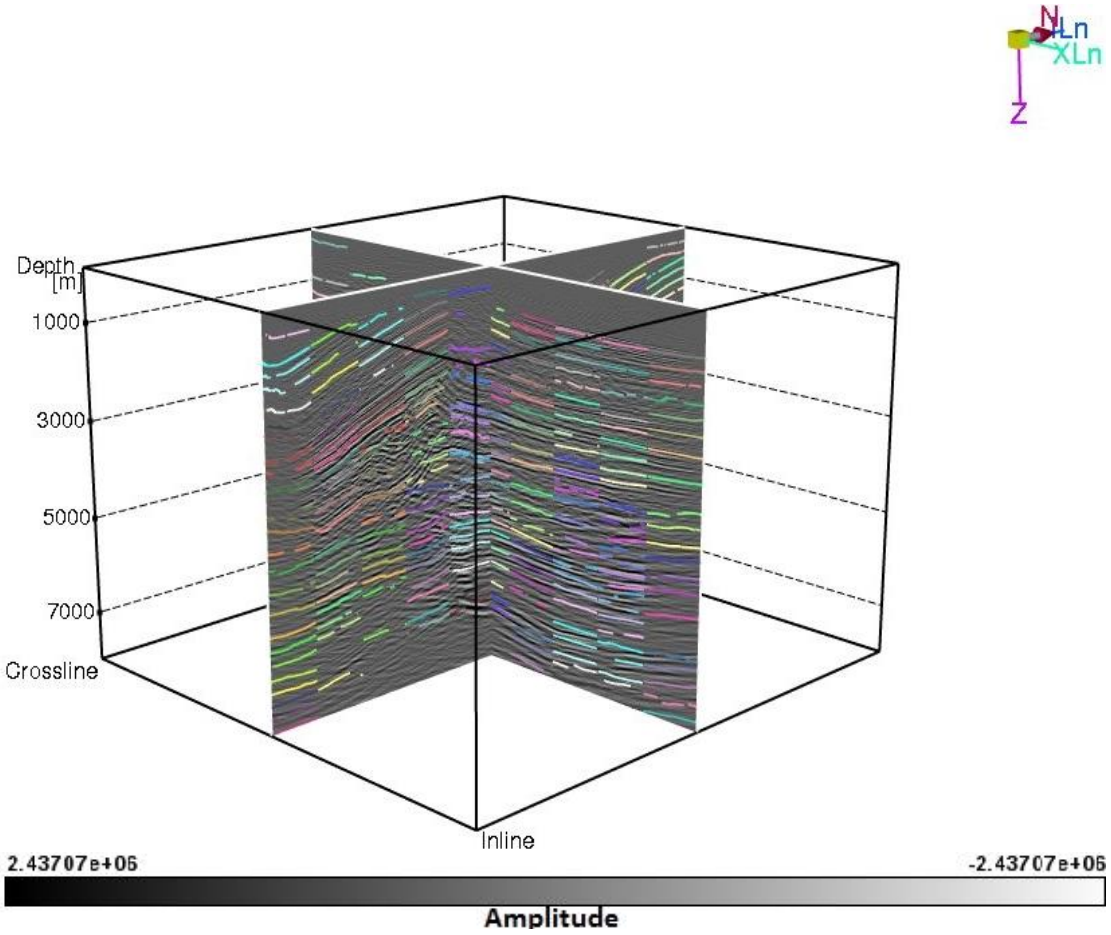

Figure 4.1: 3D view of the interlayer horizons, including inlines and crosslines. The Auto Image Picking program automatically picks and selects the horizons in the stacked data. Every color represents the continuity of each horizon.

After creating the above data, the seismic structural attributes dip, azimuth, and continuity maps are generated. These profiles are implemented by the 'Structural Attributes' application. The dip and azimuth values are computed using the plane-wave destructor method, and the continuity computation is calculated with the normalized semblance. Then, the dip and azimuth angles between the seismic traces is computed. The continuity values depend on the parameters chosen and can be adjusted by changing the power value of semblance or by weighting in the seismic section. In 3D-

grid tomography, dip, azimuth, and continuity maps are attributes from ray-shooting and smoothing in the structural model. Dip, azimuth, and continuity attributes used in tomography are seen in Figures 4.2, 4.3, and 4.4.

3D-grid tomography also creates the pencil files. These are files that contain information related to the vertical function of the data and includes information about the subsurface structural model and subsurface geological and geophysical attributes. The data are sampled according to a chosen grid and stored as pencil files. Each pencil file has a different number of points along the vertical axis that intersects with subsurface horizons.

After creating the pencil files, 'Auto Picker' is performed. The Auto Picker does pre-stack picking of the residual move-outs. Residual move-outs determine errors in flatness used for updating velocities and are used for quality checking of the coherency of the pre-stack migrated gathers. The Auto Picker uses pencil and CIG files, and outputs the error matrix for the 3D-grid tomographic solution and builds the updated velocity model. A view of the move-outs is displayed on the stacked data in Figure 4.5.

3D-grid tomography builds a matrix which is used to create an updated interval velocity. The build matrix mode in tomography was most time-consuming because of computation, memory, and disk space needs. Pencil file, interval velocity, and move-out information was input in that order; whereas the output was the tomography matrix. The workflow for 3D-grid tomography is shown in Figure 4.6.

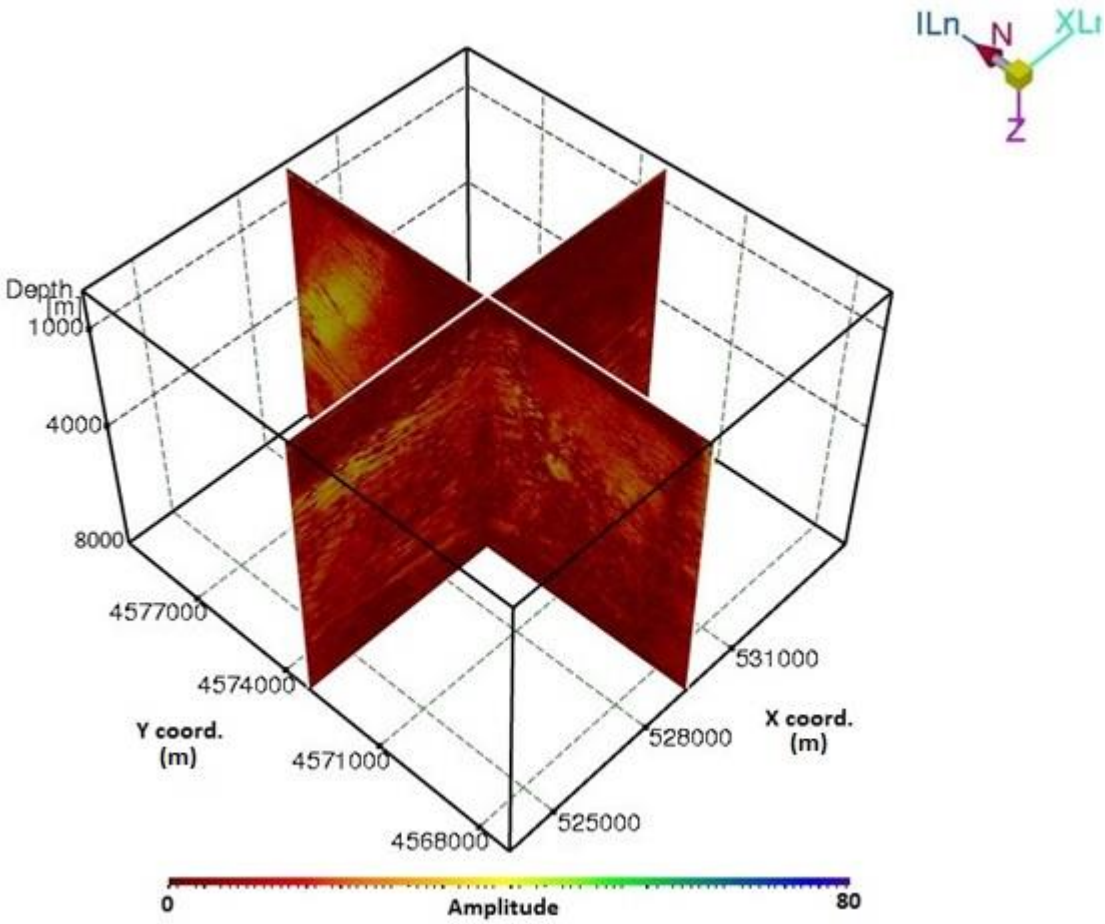

Figure 4.2: The 3D cube view of dip attribute of the seismic section, including inlines and crosslines.

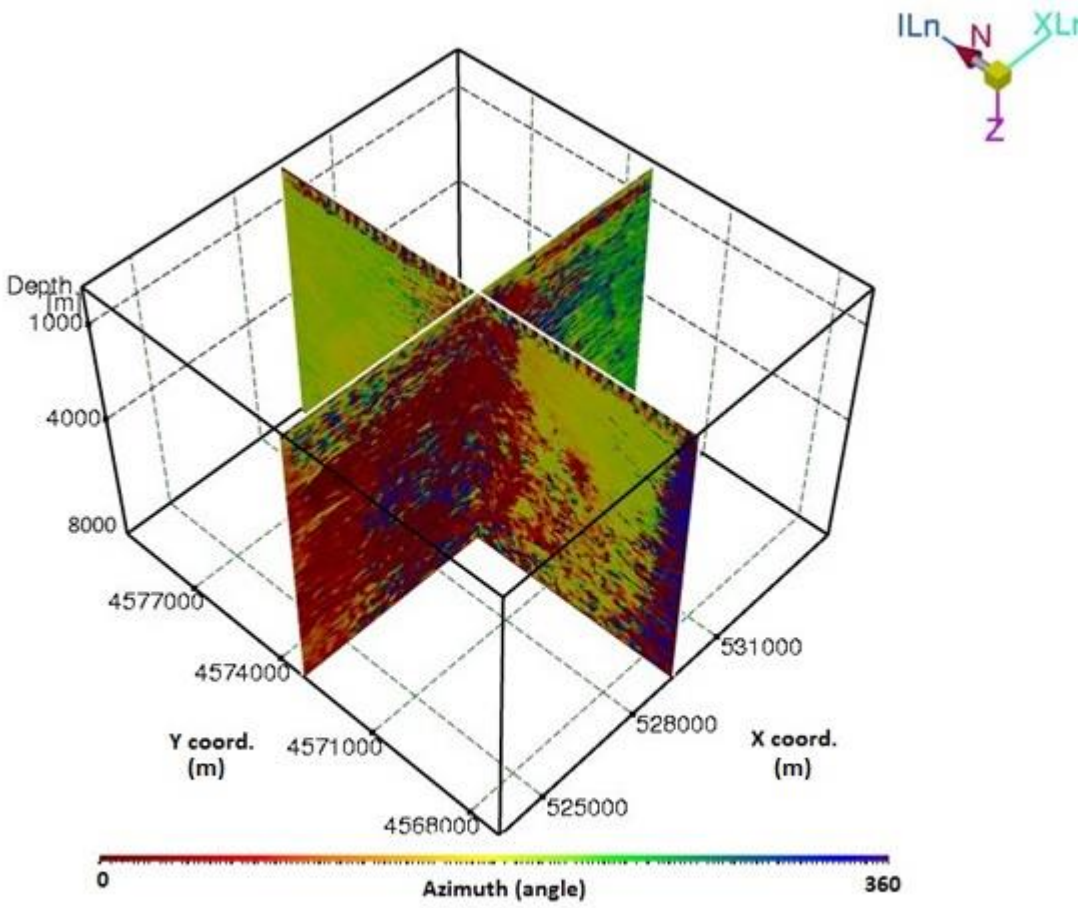

Figure 4.3: The 3D cube view of azimuth attribute of the seismic section, including inlines and crosslines.

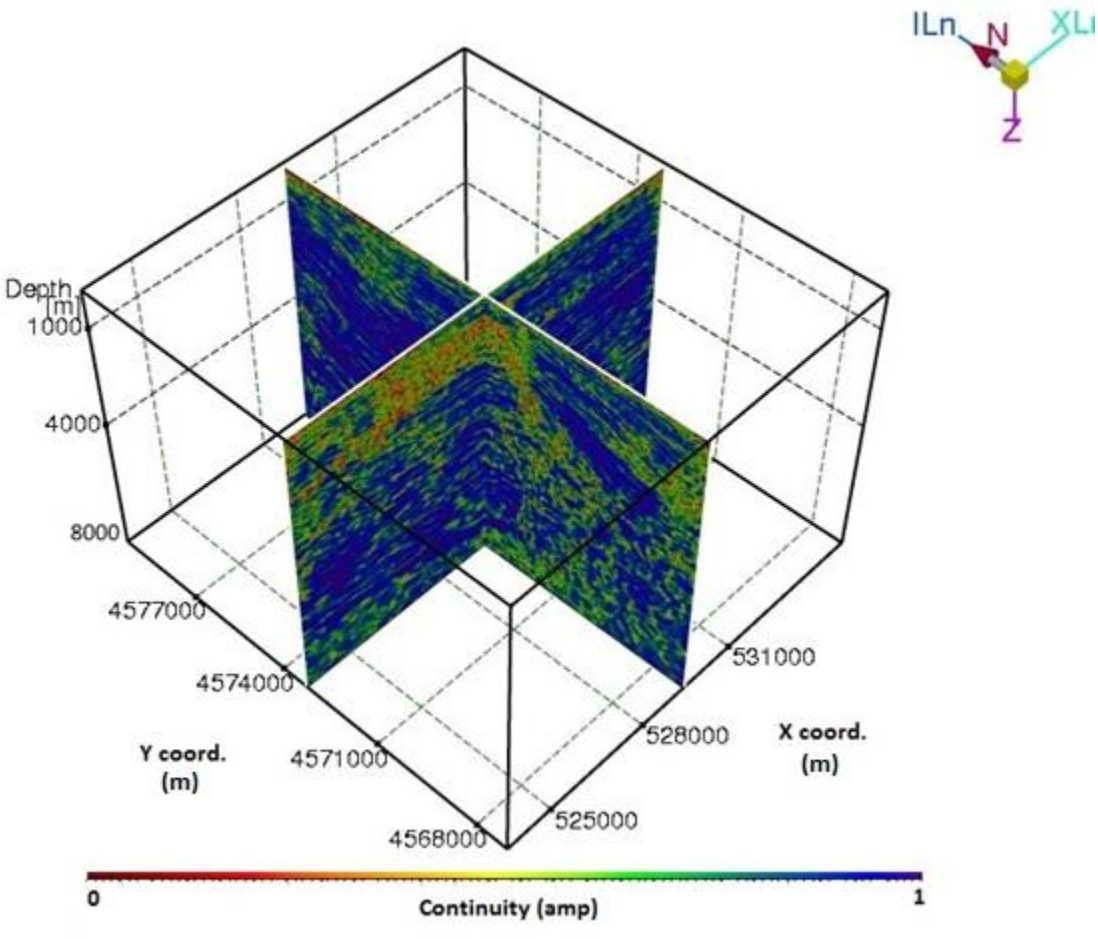

Figure 4.4: The 3D cube view of continuity attribute of the seismic section, including inlines and crosslines.

Before applying full range tomography to the data, several tests were run to check the accuracy and the reliability of the parameters. The first run was with the default parameters, but as a result, the expected upgrades in the velocity volume and the flattening of the gathers were not observed. Since I did not observe a change, I examined the initial velocity function for reliability. The shallow part of the data produced poor gathers, and instead of employing a full range of tomography to the whole depth, I primarily focused on the depth range between -100 to 3000 m. By applying this method, I examined positive changes in the gathers. In the second iteration, after updating the velocity, the new velocity input was used which changed

the depth for the full range. The parameters for the 3D Grid Tomography is described in Table 4.1.

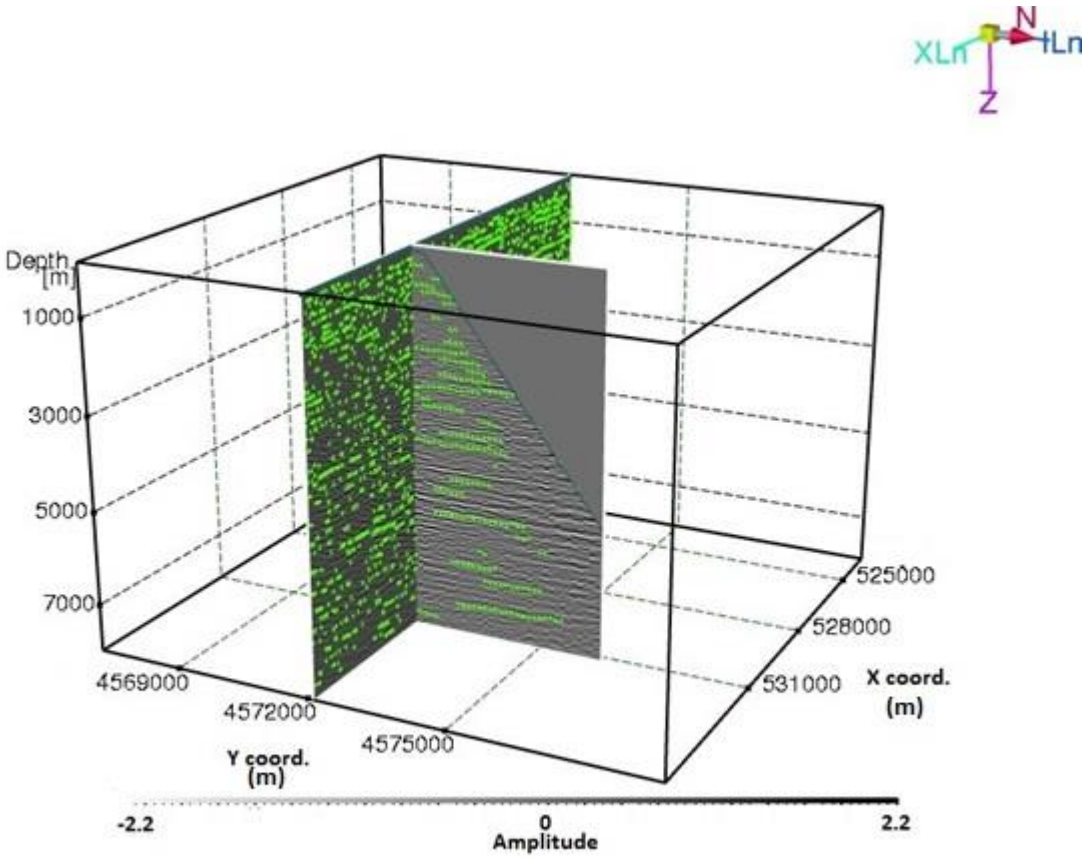

Figure 4.5: Automatically picked residual move-outs (velocity errors) shown in green color. The display shows one inline (5200) and one xline (2200) value.

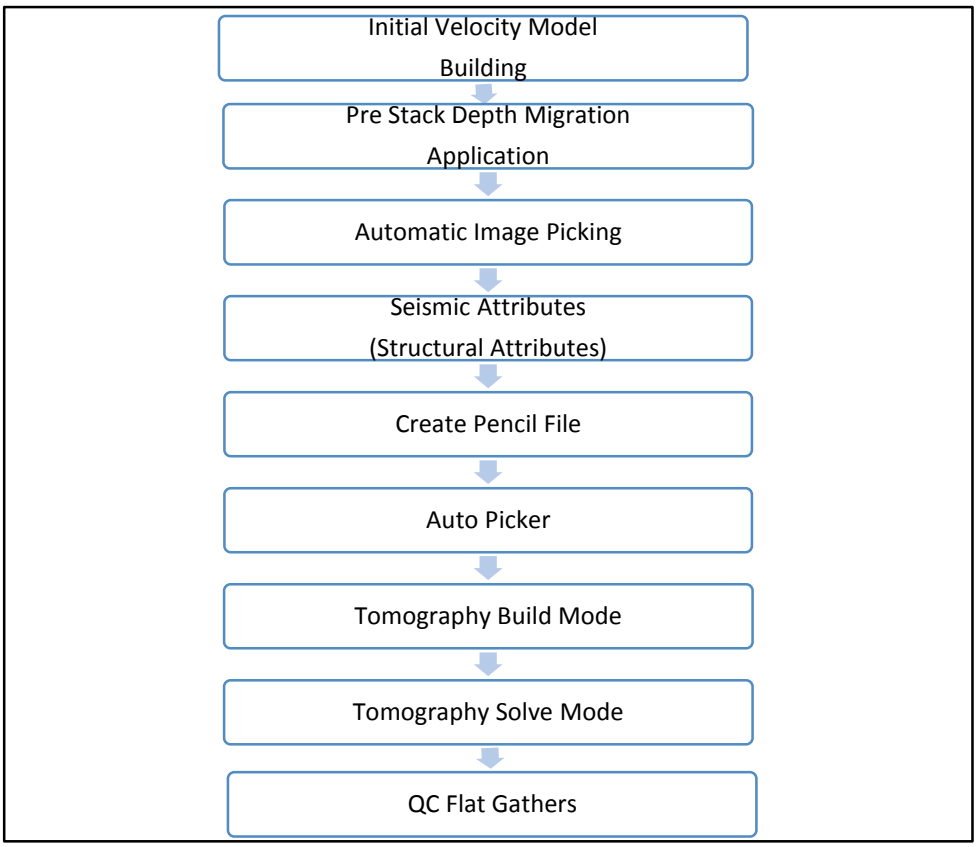

Figure 4.6: General 3D grid tomography workflow.

Table 4.1: Tomography build matrix mode parameters

Parameters	Values
Ray Shooting Grid	Along Inlines: 50 m. Along Crosslines: 50 m.
Ray Step	10 m.
Ray Frame	Aperture: 6000 m. Maximum Offset: 3400 m. Depth Range: -100 to 3200 m.
Ray Angles	Max. Half Opening Angle At Top: 40 degree At Bottom: 30 degree
Update Grid	Inline: 200 m. Crossline: 200 m. Depth: 100 m.

The solving mode was relatively similar to the build mode, but the input was the matrix file instead of a pencil file. All the related information was computed in the matrix file to produce the updated interval velocity. The same inline and crossline ranges and depths were used. In addition to the input definitions, a sensitivity factor was an essential. This global sensitivity factor multiplied the model variance. If the value is larger, larger updates were produced. However, using a large sensitivity factor may lead to failure of the iterative algorithm. I used a sensitivity factor of 20 which produced relatively flat and updated gathers.

The updated velocity from the tomography was used for the pre-stack depth migration algorithm. A new travel-time was calculated. I have chosen the spherical eikonal approach which calculates the time for an isotropic media. For the spherical eikonal travel-time solver, the parameter spheres step is defined as the distance between spheres where the travel time is calculated. The impact of this is related to the accuracy and the speed of the calculation, and a smaller value may increase the calculation time. My choice for this parameter was 50 m. Another useful parameter was the spherical grid arc length which is the length of arcs between the nodes on the spherical grid. It requires a minimum and a maximum value. I used 25 m for the minimum arc length, and 50 m for the maximum arc length. After application of those two iterations in tomography, the final interval velocity model was produced as seen in Figure 4.7.

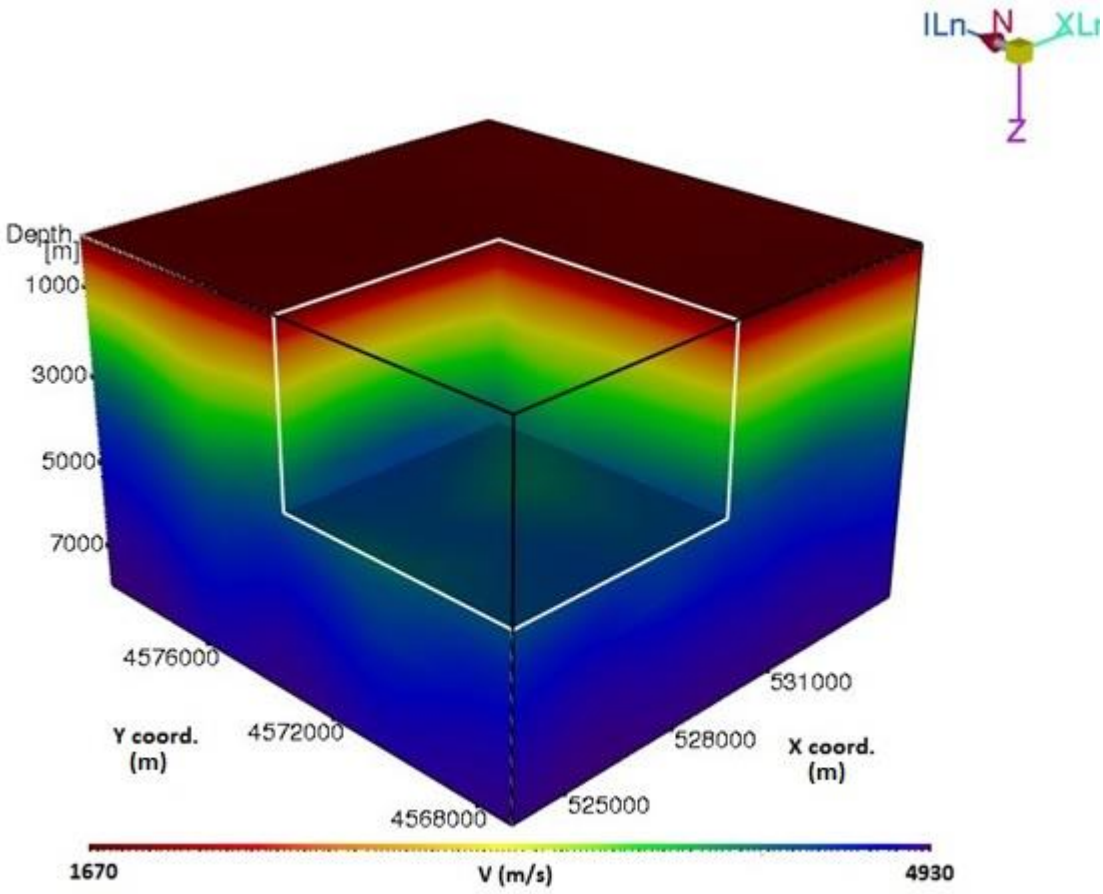

Figure 4.7: Final interval velocity volume in 3D chair view.

Using the final interval velocity volume, a final approach for Kirchhoff pre-stack depth migration has been undertaken in Figure 4.8. Common image gathers are exhibited as before tomography in Figure 4.9 and after tomography in Figure 4.10 to see the effect of refined velocity. The resulting stacks of final Kirchhoff pre-stack depth migration using the final interval velocity model are shown in Figure 4.11 to 4.15.

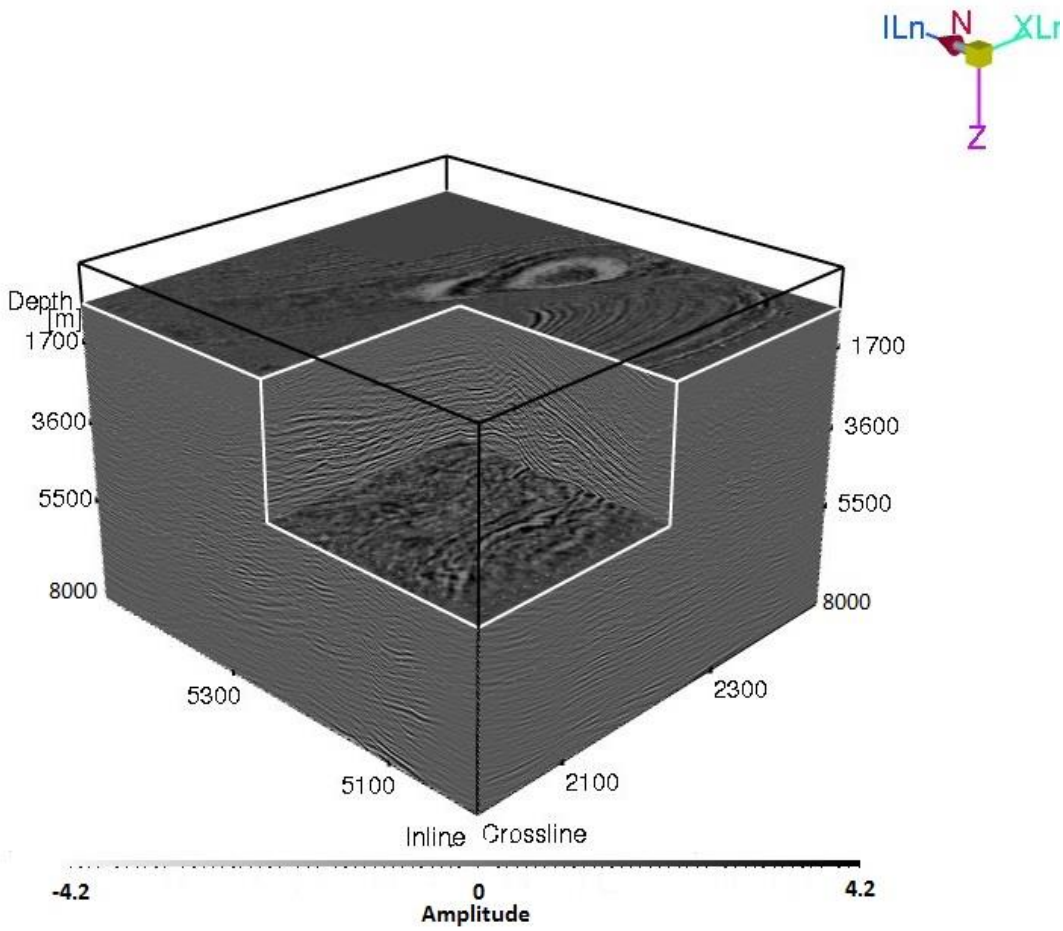

Figure 4.8: 3D chair view of the final Kirchhoff pre-stack depth migration.

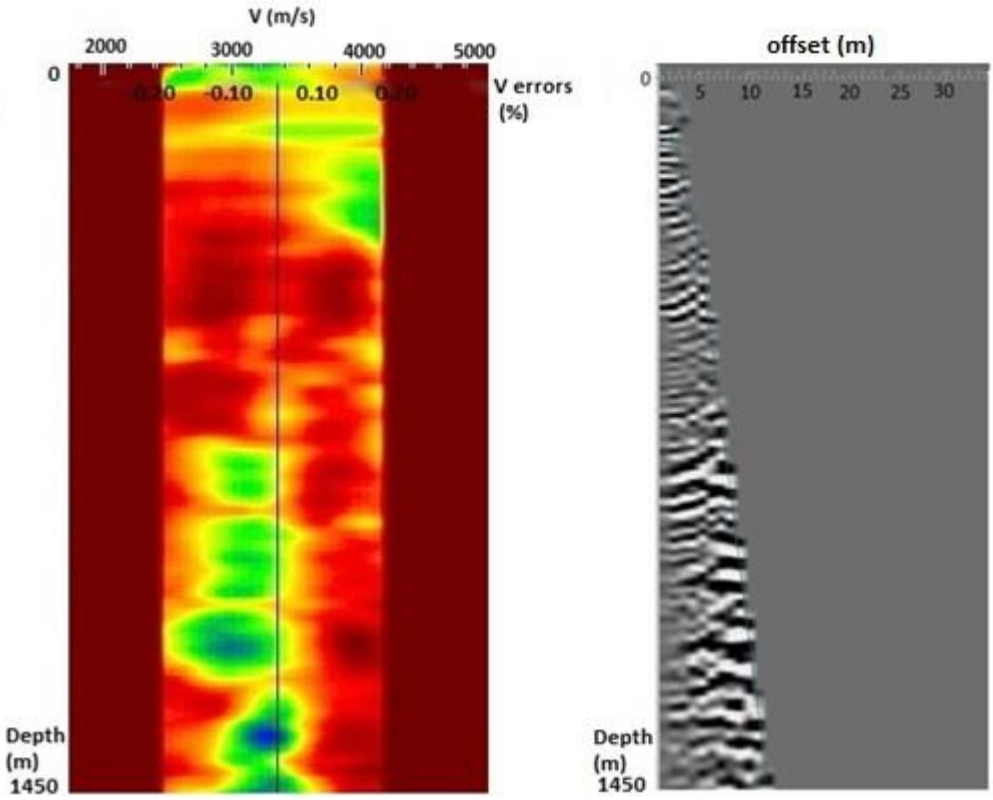

Figure 4.9: The velocity errors and the common-image-gathers before the tomography.

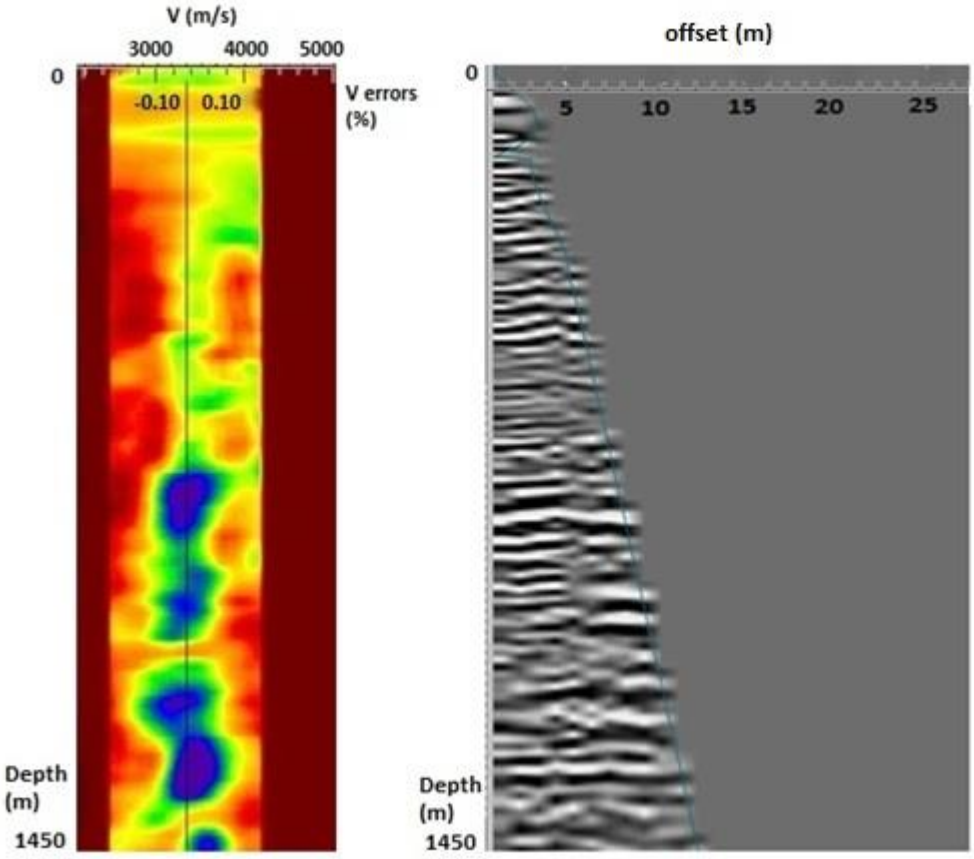

Figure 4.10: The velocity errors shown in semblance coherency plot and the common-image-gathers after the tomography.

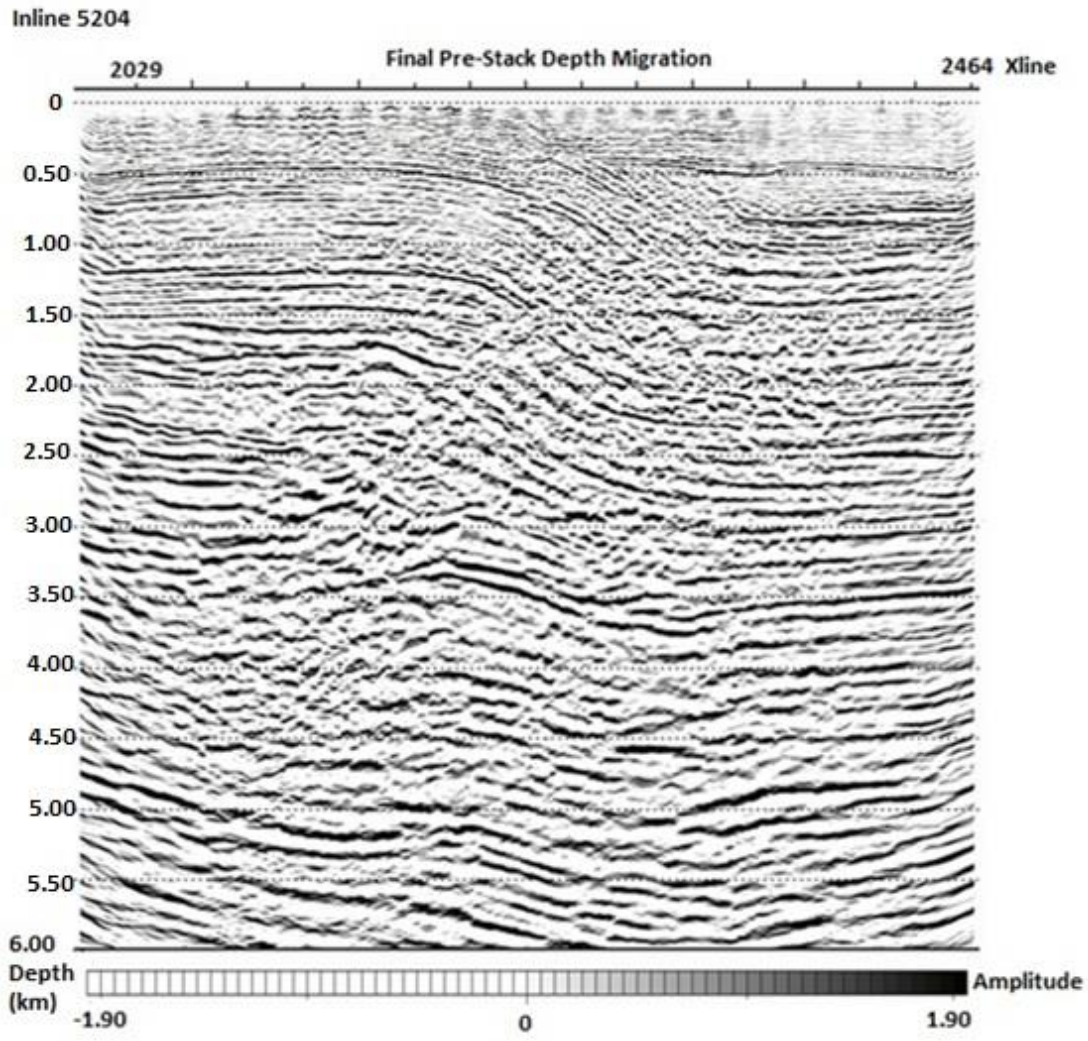

Figure 4.11: The final Kirchhoff pre-stack depth migration result of inline 5204.

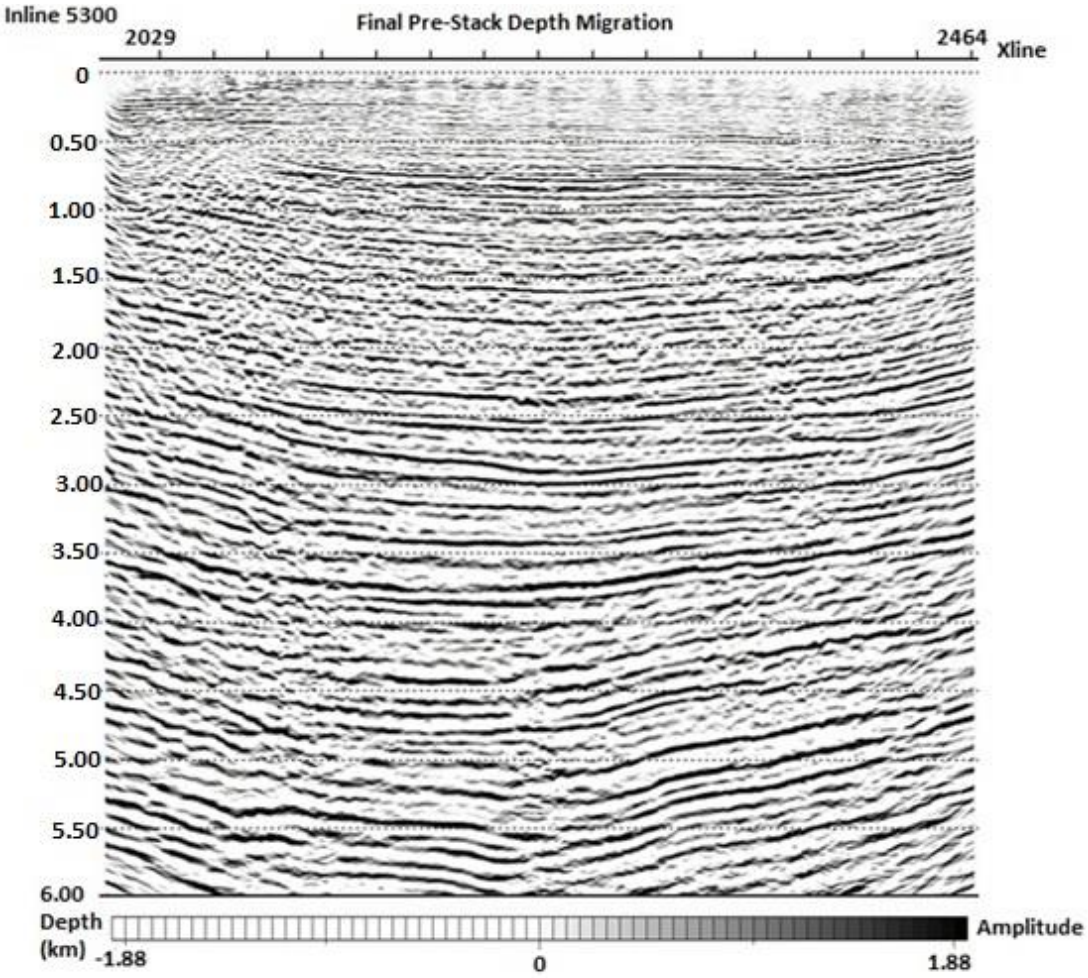

Figure 4.12: The final Kirchhoff pre-stack depth migration result of inline 5300.

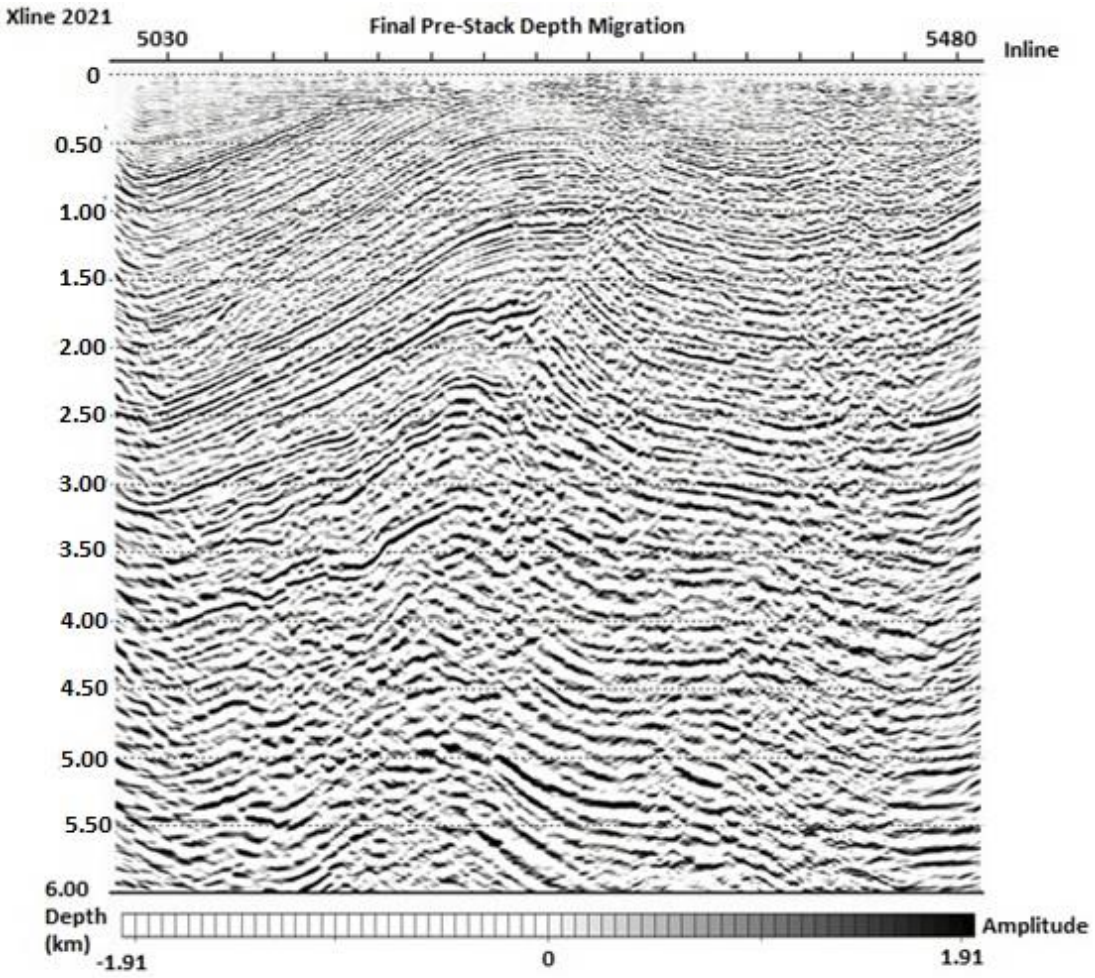

Figure 4.13: The final Kirchhoff pre-stack depth migration result of xline 2021.

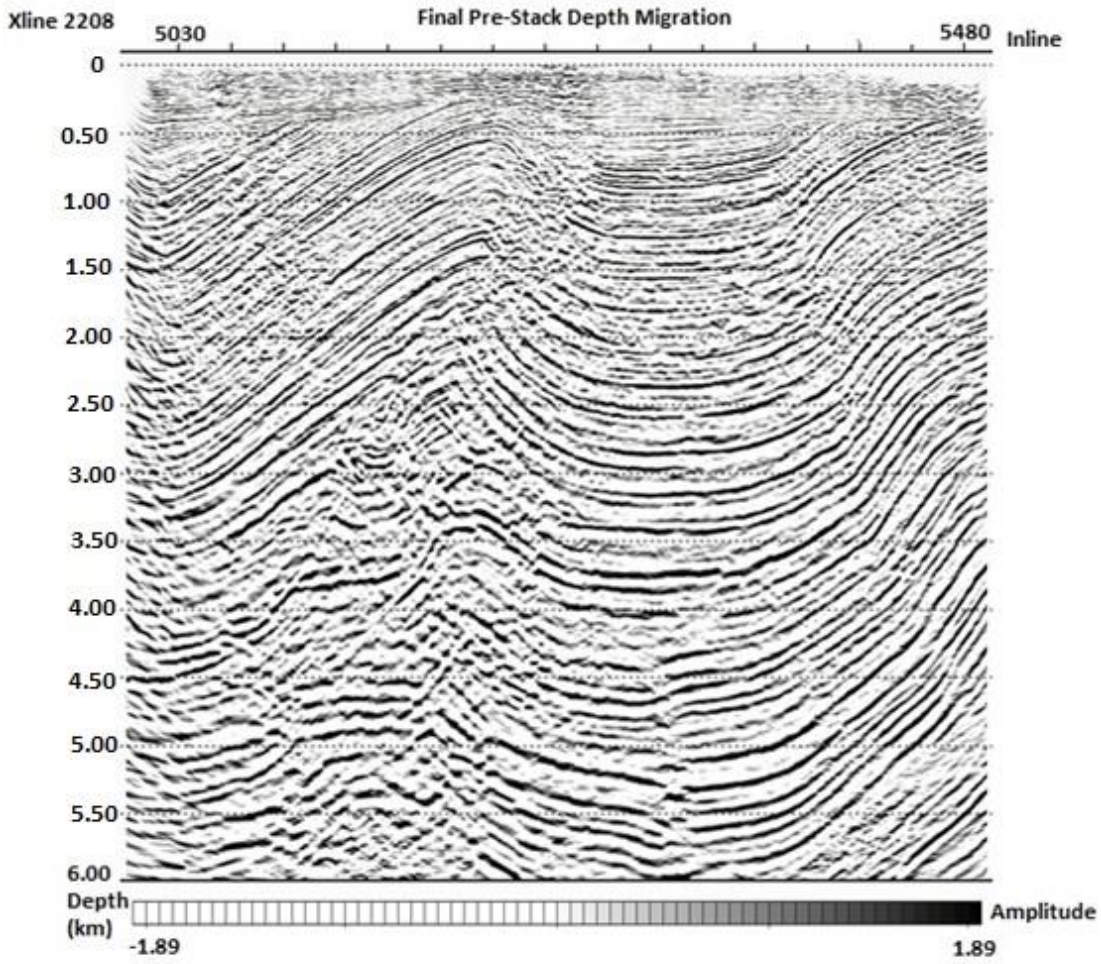

Figure 4.14: The final Kirchhoff pre-stack depth migration result of xline 2208.

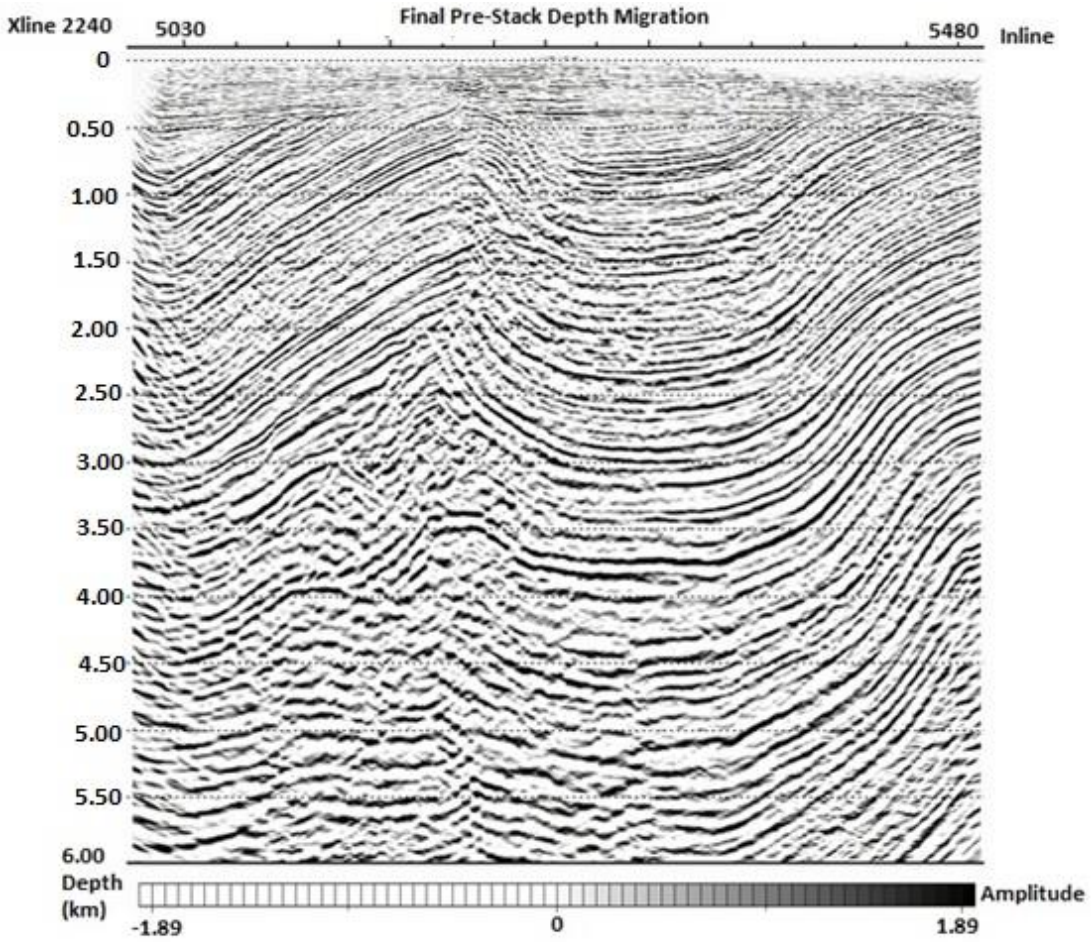

Figure 4.15: The final Kirchhoff pre-stack depth migration result of xline 2240.

Chapter 5: Reverse-Time-Migration (RTM)

In this phase of my research, I have employed reverse-time migration as a final approach to produce a better imaging of the subsurface. RTM has been a preferable imaging algorithm due to its full two-way wave equation solutions. This method accurately propagates the wave field through a complex velocity structures and has no dip limitations, such as downward continuation (Baysal et al., 1983).

For the areas with complex geometry, reverse-time migration is an essential tool, it will produce significantly better images than other imaging methods. Due to greater computation power, imaging problems are easily resolved by RTM. RTM assumes a correct interval velocity model as any other depth migration.

RTM is a shot-gather migration that images a shot gather into an output sub-volume around of each recorded shot gather. Mainly, the general procedure of this technique is modeling the source field via forward time extrapolation of the source field (modeling), and backward time extrapolation of the receiver field (recorded shot gather). Then, the imaging condition is applied by cross-correlating the corresponding equal-time wave-fields also called snapshots.

Wave propagation is at the core of the RTM algorithm. Therefore, efficient calculation of wave-field updates is absolutely necessary for an accelerated RTM application. In isotropic case, waves are propagated according to the second-order scalar acoustic wave equation:

$$\nabla^2 U = \frac{1}{c^2}\frac{\partial^2 U}{\partial^2 t} \tag{5.1}$$

Where, U is the wave-field of interest and c is the corresponding acoustic wave velocity.

All wave propagations are performed in the space-time domain. Second-order central time finite difference approximations are used as standard, so that the wave-field at time n+1 may be calculated from previous values as:

$$U^{n+1} = 2U^{n} - U^{n-1} + \Delta t^{2} c^{2} L(U^{n}) \tag{5.2}$$

Where, Δt is the temporal discretization step and the operator L represents the spatial derivatives incorporated in the $\nabla^{2} U$ term in the scalar acoustic wave equation (5.1), i.e. the left hand of the equation.

The subsurface image is constructed by application of an imaging condition. In RTM, the basic imaging condition is a point-by-point multiplication of source and receiver wave-fields at each time-step. The snapshot images at each time-step integrated over time to give the final image for the current shot;

$$\mathrm{Image}(x, y, z) = \sum_{t=T}^{t=0} S(x, y, z, t) R(x, y, z, t) \tag{5.3}$$

Where, the summation runs over the total number of computational time-steps. *S* is the source wave-field calculated at time-step t and R is the corresponding receiver wave-field.

Each shot gather is imaged into a surrounding sub-volume, where each sub-volume is a portion of the final image. These overlapping sub-volumes are accumulated to obtain the complete migration result. The final output volume as shown in Figure 5.1. Since it is a shot gather migration, it allows easy parallelization on today's clusters. The final image volume will be created by sorting the output sub-volumes into CIGs, and stacking them. Shot gather migration methods also have the advantage that a sub-sampled number of shots may be used to image the data, and then additional shots may be added to the solution as needed.

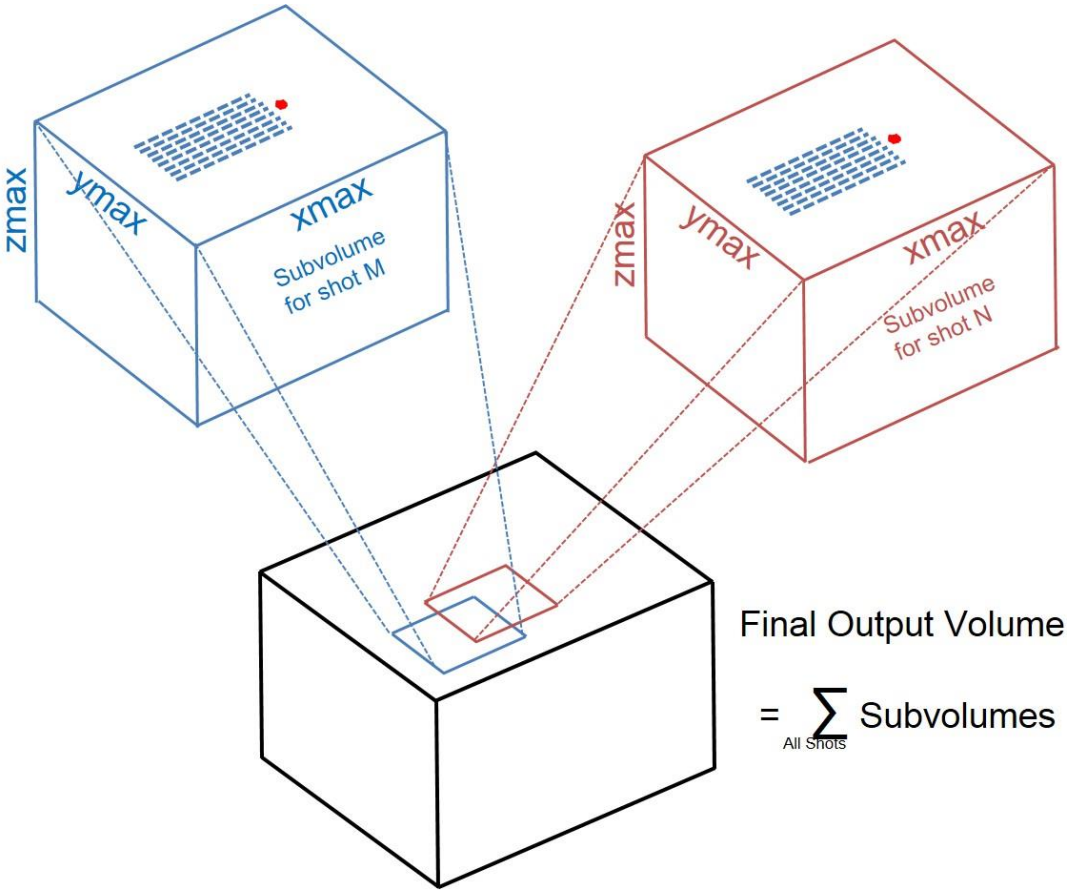

Figure 5.1: Illustration of overlapping sub-volumes, and building up the Final Image Volume. The size of the sub-volume around the shot-gather is user chosen and depends on the geology of the area, mainly in the maximum migration distances of events.

As in other imaging methods, reverse-time migration has some limitations and pre-conditions. Usually, the raw data must be the input although a lateral balancing of the shots and receivers may be desirable on some data. Spherical divergence correction should not be applied. In marine cases, SRMA (Surface Related Multiple Attenuation) would be desirable. A source wavelet is needed to capture a better imaging, since the source wavelet also helps to control the frequency band. In calculating the spatial derivatives in finite difference method, the design of the derivative operators will govern the minimum cell size in the sub-volume, and the desired maximum frequency

will define the time-step for extrapolation of the pressure fields. All these factors are effecting the computer resources needed (the size of the grid in the sub-volume will require large memory) and the run times per shot depend on the grid size and mostly on the time step size for time extrapolations. Generally, with all these considerations a desired high frequency is chosen to achieve reasonable run times. This frequency is not a cut-off frequency for the data. In other words, the frequencies higher than this maximum frequency will also migrate, but the cell size in x, y, and z, and also the time-step size will be designed. Consequently, the frequencies up to this maximum frequency would not have dispersion, and higher frequencies may have dispersion effects. As stated earlier, also a source wavelet, usually having a frequency bandwidth the maximum frequency specified, is defined and used in the source modeling, which may also control the frequencies extrapolated. The source field and receiver fields are correlated at every time-step.

All these considerations usually result in RTM images created with rather lower frequency data compared to other depth migrations, such as Kirchhoff depth migration. RTM presents slightly worse resolution, yet the most accurate image, assuming the velocity model is correct.

In my study, as a final approach, I have implemented reverse-time migration to observe a better outcome of the subsurface. I used the velocity model obtained from the velocity model building earlier, employing the Kirchhoff depth migration and tomography iteration. The input data to the RTM are the raw shot gathers which include editing and surface consistent lateral balancing only. I have presented RTM results for the same selected inlines and crosslines in Figures 5.2 to 5.6. The vertical axis,

represents depth, Z, and it is in the range of -100 m (datum for conventional processing) to 6000 m.

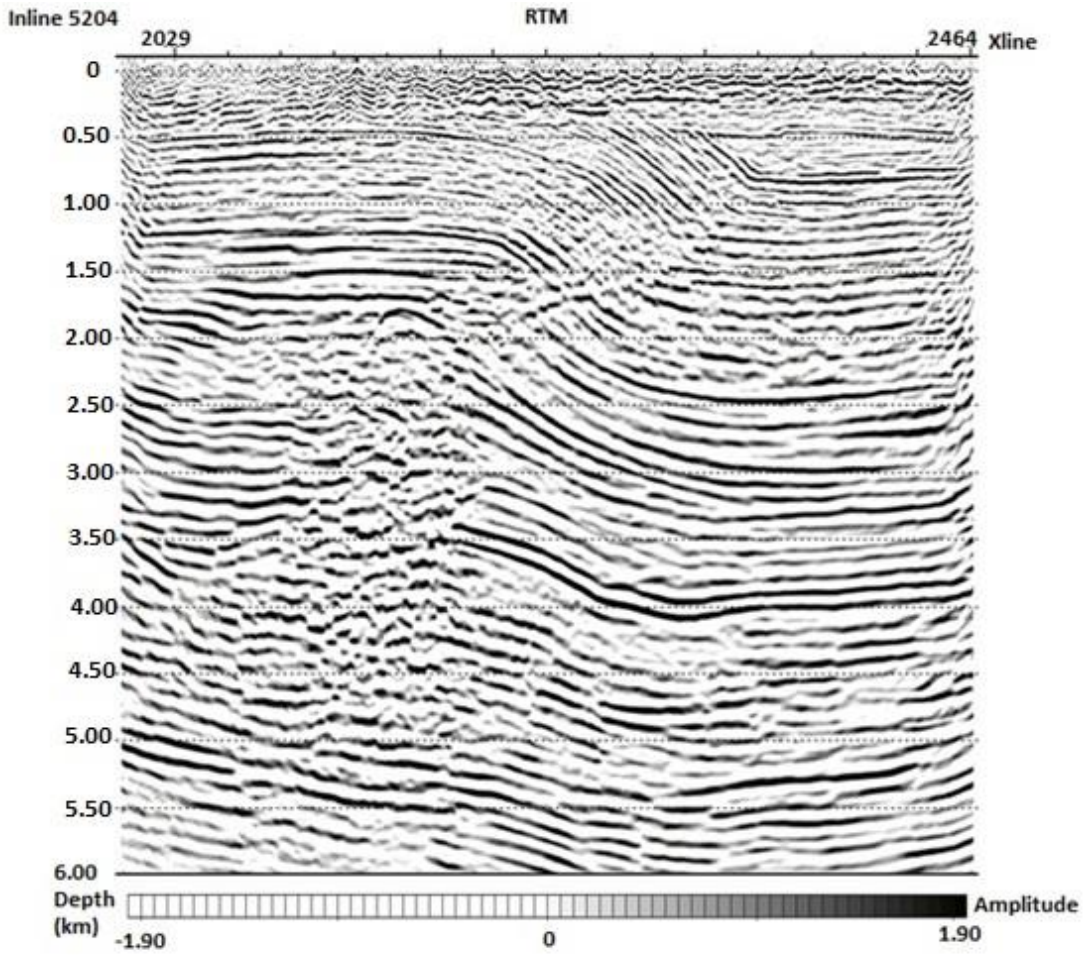

Figure 5.2: The reverse-time migration result of the data for inline 5204.

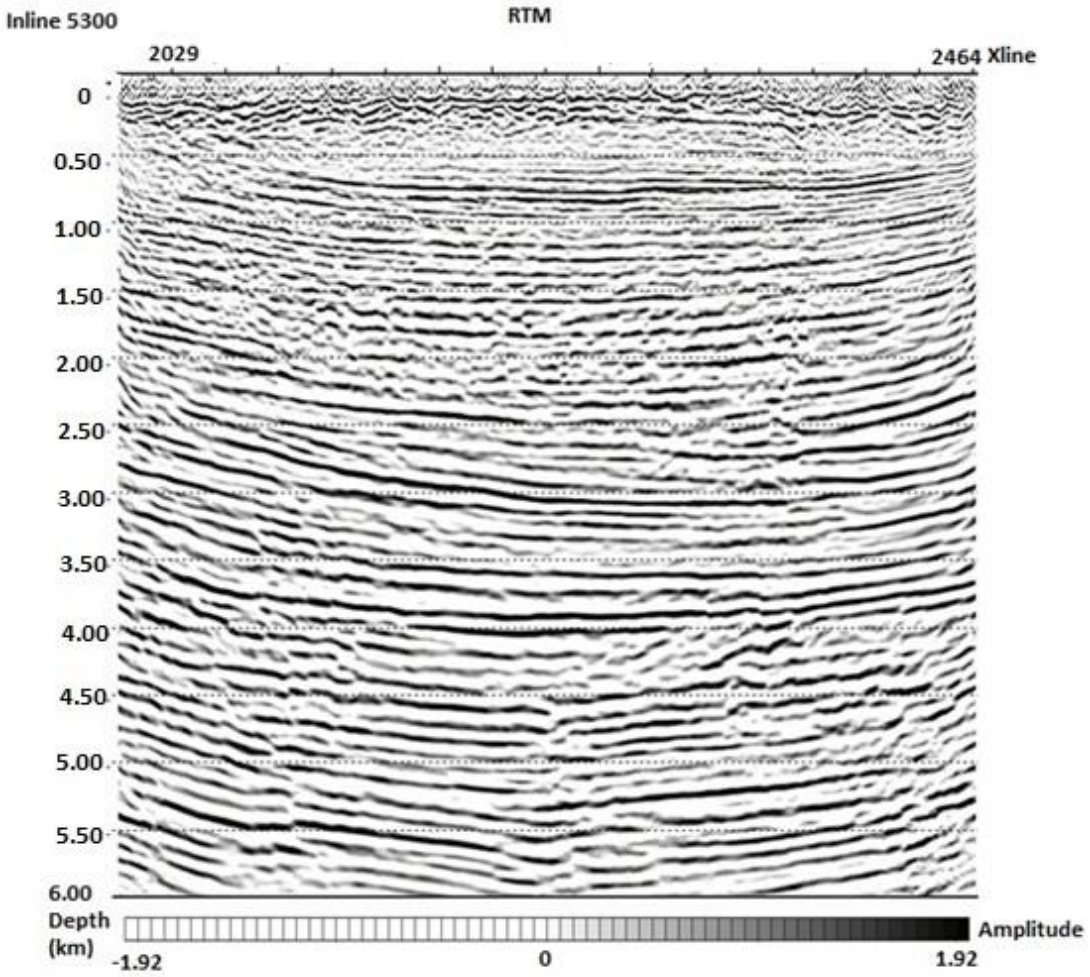

Figure 5.3: The reverse-time migration result of the data for inline 5300.

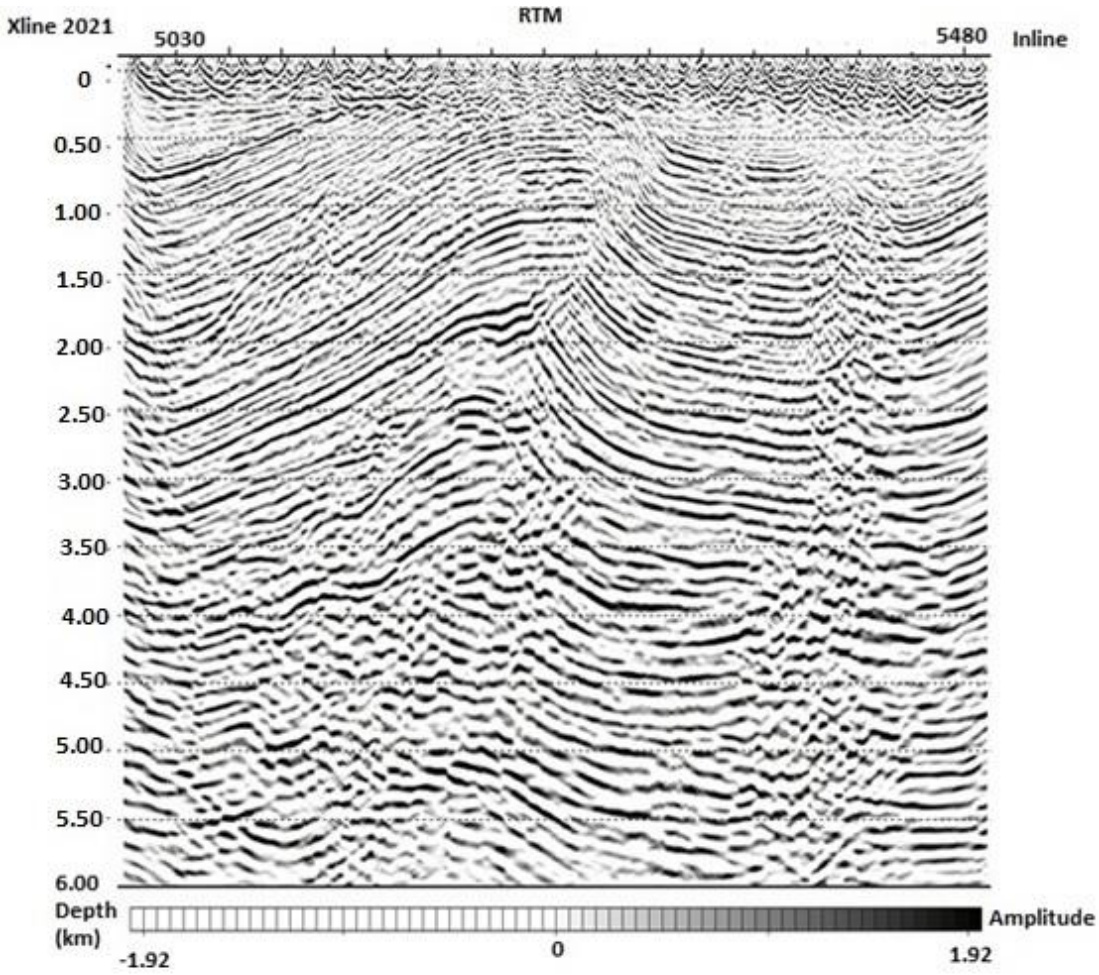

Figure 5.4: The reverse-time migration result of the data xline 2021.

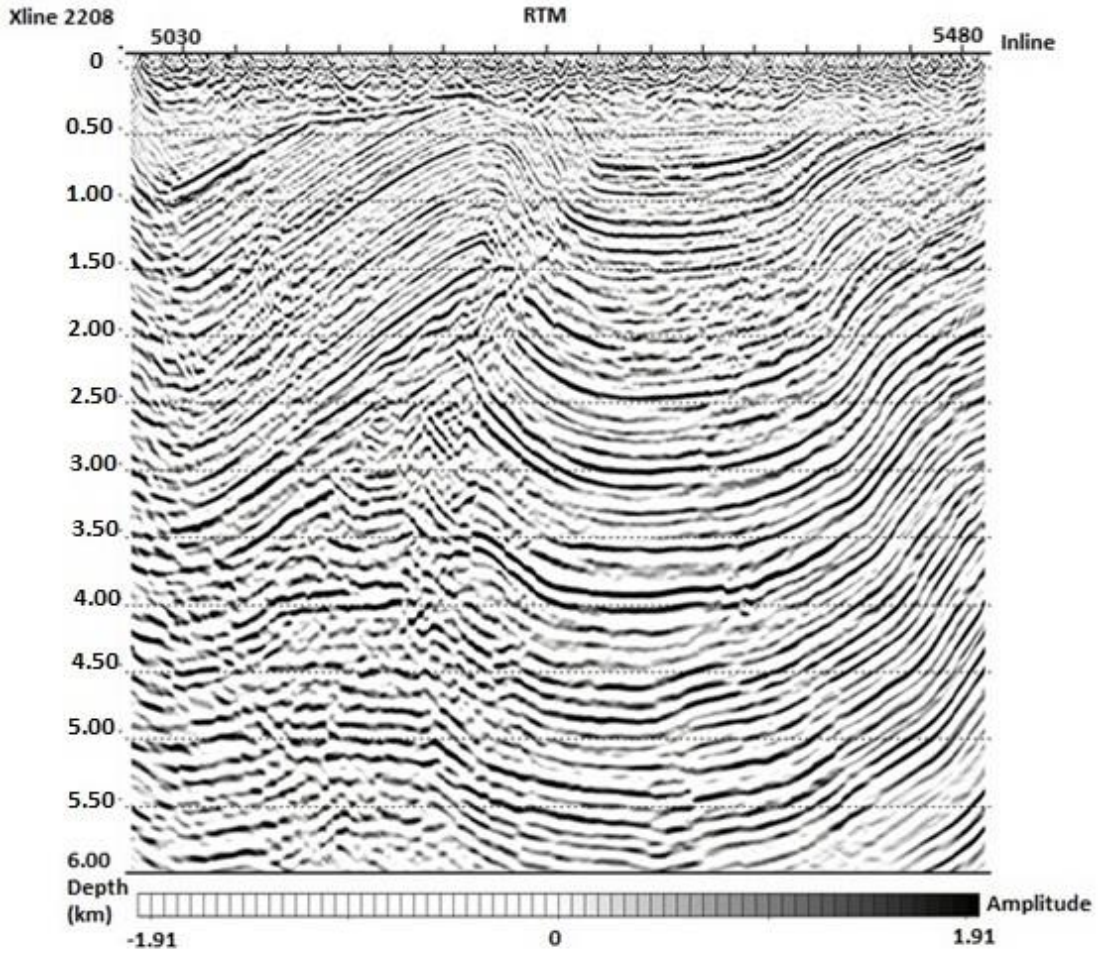

Figure 5.5: The reverse-time migration result of the data xline 2208.

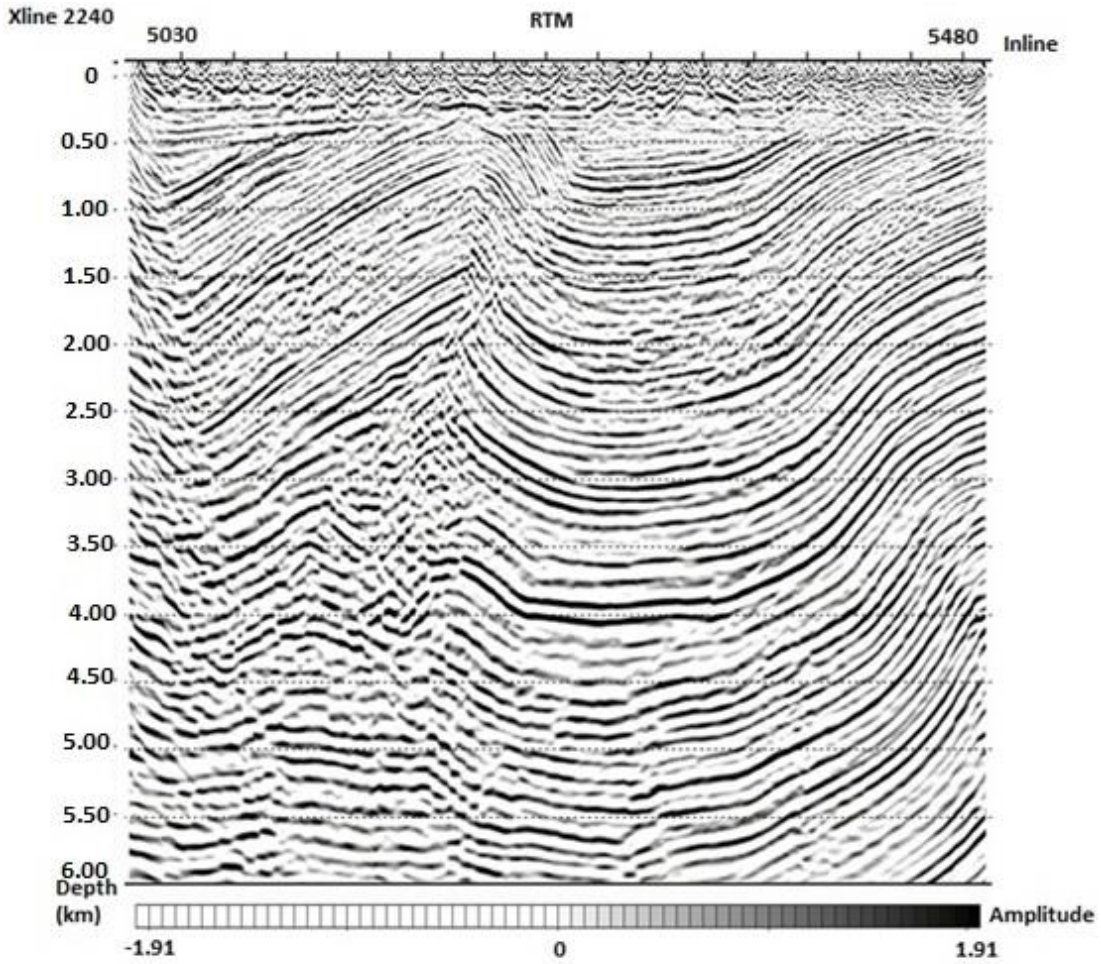

Figure 5.6: The reverse-time migration result of the data xline 2240.

Chapter 6: Conclusions

In this study, I have processed a 3D land dataset, with conventional and modern processing and imaging techniques, and velocity model building which is widely used in the industry. The data were supplied by Turkish Petroleum. It is a 3D-dataset which was acquired in the Thrace Basin of Turkey. Natural gas is main hydrocarbon produced in this region.

I started, with what we may call conventional processing, which in today's industry is fast-track processing and mainly uses common-depth-point (CDP) method and generates a CDP stack volume. This type of processing served well for many years, especially when only 2D-datasets were collected. Although CDP stacking is not the mainstream of the processing today, especially for 3D-data, it still serves as a fast-track processing for the industry. This type of processing reveals the problems and solutions for near surface (statics), various noise suppressions, and also presents a means of quality control in data acquisition. It produces a CDP stack volume to give the first interpretation of the subsurface and also produces the first guess of the effective (RMS) velocities, either stacking or NMO velocities. During this processing, I have derived the necessary pre-processing steps of the pre-stack data for different imaging methods.

Following the conventional processing, I have investigated and applied the imaging (migration) methods, post-stack, and pre-stack, time and depth imaging, and Kirchhoff and wave-equation, specifically reverse-time migration (RTM). I also applied interval velocity building flows, via iterations of Kirchhoff depth migration and tomography.

I started with the 3D-post-stack time migration of the CDP stack volume which was obtained in the conventional processing of the data. Following the post-stack migration, I have implemented 3D-pre-stack time migration. Both time migrations (post and pre-stack) that are employed are Kirchhoff migrations. It is clear that the pre-stack migration is superior to post-stack migration since the NMO and CDP stack has limitations in representing the true zero-offset volume. The pre-stack migration also allows the correctness of the effective velocity field and ways to update the stacking or NMO velocities obtained during the velocity analysis of conventional processing. Effective (RMS) velocities are needed for time migration, and may serve as an initial guess for interval velocity model using Dix inversion. It is needed for depth migrations.

For the pre-stack depth migration and interval velocity model building, again Kirchhoff depth imaging is used for its versatility and flexibility. Kirchhoff method allows target oriented migration results, without migrating the whole output volume. Selected inlines and crosslines of the output may be migrated, and tomography minimizes the errors and updates the interval velocity field. These iterations of pre-stack depth migration and tomography may be repeated as many times as necessary depending on the complexity of the geological model of the area. The tomography updates the depth and velocities of the layers in the interval velocity model by preserving the zero-offset arrival time which is unchanged for the reflections (time preserving tomography). In my study, I started with an interval velocity model estimation that is obtained via Dix inversion of the final RMS velocity volume. Rather than using the straight Dix inversion, I used a constrained Dix inversion (Koren and Ravve, 2005). The constraints applied in this method (CVI) prevents a more robust inversion, especially in areas where the Dix formulation may blow up due to unrealistic

RMS velocity values. I applied two iterations of Kirchhoff depth migration and tomography to update the interval velocity volume. The final interval velocity in depth domain is used to result in the final Kirchhoff depth image volume. The results are given for -100 to 6000 m depth range.

The modern, up-to-date depth imaging technique is reverse-time migration. RTM is a depth migration that uses the full or two-way wave-equation which allows all the complex wave phenomena to be handled better than any other migration method. It is a shot gather migration where the source modeling is performed in forward extrapolation in time, but the recorded seismic field (traces recorded by the receivers) is extrapolated in the reverse-time direction (hence, the name reverse-rime migration). It is an expensive application, and due to practical usage of RTM, the maximum frequencies used in RTM implementations are usually lower than the other depth migrations such as Kirchhoff depth migration. RTM is producing a lower resolution, especially in the shallow areas of the image compared to Kirchhoff images. In my study, I have chosen a maximum frequency of 40 Hz. The RTM imaging results are also given for -100 to 6000 m depth range.

I have used a dataset which was acquired in 2006, with the conventional processing techniques (CDP stacking) in mind. I applied the most modern, up-to-date processing flows, imaging methods to this data. I believe, I did not get most of the benefits of modern imaging and velocity model building techniques since the data are not very suitable for this purpose. The shot pattern used in the data acquisition is quite a narrow azimuth, 1800 m X 6400 m (shot being in the middle of the pattern). The azimuth distribution is an important factor in today's 3D pre-stack imaging methods. Azimuth distribution, as well as offset distribution, are important factors in better

imaging of the subsurface. Furthermore, the target for possible reservoir layers, is not too deep (1500 - 2200 m) in this area; therefore, 50 m for the station and shot distances along the receiver and shot lines may be too large for the purpose of imaging this depth zone.

References

Bancroft, C. J., Wang, S., Lawton, C. D., and Foltinek, H. D. (1996). Converted-wave pre-stack migration and migration velocity analysis. 66th International Meeting, Society of Exploration Geophysicists, Expanded Abstracts, 1575-1578.

Bancroft, C. J. (2002). A theoretical and visual description of the relationship between Kirchhoff migration and seismic inversion. SEG Technical Program Expanded Abstracts, 2154-2157.

Baysal, E., Kosloff, D. D., and Sherwood, W. C. (1983). Reverse Time Migration. Geophysics, 48, 1514-1524.

Biondi, B. (2005). Angle-domain common image gathers for anisotropic migration. SEG Technical Program Expanded Abstracts, 1922-1925.

Biondi, B. (2006). 3D Seismic imaging. Tulsa, Oklahoma. Society of Exploration Geophysicists.

Coskun, B. (2000). Influence of the Istranca-Rhodope Massifs and strands of the North Anatolian Fault on oil potential of Thrace Basin, NW Turkey. Journal of Petroleum Science and Engineering, 27(1), 1-25.

Dai, H., Li, X-Y., and Conway, C. (2004). 3D prestack Kirchhoff time migration of PS-waves and migration velocity model building. Extended Abstracts of SEG 74th Annual Meeting and 2004 International Exhibition, Denver, Colorado, 10-15

Daly, C., Diggins, C. (1988). Use of refractor elevation models in the computation of refraction statics. SEG Technical Program Expanded Abstracts, 574-577.

Dix, C. H. (1955). Seismic velocities from surface measurements. Geophysics, 20, 68–86.

Gorur, N., Okay, A. I. (1996). A fore-arc origin for the Thrace Basin, NW Turkey. Geologische Rundschau, 85(4), 662-668.

Gray, S.H. (2001). Seismic Imaging. Geophysics, 66, 15-17.

Gurgey, K., Philp, P., Clayton, C., and Siyako, M. (2005). Geochemical and isotopic approach to maturity/source/mixing estimations for natural gas and associated condensates in the Thrace Basin, NW Turkey. Applied Geochemistry, 20, 2017-2037.

Hosgormez, H., Yalcin, M. (2005). Gas-source rock correlation in Thrace basin, Turkey. Marine and Petroleum Geology, 22, 901-916.

Kearey, P., Brooks, M., and Hill, I. (2002). An Introduction To Geophysical Exploration, 3rd edition. Blackwell Science Ltd.

Koren, Z., Ravve, I. (2005). Constrained velocity inversion: SEG Technical Program Expanded Abstracts, 2289-2292.

Lawton, D.C. (1989). Computation of refraction static corrections using first-break traveltime differences. Geophysics, 54, 1289-1296.

Lovelady, D. L., Goins, N. R., Reilly, T. A., and Spratt, R. S. (1984). Amplitude balancing of seismic data. SEG Technical Program Expanded Abstracts, 512-513

Liner, L. C. (1999). Concepts of normal and dip moveout. Geophysics, 64, 1637-1647.

Sabbione, J. I., Velis, D. (2010). Automatic first-breaks picking: New strategies and algorithms. Geophysics, 75, 67–76.

Schneider, W. A. (1971). Developments in seismic data-processing and analysis. Geophysics, 36, 1043–1073.

Sheriff, R. E. (2005). Encyclopedic dictionary of applied geophysics. Society of Exploration Geophysicists, Tulsa, Oklahoma.

Siyako, M. (2006). Tertiary lithostratigraphic units of the Thrace Basin in Siyako, A., Okay, A., Yurtsever, A. Lithostratigraphic units of the Thrace region. Lithostratigraphic Units Series-2. General Directorate of Mineral Research and Exploration Publications, Ankara, 43-83.

Turgut, S., Turkaslan, M., and Perincek, D. (1991). Evolution of the Thrace Sedimentary Basin and its hydrocarbon prospectivity, in Generation, Accumulation, and Production of Europe's Hydrocarbons, edited by A. M. Spencer, Oxford University Press, 415–437.

Whitmore, N. D. (1983). Iterative depth migration by backward time propagation: SEG Technical Program Expanded Abstracts, 382-385.

Yilmaz, O. (1987). Seismic data processing: Society of Exploration Geophysicists.

Yilmaz, O. (2001) Seismic Data Analysis: Processing, Inversion, and Interpretation of Seismic Data (Investigations in Geophysics, No. 10), Society of Exploration Geophysicists, Tulsa, Oklahoma.

Zhou, H. (2014). Practical Seismic Data Analysis. Cambridge University Press.